

KADIR HAS UNIVERSITY  
GRADUATE SCHOOL OF SCIENCE AND ENGINEERING



MOLECULAR DYNAMICS STUDIES OF HUMAN DAT  
AND ITS NATURAL LIGAND DOPAMINE

SEDA DEMİRCİ

20091109008

May, 2012



Seda DEMİRÇİ

M.S. Thesis

2012

MOLECULAR DYNAMICS STUDIES OF HUMAN DAT  
AND ITS NATURAL LIGAND DOPAMINE

SEDA DEMİRCİ

B.S, Biology, Çanakkale 18 Mart University, 2009

Submitted to the Graduate School of Kadir Has University  
in partial fulfillment of the requirements for the degree of

Master of Science

in

Computational Biology and Bioinformatics

KADIR HAS UNIVERSITY

May, 2012

KADIR HAS UNIVERSITY  
GRADUATE SCHOOL OF SCIENCE AND ENGINEERING

MOLECULAR DYNAMICS STUDIES OF HUMAN DAT  
AND ITS NATURAL LIGAND DOPAMINE

SEDA DEMİRCİ

APPROVED BY:

Dr. Tuğba Arzu Özal (Kadir Has University) \_\_\_\_\_  
(Thesis Supervisor)

Prof.Dr. Kemal Yelekçi (Kadir Has University) \_\_\_\_\_

Assist.Prof.Dr. İlke Anaç (GYTE) \_\_\_\_\_

APPROVAL DATE: 22/06/2012

# MOLECULAR DYNAMICS STUDIES OF HUMAN DAT AND ITS NATURAL LIGAND DOPAMINE

## **Abstract**

The dopamine transporter (DAT), which is a member of Neurotransmitter sodium symporters (NSSs) family, takes place in dopaminergic neurotransmission. Therefore, it is a major molecular target for numerous drugs, including the widely abused psychostimulants cocaine and amphetamine as well as antidepressants. In this study, to understand the dynamics behavior of structure-function relationship of the human dopamine transporter (DAT) we performed MD studies. The dopamine DAT interactions were investigated via Molecular Dynamics (MD) simulations combined with docking analysis. We have used in this study the 3D structure of human DAT which was determined in a previous homology modeling study based on its bacterial homolog LeuT structure. Throughout our study, we developed DAT model, dopamine model and DAT-dopamine complex model, and performed a series of energy minimization and MD simulations. Comparing the outcomes of the simulation for these three cases, we aim to expose the binding properties and dynamics of DAT and dopamine. Afterwards, to study variations in the binding site affinities during the Molecular Dynamics simulation, we have investigated MD trajectory. Different conformations of DAT model were obtained with clustering analysis. To explore different binding sites and the pathway we performed docking analysis. As a result we determined two binding sites and a translocation pathway for dopamine. The binding modes of dopamine for S1 (primary binding site), S2 (secondary binding site) and S1 to intracellular translocation pathway, were determined through the binding affinities. We observed that there is a remarkable agreement between the identities of the key residues in the translocation mechanism obtained via the simulations with experimental data in the literature.

# İNSAN DAT PROTEİNİN VE DOĞAL LİGANDI DOPAMİNİN MOLEKÜLER DİNAMİK ÇALIŞMASI

## Özet

Nörotransmitter sodyum simporter (NSSs) ailesinin bir üyesi olan dopamin taşıyıcısı (DAT), dopaminerjik nörotransmisyonu gerçekleştirir. Bu nedenle, antidepresanların yanı sıra yaygın olarak istismara neden olan psikostimulanlar kokain ve amfetamin dahil olmak üzere sayısız ilaç için ana moleküler hedefdir. Bu çalışmada, dopamin taşıyıcısı (DAT) ve dopaminin yapı-işlev ilişkisinin dinamik özelliklerini anlamak için Moleküler Dinamik çalışması gerçekleştirildi. Dopamin-DAT etkileşimleri doklama analizleriyle birlikte Moleküler dinamik (MD) simülasyonları ile incelendi. Biz bu çalışmada, daha önceki çalışmada bakteriyel homoloğu LeuT örnek alınarak, homoloji modellemesi ile oluşturulan, insan DAT 3 boyutlu yapısını kullandık. Çalışmamız boyunca, DAT modeli, dopamin modeli ve DAT-dopamin tümleşik modeli geliştirdik ve bir dizi enerji minimizasyonu ve MD simülasyonu uyguladık. Bu üç durumun simülasyon sonuçlarını karşılaştırarak, DAT ve dopaminin bağlanma özelliklerini ve dinamiğini meydana çıkarmayı hedefledik. Daha sonra, Moleküler Dinamik esnasında ki bağlanma bölgelerindeki değişiklikleri ve etkileşimleri incelemek için Moleküler Dinamikten elde edilen zamana bağlı pozisyon datası kullanılmıştır. Kümeleme analizleri ile DAT modelin farklı konformasyonları elde edilmiştir. Farklı bağlanma yerleri ve yollarını keşfetmek için doklama işlemi kullandık. Bunun sonucunda dopamin için iki bağlanma bölgesi ve bir translokasyon yolu belirledik. Dopaminin S1, S2 ve S1 'den hücre içine translokasyon yolundaki bağlanma modları, bağlanma eğilimlerine göre tespit edildi. Literatürdeki simülasyon ve deneysel verilerle elde edilen translokasyon mekanizmasında ki, tanımlanan önemli residüel arasında dikkate değer bir anlaşma olduğunu gözlemledik.

## **Acknowledgements**

I would never have been able to finish my graduate study without the guidance of my advisor and other committee members, support from my family, and help from friends.

First and foremost, I would thank to my dissertation supervisor, Dr. Tuğba Arzu Özal for her courage, patience and assistance during this project. I also thank Assist. Prof. İlke Anaç for her participation in my thesis committee and important comments of my thesis. And special thanks to Prof. Dr. Kemal Yelekçi for his valuable contributions in this thesis and being in my thesis committee. Thank to Gizem Tatar for her contribution of this research at the beginning.

I wish to express thanks to my friends Sibel Çakan, Oya Karatepe, Aslı Yıldırım, Burak Kaan Kızıllan, Ozan Uzun, Gökhan Kuşçu and Çağla Mıdık for their constant support, understanding and motivation. My heartfelt gratitude all of them.

Finally, I would like to thank my parents, Musa Demirci, Dilber Demirci and my brother Abdullah Demirci for their love, patience and encouragement.



*This thesis is dedicated to my mother Dilber and my father Musa for their  
endless love and support.*

## Table of Contents

<b>Abstract</b> .....	i
<b>Özet</b> .....	ii
<b>Acknowledgements</b> .....	iii
<b>Table of Contents</b> .....	v
<b>List of Tables</b> .....	viii
<b>List of Figures</b> .....	xi
<b>List of Abbreviations</b> .....	xxi
<b>Introduction</b> .....	1
1.1 Literature Search .....	4
<b>Theoretical Background for MD Simulations</b> .....	11
2.1. Force Fields .....	11
2.2. Initialization of the System .....	13
2.3. Trajectory Analysis .....	15
2.3.1. Root Mean Square Deviation (RMSD) .....	15
2.3.2. Mean Square Fluctuation (MSF).....	15
2.3.3. Clustering Analysis .....	16
<b>Moleccular Dynamics Simulations</b> .....	17
3.1. Introduction .....	17
3.2. Methodology: Steps of MD Simulation .....	18
3.2.1. Melting of Lipid Tails .....	18
3.2.2. Minimization and Equilibration with Protein Constrained .....	19
3.2.3. Equilibration with Protein Released .....	20
3.2.4. Production Runs .....	21

3.3. Molecular Dynamics (MD) Simulations of Dopamine Transporter .....	21
3.3.1. System Preparation for MD .....	23
3.3.3. Analysis.....	27
3.4. Molecular Dynamics (MD) Simulations of Dopamine.....	42
3.4.1. Creating Topology File for Dopamine.....	42
3.4.2. System Preparation for MD .....	43
3.4.3 Simulation Details and Production MD run.....	46
3.4.4. Analysis.....	47
3.5. Molecular Dynamics (MD) Simulations of DAT-Dopamine Complex.....	53
3.5.1 Molecular Docking of Dopamine Transporter and Dopamine .....	55
3.5.2. System Preparation for MD .....	58
3.5.3 Simulation Details and Production MD run.....	61
3.5.4 Analysis.....	62
<b>Clustering Analysis .....</b>	<b>71</b>
4.1 Clustering Analysis Methodology .....	71
4.2 Clustering Results of MD Trajectory Snapshots.....	72
<b>Docking Analysis .....</b>	<b>81</b>
5.1 Methodology .....	82
5.2 Results and Discussion.....	84
5.2.1 Binding Energies For Different Conformations of DAT Clustered With Respect to Overall Structure .....	84
5.2.2 Binding Site Residues and Interactions in DAT model Subclusters (Radius of 3.0 Å) with Dopamine .....	86
5.2.3 Binding Energies For Different Conformations of DAT Clustered With Respect to Binding Site.....	100
5.2.4 Binding Site Residues and Interactions in DAT model Subclusters (Radius of 1.3 Å) with Dopamine .....	101

5.2.5 The S1 and S2 binding sites and the substrate translocation pathway of DAT .....	112
<b>Conclusion</b> .....	121
<b>REFERENCES</b> .....	127

## List of Tables

<b>Table 3.1.</b> Total number of atoms and water molecules at three simulations. ....	21
<b>Table 3.2.</b> The DAT, cell membrane and system dimensions.....	25
<b>Table 3.3</b> DAT simulation system details. ....	26
<b>Table 3.4.</b> Start and end points of TMHs detected in the experimental studies of human dopamine transporter (DAT).....	33
<b>Table 3.5.</b> Start and end points of transmembrane helices (TMHs) of initial DAT model detected computationally by using VMD program. ....	33
<b>Table 3.6.</b> The positions of the aminoacid sequence of the transmembrane helix regions were detected in the initial DAT model corresponding to experimental studies.....	34
<b>Table 3.7.</b> Start and end points of transmembrane helices (TMHs) of after MD DAT model detected computationally by using VMD program. ....	36
<b>Table 3.8.</b> The positions of amino acid sequence of transmembrane helices obtained in the after MD simulation DAT model corresponding to experimental studies.....	36
<b>Table 3.9.</b> Comparison of the initial and after MD simulation DAT helices structures and RMSD values. ....	41
<b>Table 3.10.</b> The dopamine, cell membrane and system dimensions. ....	45

<b>Table 3.11</b> Dopamine simulation system details.....	47
<b>Table 3.12.</b> The DAT complex structure, cell membrane and system dimensions. ...	60
<b>Table 3.13</b> DAT complex simulation system details.....	61
<b>Table 3.14.</b> The residues in the binding sites pertaining to the before and after MD-simulated DAT-dopamine complexes. Common residues found in these regions are shown in dark. ....	65
<b>Table 4.1</b> Cluster members and best members (BM) resulting from cluster radius of 3.0 Å with overall structural considerations. ....	73
<b>Table 4.2</b> Cluster members and best members (BM) resulting from cluster radius of 1.3 Å when binding-site is taken as reference.....	74
<b>Table 5.1</b> Docking results for DAT model subclusters (radius of 3.0 Å) - dopamine with AutoDock 4.0.....	85
<b>Table 5.2</b> Binding site residues of the DAT model subclusters (radius of 3.0 Å).....	87
<b>Table 5.3</b> Docking results for DAT model subclusters (radius of 1.3 Å) - dopamine with AutoDock 4.0.....	100
<b>Table 5.4</b> Binding site residues of the DAT model subclusters (radius of 1.3 Å)...	102
<b>Table 5.5</b> Comparison of S1 site residues. Same residues found in these regions are shown in dark. ....	115
<b>Table 5.6</b> Comparison of S2 site residues. Same residues found in these regions are shown in dark. ....	116
<b>Table 5.7</b> Docking results for initial DAT model-ligand dopamine with AutoDock 4.0 (result of top 10).....	116

**Table 5.8** Comparison of translocation pathway from the S1 site to the intracellular site residues. Same residues found in these regions are shown in dark. .... 119

## List of Figures

<b>Figure 1.1.</b> Designated three cases in our study, which is first case with the dopamine transporter as ‘DAT’ model, second case with dopamine as ‘dopamine’ model and third model with dopamine transporter-dopamine complex as ‘DAT-dopamine complex’ model.....	2
<b>Figure 1.2.</b> Active sites and translocation pathway of dopamine in DAT which are defined in our study.....	3
<b>Figure 1.3</b> 2D representation of human dopamine transporter. hDAT contains 620 amino acid residues packed onto 12 TMs. N-and C- termini are both in intracellular region [11].....	5
<b>Figure 1.4</b> Secondary structure of LeuT. The leucine transporter forms 12 TMH. The leucine molecule is displayed as a yellow triangle and the two sodium ions are blue circles [11].....	6
<b>Figure 1.5</b> Suggested transport mechanism of dopamine in DAT and effect of Na <sup>+</sup> ions [adapted from 32]. .....	7
<b>Figure 2.1.</b> Interactions included in representative potential energy function for MD simulations [69].....	12
<b>Figure 3.1.</b> Representation of the melting lipid tails, (a) before the melting of lipid tails, (b) after the melting of lipid tails.....	19
<b>Figure 3.2.</b> Achieving a good packing of lipids around the protein, (a) before the third preparation stage, here can be seen the gaps in the membrane- protein interface, (b) an equilibrated system. ....	20



<b>Figure 3.3.1.</b> Initial structural model of human DAT which is represented as cylindrical helices in gray, with two Na <sup>+</sup> ions in cyan.....	22
<b>Figure 3.3.2.</b> The human DAT model in the cell membrane represented as a cyan cartoon and two Na <sup>+</sup> ions represented as a yellow spheres.....	23
<b>Figure 3.3.3</b> The position of the DAT model in a room which is made for DAT in the cell membrane. ....	24
<b>Figure 3.3.4</b> Initial structural model of human DAT in the physiological environment used for MD simulations. DAT protein is represented as cylindrical helices in cyan, water molecules are shown in blue and lipid molecules are indicated as sticks in pink. ....	25
<b>Figure 3.3.5.</b> Left one initial structural model of human DAT which is represented as cartoon in cyan.Right one after molecular dynamics simulation structural model of human DAT which is represented as cartoon in gray. ....	27
<b>Figure 3.3.6.</b> Structural model of human DAT after molecular dynamics which is represented as cartoon in gray and initial structural model of human DAT which is represented as cartoon in cyan, structural alignment. ....	28
<b>Figure 3.3.7.</b> RMSD values which were obtained from 200 ns MD simulations for DAT model. ....	29
<b>Figure 3.3.8.</b> RMSF profile of DAT model. ....	30
<b>Figure 3.3.9.</b> The positions of the most mobile regions on the structure of DAT model.First loop is shown in magenta, second loop is shown in cyan and third loop is illustrated in blue.....	30
<b>Figure 3.3.10.</b> Kinetic, potential and total energy values of DAT model, which is obtained from MD simulations. ....	31

<b>Figure 3.3.11.</b> The human DAT cDNA clone amino acid sequences. Boxed regions indicate 12 TMH domains [91].	32
<b>Figure 3.3.12.</b> Representation of the initial DAT model 12 alpha helices. Cyan represents TMH1a-TMH1b, deep blue TMH2, marine blue TMH3, pink TMH4, magenta TMH5, raspberry TMH6a-TMH6b, orange TMH7, green TMH8, teal TMH9, black TMH10, pale-yellow TMH11, deep-purple TMH12.	35
<b>Figure 3.3.13.</b> Representation of the after MD simulation DAT model 12 alpha helices. Cyan TMH1a-TMH1b, deep blue TMH2, marine blue TMH3, pink TMH4, magenta TMH5, raspberry TMH6a-TMH6b, orange TMH7, green TMH8, teal TMH9, black TMH10, pale-yellow TMH11, deep-purple TMH12.	37
<b>Figure 3.3.14.</b> Root Mean Square Deviation values which were obtained from 200 ns MD simulations for all structure and helix regions.	38
<b>Figure 3.3.15.</b> RMSF about the average position plotted for residues which were obtained from 200 ns MD simulations for all structure and helix regions.	39
<b>Figure 3.3.16.</b> RMSD values which were obtained from 200 ns MD simulations for all helix regions on DAT model.	40
<b>Figure 3.4.1.</b> Molecular model and 3D structure of neurotransmitter dopamine.	42
<b>Figure 3.4.2.</b> The neurotransmitter dopamine in the cell membrane represented as a cyan dots.	44
<b>Figure 3.4.3</b> The position of the Dopamine in the cell membrane.	45
<b>Figure 3.4.4</b> Neurotransmitter dopamine in the physiological environment used for MD simulations. Dopamine molecule is represented as dots in cyan, water molecules are shown in blue and lipid molecules are indicated as sticks in pink.	46

<b>Figure 3.4.5</b> First (left one) and second (right one) snapshots of dopamine in the membrane. Dopamine molecule is represented as dots in purple. ....	48
<b>Figure 3.4.6</b> Third (left one) and fourth (right one) snapshots of dopamine in the membrane. Dopamine molecule is represented as dots in purple. ....	49
<b>Figure 3.4.7</b> Fifth (left one) and sixth (right one) snapshots of dopamine in the membrane. Dopamine molecule is represented as dots in purple. ....	49
<b>Figure 3.4.8</b> Seventh snapshots of dopamine in the membrane. Dopamine molecule is represented as dots in purple. ....	50
<b>Figure 3.4.9</b> The displacement of the dopamine in the 15 ns MD simulations for Dopamine model. ....	51
<b>Figure 3.4.10</b> Movement of dopamine ligand, step by step in the membrane. ....	52
<b>Figure 3.4.11.</b> Kinetic, potential and total energy values of Dopamine model, which is obtained from MD simulations. ....	53
<b>Figure 3.5.1.</b> Structural model of human DAT and dopamine complex. DAT is represented as cylindrical helices in gray, dopamine shown in cyan dots with two Na <sup>+</sup> ions in magenta. ....	54
<b>Figure 3.5.2.</b> Figure above is typical structure of the DAT-dopamine binding complex, snapshottaken from after Autodock. Viewing the dopamine molecule (shown as ball-and-stick) in the complex model. Only helix part of the DAT is shown as cylindrical helices, two Na ions shown as dots in magenta and Cl ions shown as dots in green. Helices 1, 6 and 10 are represented in cyan to indicate the relative position of dopamine in DAT. Figure below one shows that dopamine in the binding site interacts basically with residues of TMH 1,6 and 10. Residues from DAT within 5 Å of dopamine are labeled and shown in stick style, while dopamine is shown in purple stick. ....	57

**Figure 3.5.3.** The human DAT and dopamine complex model in the cell membrane  
 DAT represented as a cyan cartoon, dopamine represented as a blue dots and two  
 $\text{Na}^+$  ions represented as a yellow spheres. .... 58

**Figure 3.5.4** The position of the DAT-dopamine complex model in the cell  
 membrane..... 59

**Figure 3.5.5** Structural model of human DAT and dopamine complex in the  
 physiological environment used for MD simulations. DAT protein is represented as  
 cylindrical helices in cyan, dopamine shown in orange, water molecules are shown in  
 blue and lipid molecules are indicated as sticks in pink. .... 60

**Figure 3.5.6.** Right Figure is after molecular dynamics simulation structural model  
 of human DAT and dopamine complex. DAT is represented as a cylindrical helices  
 in gray, dopamine shown in cyan dots with two  $\text{Na}^+$  ions in magenta. Left Figure is  
 structural alignment of complex structures, after and before molecular dynamics  
 simulation and positions of dopamine. Before md simulation complex structure is  
 represented as cylindrical helices in blue, dopamine shown in red dots, after md  
 simulation complex model is represented as similar as in the right figure. .... 63

**Figure 3.5.7.** Figure above is typical structure of the DAT-dopamine binding  
 complex, snapshottaken from after MD simulation. Viewing the dopamine molecule  
 (shown as ball-and-stick) in the complex model. Only helix part of the DAT is shown  
 as cylindiral helices, two Na ions shown as dots in magenta and Cl ion shown as dots  
 too in green. Helices 1, 8 and 10 are represented in cyan to indicate the relative  
 position of dopamine in DAT. Figure below one shown that dopamine in the binding  
 site interacts basicly with residues of TMH 1, 8 and 10. Residues from DAT within 5  
 Å of dopamine are labeled and shown in stick style, while dopamin is shown in  
 purple stick..... 64

**Figure 3.5.8.** RMSD values which were obtained from 20 ns MD simulations for  
 DAT-dopamine complex model..... 66

<b>Figure 3.5.10</b> RMSD about the average position plotted for $C\alpha$ atoms of residues for MD result.....	67
<b>Figure 3.5.11</b> RMSF about the average position plotted for residues which were obtained from 200 ns MD simulations of only DAT for all structure and 20 ns MD simulations of DAT with dopamine.....	68
<b>Figure 3.5.12</b> Root Mean Square Deviation values which were obtained from 20 ns MD simulations for all helix regions on DAT-dopamine complex model. ....	69
<b>Figure 3.5.13.</b> Kinetic, potential and total energy values of DAT-dopamine complex model, which is obtained from MD simulations.....	70
<b>Figure 4.1</b> Clustering of the simulation according to all structural information using a RMSD threshold of 3.00 Å.....	75
<b>Figure 4.2</b> Clustering of the simulation according to binding site region using a RMSD threshold of 1.3 Å. ....	75
<b>Figure 4.3 cont.</b> The best representative members of the first clustering proces, clusters are aligned on initial structure. Initial structure represented as a cartoon in blue and representative from (a) gray: Cluster1; (b) orange: Cluster2 ; (c) cyan: Cluster3; (d) magenta: Cluster4; (e) yellow: Cluster5; (f) purple: Cluster6; (g) green: Cluster7; (h) brown: Cluster8; (i) red: Cluster9; (j) light pink: Cluster10; (k) dark blue: Cluster11. ....	77
<b>Figure 4.4 cont.</b> The best representative members of the second cluster proces, clusters are aligned on initial structure. Initial structure represented as a cartoon in blue and representative from (a) yellow: Cluster1; (b) pink: Cluster2 ; (c) red: Cluster3; (d) gray: Cluster4; (e) orange: Cluster5; (f) green: Cluster6; (g) purple: Cluster7; (h) cyan: Cluster8. ....	79

<b>Figure 5.1.</b> A snapshot taken from docking studies of DAT (subcluster at1)-dopamine binding complex (a) and 2D representation of the atomic interactions between the DAT and dopamine (b). .....	88
<b>Figure 5.2</b> A snapshot taken from docking studies of the DAT (subcluster at2)-dopamine binding complex (a). 2D representation of the atomic interactions between the DAT and dopamine (b). .....	89
<b>Figure 5.3</b> A snapshot taken from docking studies of the DAT (subcluster at3)-dopamine binding complex (a). 2D representation of the atomic interactions between the DAT and dopamine (b). .....	90
<b>Figure 5.4.</b> A snapshot taken from docking studies of the DAT (subcluster at4)-dopamine binding complex (a). 2D representation of the atomic interactions between the DAT and dopamine (b). .....	91
<b>Figure 5.5.</b> A snapshot taken from docking studies of the DAT (subcluster at5)-dopamine binding complex (a). 2D representation of the atomic interactions between the DAT and dopamine (b). .....	92
<b>Figure 5.6.</b> A snapshot taken from docking studies of the DAT (subcluster at6)-dopamine binding complex (a). 2D representation of the atomic interactions between the DAT and dopamine (b). .....	93
<b>Figure 5.7.</b> A snapshot taken from docking studies of the DAT (subcluster at7)-dopamine binding complex (a). 2D representation of the atomic interactions between the DAT and dopamine (b). .....	94
<b>Figure 5.8.</b> A snapshot taken from docking studies of the DAT (subcluster at8)-dopamine binding complex (a). 2D representation of the atomic interactions between the DAT and dopamine (b). .....	95

<b>Figure 5.9.</b> A snapshot taken from docking studies of the DAT (subcluster at9)-dopamine binding complex (a). 2D representation of the atomic interactions between the DAT and dopamine (b). .....	96
<b>Figure 5.10.</b> A snapshot taken from docking studies of the DAT (subcluster at10)-dopamine binding complex (a). 2D representation of the atomic interactions between the DAT and dopamine (b). .....	97
<b>Figure 5.11.</b> A snapshot taken from docking studies of the DAT (subcluster at11)-dopamine binding complex (a). 2D representation of the atomic interactions between the DAT and dopamine (b). .....	98
<b>Figure 5.12.</b> Autodock different binding site results of dopamine and DAT model subclusters clustering of all simulations according to the overall structure using a RMSD threshold of 3 Å. Viewing the dopamine in the binding pocket. The binding pocket is represented in molecular surface format, colored with cyan. The dopamine molecule shown as dots in green, in the complex model. ....	99
<b>Figure 5.13.</b> DAT (subcluster at1)-dopamine binding complex snapshot which is taken from docking studies (a). 2D representation of the atomic interactions between the DAT and dopamine (b). .....	103
<b>Figure 5.14.</b> DAT (subcluster at2)-dopamine binding complex snapshot which is taken from docking studies (a). 2D representation of the atomic interactions between the DAT and dopamine (b). .....	104
<b>Figure 5.15.</b> DAT (subcluster at3)-dopamine binding complex snapshot which is taken from docking studies (a). 2D representation of the atomic interactions between the DAT and dopamine (b). .....	105
<b>Figure 5.16.</b> DAT (subcluster at4)-dopamine binding complex snapshot which is taken from docking studies (a). 2D representation of the atomic interactions between the DAT and dopamine (b). .....	106

**Figure 5.17.** DAT (subcluster at5)-dopamine binding complex snapshot which is taken from docking studies (a). 2D representation of the atomic interactions between the DAT and dopamine (b). ..... 107

**Figure 5.18.** DAT (subcluster at6)-dopamine binding complex snapshot which is taken from docking studies (a). 2D representation of the atomic interactions between the DAT and dopamine (b). ..... 108

**Figure 5.19.** DAT (subcluster at7)-dopamine binding complex snapshot which is taken from docking studies (a). 2D representation of the atomic interactions between the DAT and dopamine (b). ..... 109

**Figure 5.20.** DAT (subcluster at8)-dopamine binding complex snapshot which is taken from docking studies (a). 2D representation of the atomic interactions between the DAT and dopamine (b). ..... 110

**Figure 5.21.** Autodock different binding site results of dopamine and DAT model subclusters. Clustering was performed based on the binding site regions using a RMSD threshold of 1.3 Å for all simulations. Dopamine is shown in the binding pocket as dots in green, while the binding pocket is represented as molecular surface format, colored with blue. .... 111

**Figure 5.22** Different binding site results of dopamine and DAT model subclusters clustering of all simulations according to the overall structure using a RMSD threshold of 3 Å. DAT is shown as helices in transparent gray. Positions of dopamine in different subclusters representat as dots which is; subcluster 1 in red, subcluster 2 in green,subcluster 3 in blue, subcluster 4 in yellow, subcluster 5 in magenta, subcluster 6 in cyan,subcluster 7 in orange, subcluster 8 in gray,subcluster 9 in brown, subcluster 10 in limon and subcluster 11 in dirty violet. .... 113

**Figure 5.23** Different binding site results of dopamine and DAT model subclusters clustering of all simulations according to the binding site regions using a RMSD threshold of 1.3 Å. DAT is shown as helices in transparent pink. Positions of dopamine in different subclusters representat as dots which is; subcluster 1 in red,



subcluster 2 in green, subcluster 3 in blue, subcluster 4 in yellow, subcluster 5 in magenta, subcluster 6 in cyan, subcluster 7 in orange and subcluster 8 in gray..... 114

**Figure 5.24** Autodock binding site result of dopamine and initial DAT model. The binding pocket is represented in molecular surface format, colored with cyan. The dopamine molecule shown as dots in blue, in the complex model. .... 117

**Figure 5.25** The substrate binding sites of DAT. S1 site is represented as spheres, colored with red and S2 site is represented as spheres too and colored with cyan. The TMHs 1, 3, 6, 8 and 10 which are interacting with S1 and S2, are shown as a cylindrical helices in gray. .... 118

**Figure 5.26** Different binding site results of dopamine and DAT model subclusters which are obtained from; clustering of all simulations according to the binding site regions using a RMSD threshold of 3 Å (left one) and clustering of all simulations according to the binding site regions using a RMSD threshold of 1.3 Å (right one). DAT is shown as helices in transparent gray (cluster 3) and pink (cluster 1.3). Positions of dopamine in different subclusters are labeled and represented as dots which is; S1 in red, S2 in cyan, the substrate translocation pathway from the S1 site to the intracellular site in green and finally purple is untitled..... 119

**Figure 5.27** Active sites and translocation pathway of dopamine in DAT which are defined in our study. Positions of dopamine through the simulation are labeled and represented as spheres which is; S1 in red, S2 in cyan, the substrate translocation pathway from the S1 site to the intracellular site in green. .... 120

## List of Abbreviations

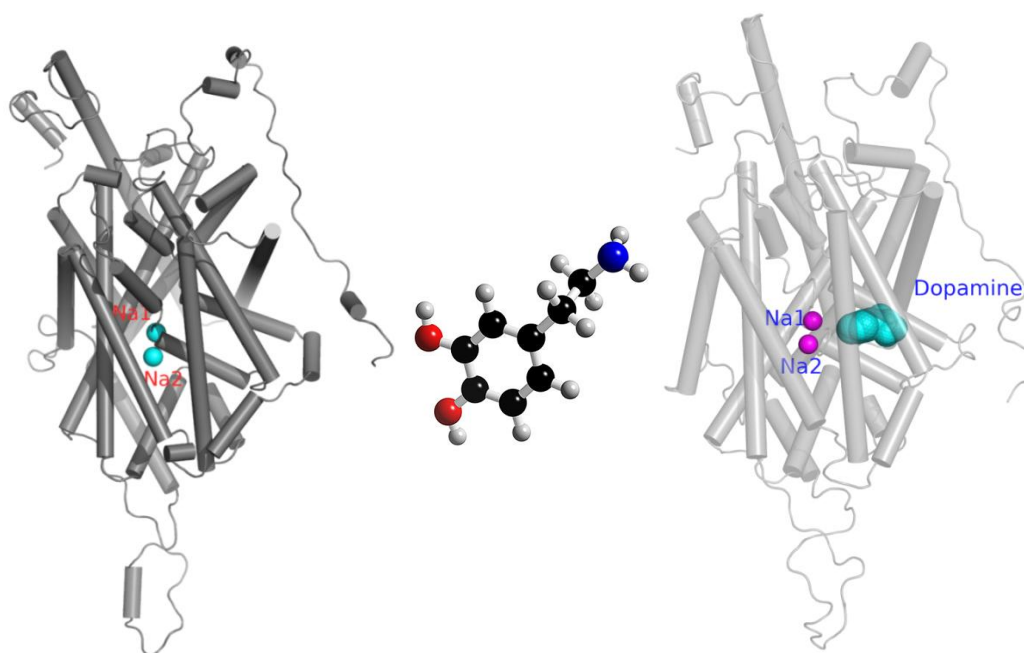
DAT	Dopamine Transporter
SERT	Serotonin
NET	Norepinephrine
GAT	Gama-aminobutyric acid
HEK	Human embryonic kidney cells
LeuT	Leucine Transporter
NSS	Neurotransmitter sodium symporters
BM	Best Members
S1	Primary binding site
S2	Secondary binding site
TMH	Transmembrane helices
POPC	Palmitoyloleoyl phosphatidylcholine
VMD	Visual Molecular Dynamics
NAMD	Nanoscale Molecular Dynamics
PDB	Protein Data Bank
RMSD	Root Mean Square Deviation
RMSF	Root Mean Square Fluctuation
MD	Molecular Dynamics

## **Chapter 1**

### **Introduction**

In this thesis, firstly the structure-function relationship of the human dopamine transporter (DAT) and the dopamine is addressed via Molecular Dynamics (MD) simulations. Throughout the study, we developed three cases. The first case is the dopamine transporter as a ‘DAT’ model, the second is the ‘dopamine’ model and the third is the ‘DAT-dopamine complex’ model. Comparing the outcomes of the simulation for these three cases, we wanted to reveal the binding properties and dynamics of DAT and dopamine. Afterwards, for study the dopamine translocation mechanism, we used different conformations of DAT model which are obtained from clustering analysis as explained in the next chapter. To explore the pathway and different binding sites, we have performed binding analysis. DAT and dopamine for the binding analysis we used a docking software, AutoDock 4.0. The dopamine-binding modes were determined through the calculation of binding free energies. We observed that there is a striking accordance between the identities of the key residues in the transport mechanism. Our results were in a good agreement with the experimental datas in the literature.

In Chapter 2, we give the basic theory of Molecular Dynamics and mention the how it is applied. There we give a brief explanation of Force Field interactions and how it initializes the system in MD. Furthermore, we introduce the algorithms used for these process. And than trajectory analysis is explained, briefly, which are RMSD, RMSF and Clustering.

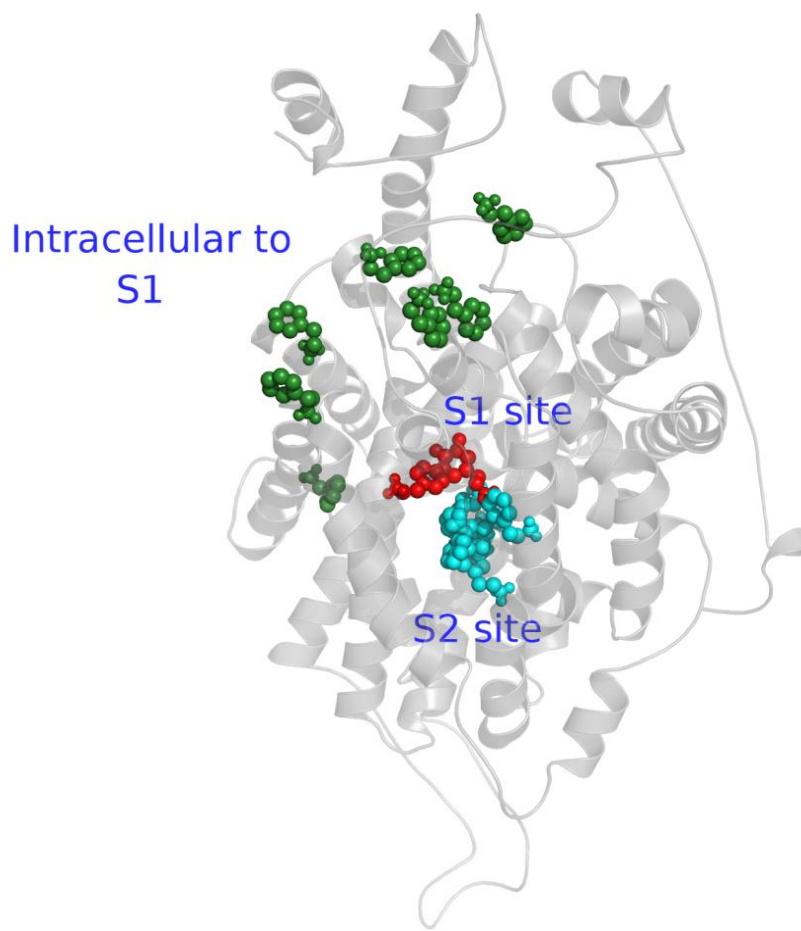


**Figure 1.1.** Designated three cases in our study, which is first case with the dopamine transporter as ‘DAT’ model, second case with dopamine as ‘dopamine’ model and third model with dopamine transporter-dopamine complex as ‘DAT-dopamine complex’ model.

In Chapter 3, we introduce the methods that we used to perform MD simulations in the membrane for our three cases which are “DAT” model, “dopamine” model and “DAT-dopamine complex” model, shown in Figure 1.1.

In the Chapter 4, we introduce the process of clustering which is performed on “DAT” model long MD simulation result. As a result of this process, we obtained 19 different conformations of DAT.

Chapter 5 and Chapter 6 encompass the basic theory of molecular docking and interaction of protein- ligand which have two main categories scoring function and docking algorithm, and methods of AutoDock 4.0.



**Figure 1.2.** Active sites and translocation pathway of dopamine in DAT which are defined in our study.

Finally, in Chapter 7 by using Autodock 4.0 program, DAT's natural ligand dopamine docked with DAT model at different conformations which are obtained from clustering process. Then we analyzed the different binding sites and translocation pathway of dopamine on DAT shown in Figure 1.2.

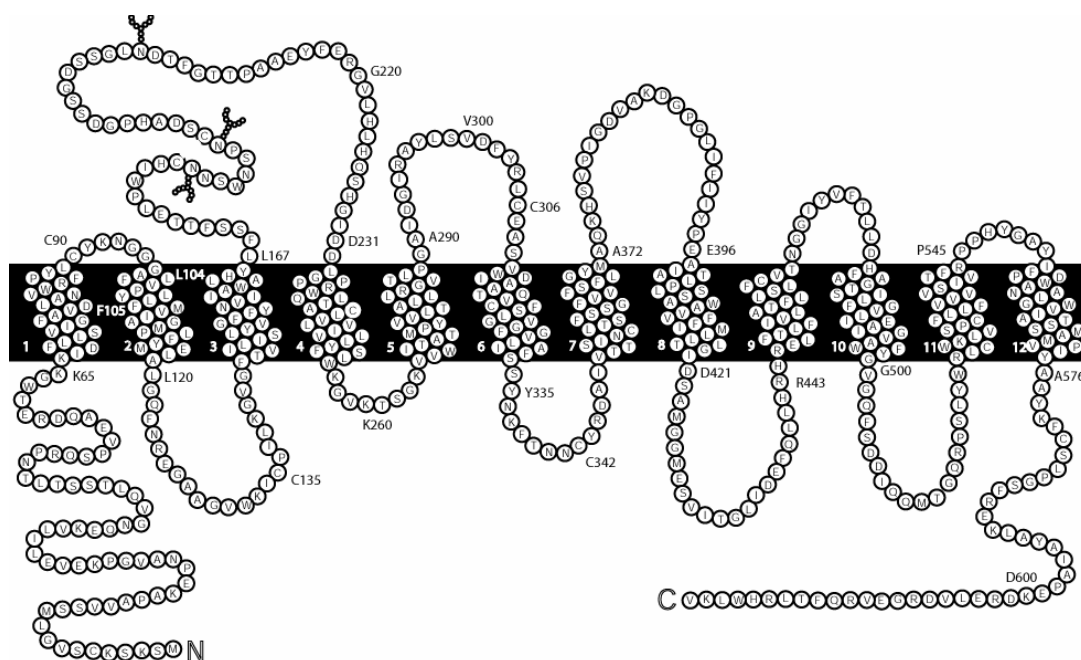
## 1.1 Literature Search

Cell membranes do not allow across extracellular water-soluble ligands to inside of the cell [1,2]. Critical ligands and ions across the membrane within the specialized molecules which are developed by cells catalyze the transportation. A class of these molecules is known as transmembrane spanning proteins which helps external solutes to across the membrane .

Membrane proteins are responsible for vital physiological activities, and they comprise one third of all proteins encoded by eukaryotic genome and occupy approximately 50 % of the volume of all biological membranes [3,4]. The human dopamine transporter (hDAT) exhibits the general properties of membrane proteins [5]. Transmembrane proteins are amphiphilic proteins and their structure is defined by the interaction of the hydrophobic lipid bilayer with the polar peptide bonds. These proteins form secondary structures, in order to adapt to the hydrophobic environment. The majority of membrane proteins, including the dopamine transporter, form  $\alpha$ -helical structures with hydrogen bonds between carbonyl and amide groups [6,7].

Despite the importance and abundance of transmembrane proteins, few have been structurally determined because they are very difficult to study due their low expression levels and solubilization challenges [8,9].

As mentioned before, the dopamine transporter (DAT) shares properties of membrane proteins and it is situated on the presynaptic membrane of dopaminergic neurons [10]. Its 620 amino acids are organized into 12 transmembrane domains with N- and C-terminals situated intracellularly represented in Figure 1.3. In most integral proteins, the disulfide bond between C180 and C189 in extracellular loop 2 facilitates the secondary structure of the transporter [10].



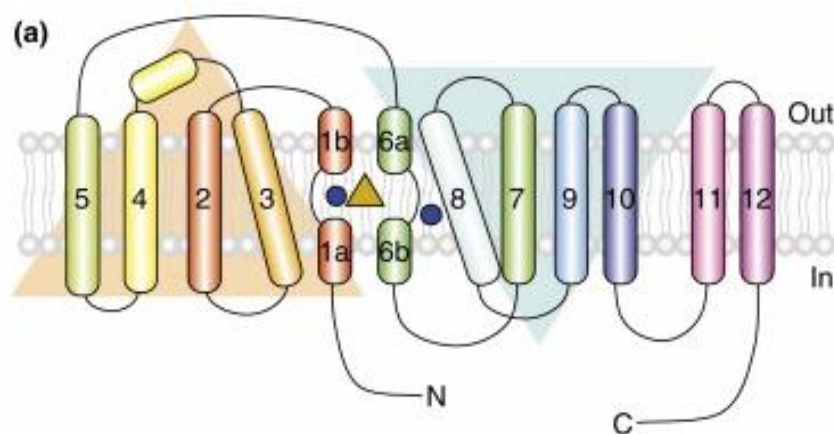
**Figure 1.3** 2D representation of human dopamine transporter. hDAT contains 620 amino acid residues packed onto 12 TMs. N- and C- termini are both in intracellular region [11].

Neurotransmitter sodium symporters (NSS) terminate synaptic transmission and recycle neurotransmitters for reuse in the nervous system and the human dopamine transporter belongs to this family [12-14]. NSSs family is also called the *sodium- and chloride-dependent neurotransmitter transporter family* (SLC6) according to the Human Genome Organization nomenclature [15]. The mentioned proteins serve as secondary active transporters by using the  $\text{Na}^+$  gradient through plasma membrane of presynaptic neuron. This action accelerates the re-ingestion and ingestion of several neurotransmitters from extracellular cytoplasm as opposed to their concentration gradient regarding a symport mechanism. [8,16]. Neurotransmitter sodium symporters are placed in the plasma membranes of neuronal/astroglial cells and the uptake of neurotransmitters is one of the mechanisms that ends neurotransmission [17].

Biogenic amines and its transporters, such as, dopamine (DAT),  $\gamma$ -aminobutyric acid (GAT), norepinephrine (NET), glycine and serotonin (SERT) transporters belong to NSS family [18-19]. First studies to understand the NSS structure *Aquifex aeolicus'* leucine transporter (LeuTAA), a member of NSS family, crystal structure was used

[20]. The sequence identities between prokaryotic LeuT and eukaryotic is low level identity; DAT (20%), SERT (21%), and NET (24%), respectively [21]. Despite this overall low sequence homology, a few regions are greatly preserved throughout the family. Therefore, the crystal structure of LeuT has the relevant information available regarding the NSS family structure [21-23]. The conservation of TMH 3, 8, 6, and 1, which form the ligand binding site in leucine transporter, suggests that they are involved in substrate transport and are essential for function [20].

The LeuT consists of 12 transmembrane domains that are organized in such way that the leucine (the substrate) binding pocket of the transporter is formed by pseudo-twofold packing of TM1-TM5 and TM6-TM10 superimposed domains shown in Figure 1.4 and these TMs are in direct contact with the sodium ions. When correlated the molecular structure of LeuT and other  $\text{Na}^+/\text{Cl}^-$  dependent transporters, is determined TM1 and TM6 are placed near the leucine binding site play a vital role in the substrate binding of DAT, NET, and SERT as well, and additionally, TM3 and TM8 are participating in the substrate and  $\text{Na}^+$  ion binding [20]. Like all NSS family members, the molecular structure of human DAT shares similarities with the structure of leucine transporter and contains 12 TMH attached by extracellular and intracellular loops.

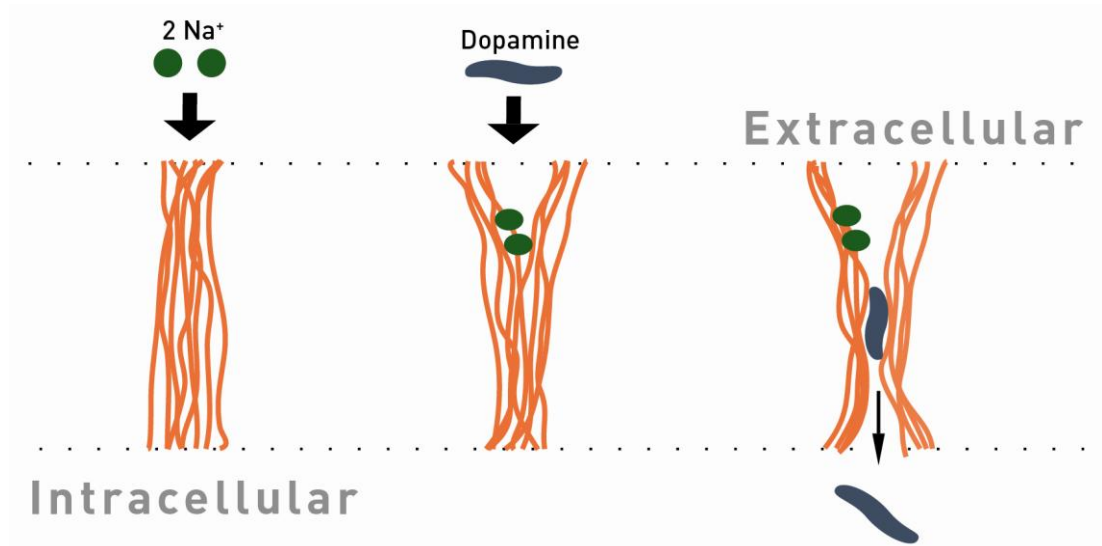


**Figure 1.4** Secondary structure of LeuT. The leucine transporter forms 12 TMH. The leucine molecule is displayed as a yellow triangle and the two sodium ions are blue circles [11].



The focus of my thesis is on human dopamine transporter (hDAT) and its function. Its function is simply re-uptake of dopamine which helps regulate the concentration and duration of dopaminergic transmission [24,25]. All of in NSS family members, DAT is of particular interest because it is targets for the action of legion drugs, incorporating the extensively abused psychostimulants amphetamine and cocaine, as well as for antidepressant drugs [1,26]. A particularly well-studied biogenic amine is dopamine (a catecholamine intermediate in the biosynthesis of epinephrine and norepinephrine), whose receptors are important targets for especially curing schizophrenia and Parkinson's diseases [27,28]. Hence, dopaminergic neurotransmission is very important for mediating lots physiologic treats incorporating reward-seeking behavior, addiction, lactation and movement [29,30].

Figure 1.5 shows the neurotransmission in the dopamine synapse, simply. The dopamine molecules bind to the dopamine receptors of the postsynaptic membrane, leading to the further propagation of the signal and cellular response.



**Figure 1.5** Suggested transport mechanism of dopamine in DAT and effect of  $Na^+$  ions [adapted from 32].

The reuptake mechanism of dopamine is dependent co-transport of  $Na^+$  and  $Cl^-$ , and follows a sequence of events where one dopamine molecule or two sodium ions

initially bind to the DAT, followed by binding of one chloride ion to the transporter [32]. The inwardly directed  $Na^+$  slope supplies energy for an inward repositioning of dopamine molecule against a density slope [33]. For the replacement of dopamine  $Na^+$  is needed by the transporter and it has been considered that, when the dopamine recognizes the dopamine transporter and interacts with it, it means that uptake cycle is starting [34]. However, the role of  $Na^+$  in this initial identification stage is under debate [35].

According to recent studies, co-transportation of two  $Na^+$  ions and one  $Cl^-$  ion with a dopamine molecule is simpler than the interaction of these ions with the transporter of dopamine [33,35-39].  $Na^+$ -dependent dopamine molecule uptake kinetic analysis by human embryonic kidney cells (HEK) indicating the human DAT propose a sequential binding order of dopamine molecule and  $Na^+$  with  $Na^+$  binding a head of dopamine [36,37]. Electrophysiological reckonings on oocytes expressing the human dopamine transporter indicate obstructe of transporter-mediated leak streams by dopamine molecule in the conclude non-attendance of  $Na^+$ . Although the later examination negates an accurate requisite for  $Na^+$  in dopamine binding, a stimulatory character for  $Na^+$  is still a chance [35].

Investigation of the structural needs for the interaction of substances with DAT have been carried out in different study and it has been performed with the help of observing the phenylethylamine derivatives which passes through the preparations. According to studies mentioned, a phenyl ring bearing a ethylamine side chain is required for optimum activity of dopamine transporter and it has been seen that transportation of  $\beta$  rotamer of the full scale configuration of catecholamines favorably occurs. It has been suggested that the recognition of substrate has been carried out via reconciliation of catechol when the structural alteration of the transporter has been enabled by the amine side chain, thus the transportation of dopamine through the membrane takes place [40].

As mentioned above DAT's structure-function affiliations have been experimentally studied commonly, using both deletion mutagenesis and cross-linking, in addition site-directed, engineering of metal binding sites, and replaced cysteine accessibility

ways [41-48]. However, dopamine transporter dynamics transport mechanism details, is still not very clear.

Dopamine transporter in Human has a bacterial homolog which is LeuT. Recently crystallized structure of LeuT, provides insight into the three dimensional structure of dopamine transporter [49-54]. Although previous studies about LeuT support the significant structural data of DAT, they do not give any important information about the transportation mechanism.

The substrate is at the center of the protein in the initial LeuT structure. To better understanding the mechanism of LeuT and other NSS transporters, several ways have been suggested in spite of the abundance of the current studies of LeuT and other transporters which provides necessary structural information [55]. For instance, Gouaux et al. have suggested that there are two other conformations which are outward-facing and inward-facing [54] and this procedure is consistent with the previous studies of transporters [56]. Structural modeling studies carried out by experimentalists reveals the symmetry properties of NSS family [57,58]. The functional mechanisms of the proteins which resemble to LeuT according to their structures have been investigated by computational simulations with utilizing high resolution structural data (eg., see [59-67]). Although cooperation of experimental and computational studies is not complete yet, it proposes that functional mechanisms of the human neurotransmitter transporters in NSS family is not as simple as expected in the transition between inward-facing and outward-facing form [68].

On the other hand, Jufang et al. have performed the flux and binding experiments and have suggested that the substrate which fills the S1 and S2 site and in the extracellular S2 site also serves as a “symport effector” by initiating the release of  $Na^+$  into the cell [55].

With combining all computational and experimental studies explained in this part, it has been concluded that former MD simulations helps revealing the information about the structural elements which are essential for binding state of substrate and DAT occluded state formation but there are still doubts about the role of LeuT-like

S2 binding site and whether S2-bound substrate plays also role in adjusting DAT function like in Leut case or not.

## Chapter 2

### Theoretical Background for MD Simulations

MD simulation is one of the main tools in the theoretical study of dynamics behavior of biological macromolecules. By this computational technique, the time dependent behavior of a biomolecular system is calculated. Atoms may interact with each other by using empirical potential energy functions or force fields and forces acting on atoms are calculated for a given configuration based on these functions or fields. With the help of the integration of Newton's equation of motion (shown below), a successive configuration of the system along the time trajectory is obtained.

$$\frac{d^2 R_i}{dt^2} = \frac{F_i}{m_i} \quad (2.1)$$

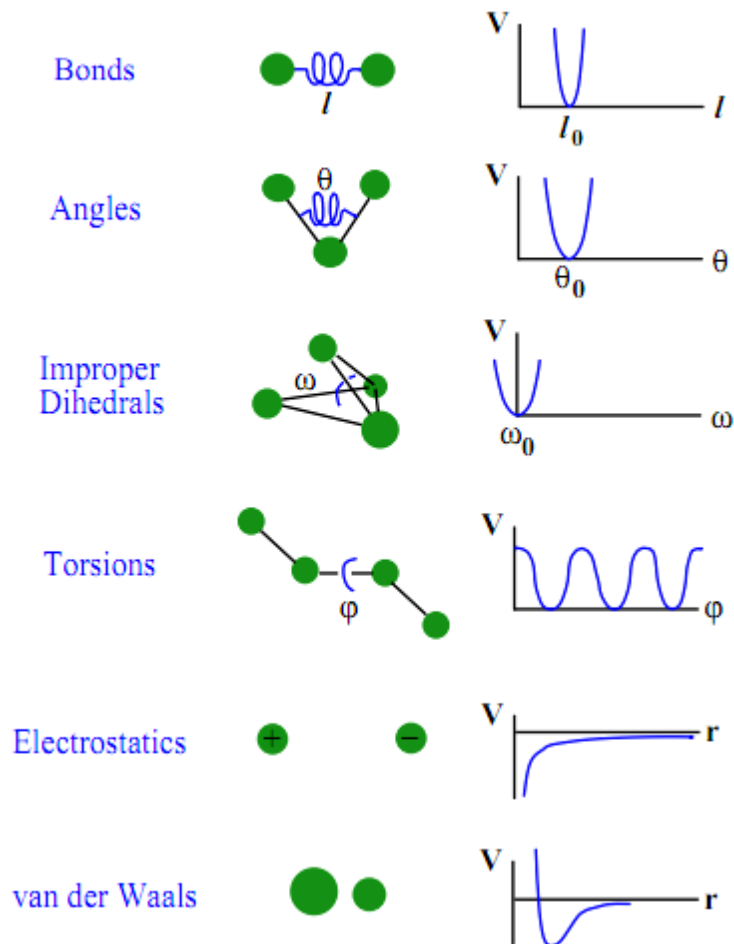
Here,  $R_i$  represents the position of particle  $i$ , and  $F_i$  is the total force acting on particle  $i$  exerted by all other molecules, and  $m_i$  its the molecular mass.

#### 2.1. Force Fields

To describe the association of chemical structure to energy, mathematical equations are applied in theoretical chemistry. The potential energy of a system is described by force fields as a function of the atomic positions/coordinates. As shown in Figure 2.1, Molecular Dynamic simulations are modelled on empirical model of interactions within a system that involves stretching of bonds, bending and also non-bonded interactions,

$$\begin{aligned}
V(R_1, \dots, R_N) = & \sum_{\text{bonds}} \frac{k_{li}}{2} (l_{li} - l_{i,0})^2 + && \text{"Bond Stretching"} \\
& \sum_{\text{angles}} \frac{k_{\theta i}}{2} (\theta_i - \theta_{i,0})^2 + && \text{"Angle Bending"} \quad (2.2) \\
& \sum_{\text{torsions}} \frac{V_n}{2} (1 + \cos(n\phi_i - \delta_i)) + && \text{"Bond Rotation (torsion)"} \\
& \sum_{i=1}^N \sum_{j=i+1}^N \left( 4\epsilon_{ij} \left[ \left( \frac{\sigma_{ij}}{r_{ij}} \right)^{12} - \left( \frac{\sigma_{ij}}{r_{ij}} \right)^6 \right] + \frac{q_i q_j}{4\pi\epsilon_0 r_{ij}} \right) && \text{"Nonbonded interactions"}
\end{aligned}$$

## Empirical Potential Energy Function



**Figure 2.1.** Interactions included in representative potential energy function for MD simulations [69].

In the equation above,  $V(R_1, \dots, R_N)$  represent the potential energy and this is a function of the coordinates ( $R_i$ ) of  $N$  atoms or particles. In the equation the first term represents the interaction of pairs of bonded atoms and  $l_i$  is the bond length. The second term is based on Hooke's Law and it is the sum of the angles in the molecule which is modeled as a harmonic potential, where  $\theta_i$  and  $\theta_{i,0}$  are the instantaneous and the equilibrium angle of the bond, respectively. In the equation, the third term describes the torsional potential and the fourth equation represents the non--bonded interactions which are represented by two different potentials. The first one is the Lennard-Jones 12-6 potential function that accounts van der Waals interactions, while the second one is the Coulomb potential for electrostatic interactions [70,71].

## 2.2. Initialization of the System

To perform an MD simulation, it is necessary to designate a preliminary configuration of the system by specifying  $3N$  atomic coordinates ( $R_i$ ) at time = 0. The preliminary configuration can be produced by using empirical data such as X-ray crystal structure. The preliminary velocities can be determined in accordance with the Maxwell-Boltzmann distribution at the initial temperature after the preliminary configuration of the system is minimized in a solvent box or cell membrane [70]. After the setting up of the system, the potential energy is calculated by the following equation;

$$F_i = -\nabla U_i(R_1, \dots, R_N) = \frac{\partial U(R_1, \dots, R_N)}{\partial R_i} \quad (2.3)$$

After the calculation of the force by potential energy function on each atom at time  $t$ , the next step is to generate the new conformation at time  $t + \Delta t$  according to the Equation (2.1). There are various numerical algorithms to perform the integration of Equation 2.1. One of the most commonly used algorithms in MD simulations is Verlet algorithm [4]. Verlet algorithm works by the addition and subtraction of the Taylor series expansions for the time dependence of the coordinates  $R_i$  at times  $t - \Delta t$  and  $t + \Delta t$ .

$$R_i(t + \Delta t) = R_i(t) + V_i(t)\Delta t + \frac{1}{2}a_i(t)\Delta t^2 + \dots \quad (2.4)$$

$$R_i(t - \Delta t) = R_i(t) - V_i(t)\Delta t + \frac{1}{2}a_i(t)\Delta t^2 + \dots \quad (2.5)$$

Adding these equations together and combining with Equation (2.1) produces:

$$R_i(t + \Delta t) \approx -R_i(t - \Delta t) + 2R_i(t) + \Delta t^2 a_i(t) \quad (2.6)$$

The velocities can be accounted by the difference of the locations at  $t - \Delta t$  and  $t + \Delta t$  :

$$V_i(t) \approx \frac{1}{2\Delta t} [R_i(t + \Delta t) - R_i(t - \Delta t)] \quad (2.7)$$

A bit different versions of the Verlet algorithm have been offered to raise the accuracy in calculation of positions and velocities like Leap-frog algorithm [73] and the velocity Verlet method [74]. The velocity Verlet method, accelerations velocities, and positions, at time  $t + \Delta t$  are taken from the same quantities at time  $t$ . Furthermore, this method does not involve precision [70,71].

$$R_i(t + \Delta t) = R_i(t) + V_i(t)\Delta t + \frac{1}{2}a_i(t)\Delta t^2 \quad (2.8)$$

$$V_i(t + \Delta t) = V_i(t) + \frac{1}{2}\Delta t[a_i(t) + a_i(t + \Delta t)] \quad (2.9)$$

The algorithm is carried out as a three-stage procedure because as can be seen from Equation (2.8), the accelerations at  $t$  and  $t + \Delta t$  should calculate new velocities. First, positions at  $t + \Delta t$  are calculated in accordance with Equation (2.7) and the velocities at time  $t + \Delta t/2$  are assessed by the following equation:

$$V_i\left(t + \frac{\Delta t}{2}\right) = V_i(t) + \frac{1}{2}\Delta t a_i(t) \quad (2.10)$$

Then, forces are calculated from the current positions to obtain the acceleration,  $a(t + \Delta t)$ . In the final step, the velocities at time  $t + \Delta t$  are computed by:



$$V_i(t + \Delta t) = V_i\left(t + \frac{1}{2}\Delta t\right) + \frac{1}{2}\Delta t a_i(t + \Delta t) \quad (2.11)$$

## 2.3. Trajectory Analysis

### 2.3.1. Root Mean Square Deviation (RMSD)

RMSD is the square root of the summation of the squares of the distances between corresponding atoms of x and y (Equation 2.12). RMSD is a measure of average atomic displacement between two conformations. In terms of formule, given N atom positions from structure x and the corresponding N atoms from structure y; the RMSD is defined as:

$$rmsd = \frac{\sqrt{\sum_{i=1}^N (d_i^2)}}{N} \quad (2.12)$$

### 2.3.2. Mean Square Fluctuation (MSF)

The mean square fluctuation (MSF) is a measure of the variation of the position of the atoms from the average structure. MSF is based on the mobility of structure [71]. It is determined by the following equation:

$$MSF = \langle (R_i(t) - \langle R_i \rangle)^T (R_i(t) - \langle R_i \rangle) \rangle \quad (2.13)$$

Where  $\langle R_i \rangle$  is the vector of time average of the cartesian coordinates of the C $\alpha$  atom of the  $i^{th}$  residue, and is the vector of the cartesian coordinates of the C $\alpha$  atom of the same residue at time t. The square root of MSF is Root Mean Square Fluctuation (RMSF) [71].

### 2.3.3. Clustering Analysis

With the help of MD simulations, large number of conformations is produced. *k*-means clustering method that is part of the kclust module of Multiscale Modeling Tools for Structural Biology (MMTSB) Tool Set [75] is used to reduce the conformational space and identify a few distinct clusters or conformational states that are generated during the simulation. For every cluster, there is a centroid or an average structure of all the constituents in the cluster. Frames are designated to clusters based on their RMSD value with regard to the centroids of the clusters. *k*-means clustering seeks to minimize the within cluster summation of squares of distances of each element from the centroid. This process is repeated until all the frames are designated to a cluster. After each iteration step, the centroids and the clusters are updated. Lastly, the conformation -which is closest to the centroid- is opted as the representative snapshot of that cluster [71].

## Chapter 3

### Molecullar Dynamics Simulations

#### 3.1. Introduction

Membrane proteins are important in many biological aspects. Membrane proteins which are thought to constitute approximately 30% of genomes are the targets of more than half of all drugs [76,77]. High resolution crystal structures of membrane proteins is less than 1% of the total number of structures, because the crystallization and expression problems. Eliciting of protein structures and variations of this structures are very important for the drug design.

Most of membrane proteins change their conformations a lot during completing their function. Experimentally, crystallography is not able to catch all these conformational changes. On the other hand, by computational means it is possible to observe the dynamics time variable behavior. Therefore, *in silico* methods are used in this thesis work. MD is one of the powerful computational tools that, additionally provides information with respect to the stability of a membrane protein, can also yield insight into the dynamic behavior in which these distinct states [78]. To investigating trial hypotheses in idealised systems in which one can discover fundamental biophysical principals governing a process can be obtained by MD simulations and also it represents *in vivo* systems as closely as possible [78,79].

In this thesis, the structure-function relationship of the human DAT and the dopamine is addressed via MD simulations. Throughout the studies, we designated three cases, first case with the dopamine transporter as DAT model, second case with dopamine as dopamine model and third model with dopamine transporter-dopamine complex as DAT-dopamine complex model. Comparing the outcomes of the

simulation for these three cases, we wanted to reveal the binding properties and dynamics of DAT and dopamine.

### **3.2. Methodology: Steps of MD Simulation**

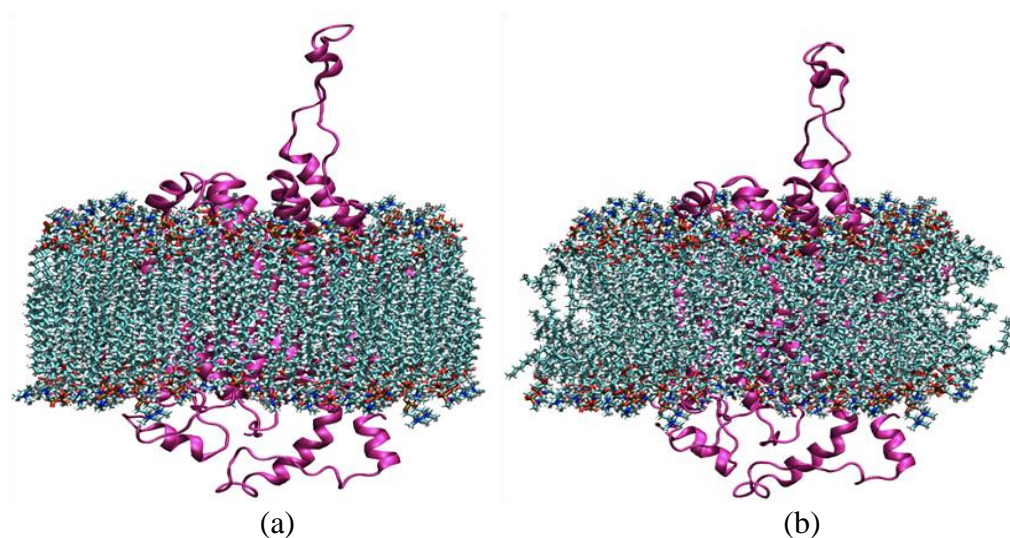
The system preparation of an MD simulation consists of five stages: obtaining a pre-equilibrated lipid bilayer, alignment of protein in the lipid bilayer, removal of overlapping lipid molecules, equilibration of new system and production. Furthermore, during the run of MD simulation there are two main stages, equilibrium and production.

As stated in the common methodology, determination of simulation time depends on the enough equilibration of the system. In this work, before the equilibration, a pre-equilibration is applied. The alignment of the pre-equilibrated lipid bilayer with the protein is performed artificially. Protein is embedded in pre-equilibrated lipid bilayer and overlapping lipids eliminated. The resulting system that have a vacuum in between the lipid molecule and the protein provide an elimination of whole overlapping lipid molecules. Lipid molecules relax around the protein during the first stage of the equilibration. Following these, water molecules which are required as the system features, are added to the system and the system is ionized for neutralization. After this stage, the system is ready for MD and it is exposed to energy minimization and production runs upto number of steps depending on the system properties. The simulation protocols were performed as explained below in four different MD simulation steps.

#### **3.2.1. Melting of Lipid Tails**

Lipid molecules are the basic components of the biomembranes. They have large number of structural forms. The most abundant lipids are the glycerophospholipids (or phosphoglycerides) [80]. Melting of the lipid hydrocarbon ends is the initial protocol of MD simulations. The lipid bilayer was generated using the membrane builder plugin available in the Visual Molecular Dynamics (VMD) software and comprise of a bilayer of palmitoyloleoyl phosphatidylcholine (POPC) residues. This

first stage melting refers to a process that gives the cell membrane a fluid-like bilayer. VMD is made of lipid molecules unrealistically smooth shown in Figure 3.1 (a). For this reason, in this stage of simulation everything (lipid headgroups, ions, water, protein) is fixed except the lipid tails, lipids allowed to move freely. The system was run 1000 steps of minimization under these conditions, then velocities were reset according to the desired temperature, and then it was run for 0.5 ns (using a 2 fs timestep). After these procedures, the structure of lipid molecules have gained a more realistic liquid form shown in Figure 3.1 (b).



**Figure 3.1.** Representation of the melting lipid tails, (a) before the melting of lipid tails, (b) after the melting of lipid tails.

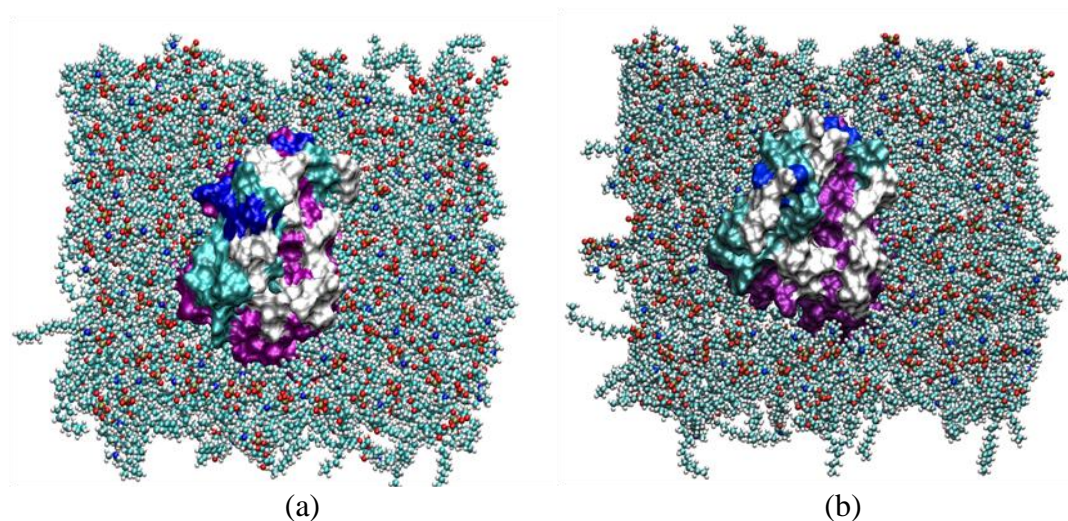
### 3.2.2. Minimization and Equilibration with Protein Constrained

The system is still not ready for running dynamics. Because of many unnatural atomistic positions MD be can safely run. Minimization will be then followed by an equilibration with the protein constrained, so as to permit the cell membrane and water molecules to relax first. The system under these conditions Nanoscale Molecular Dynamics (NAMD) was run 10000 steps of minimization and then it was run dynamics for 0.5 ns (using a 2 fs timestep). During the equilibration, some forces are applied on water molecules, which are the close enough to get into the cell

membrane, in order to prevent hydration of the membrane-protein interface. At this stage, the system reaches the local minimum faster with the protein constrained.

### 3.2.3. Equilibration with Protein Released

Following the earlier stage, where lipids are well packed around the protein, while water has not entered forbidden regions, the harmonic constraints are released and further the whole system is equilibrated. In third preparation step, a little shrink has occurred at the surface area of xy plane of the cell membrane shown in Figure 3.2. The lipid molecules, which tend to get closer to the protein is caused the reduction in volume. The decrease in volume in x-y directions is compensated by an increase in volume in the z direction, so that the system could keep its initial volume and pressure of 1 atm. The system under these conditions is exposed to MD simulation of 0.5 ns (using a 2 fs timestep).



**Figure 3.2.** Achieving a good packing of lipids around the protein, (a) before the third preparation stage, here can be seen the gaps in the membrane- protein interface, (b) an equilibrated system.

### 3.2.4. Production Runs

After a detailed preparation stage consisting of melting of lipid tails and relaxation of water and lipids, we have a more equilibrated solvated system containing the protein of interest, and we started a production simulation. A series of energy minimization and MD simulations of 200 ns for the DAT model, 15 ns for the dopamine model and 20 ns for the DAT-dopamine complex model have been performed by using NAMD 2.7 software package. NAMD is a parallelized MD program which is designed to run on multiple cores [81], and therefore we have performed our runs in parallel. For the interaction potentials, CHARMM22 force field for protein and CHARMM27 force field for lipids was used. TIP3W model was used for all water molecules. All of the simulations have been performed at 310K within phosphatidylglycerol membrane (POPC). The total number of atoms in each system is given in following Table 3.1.

**Table 3.1.** Total number of atoms and water molecules at three simulations.

Model	DAT	dopamine	DAT-dopamine complex
Lipid	43.952	52.126	43.684
Water	33.882	35.164	34.310
Ion ( $Na^+/Cl^-$ )	2/-	1/8	2/5
Totally	155.293	158.100	156.188

### 3.3. Molecular Dynamics (MD) Simulations of Dopamine Transporter

In examining the dynamic structure of proteins, especially membrane proteins, physiological environment have a major effect. Therefore, the protein has been studied along with, water molecules and lipid cell membrane which is its natural environment. To be able to perform MD studies, an initial 3D structure of the protein is required. Homology modeling studies were performed for that purpose before hand in a previous thesis work of a colleague [133].

Homology modeling also known as comparative modeling, is a tool for the estimation of three-dimensional (3-D) structure of a protein by performing amino acid sequence alignment to template proteins whose 3-D structures are already resolved experimentally. The first experimental study of DAT in literature is the determination of the 3D structure of LeuT<sub>Aa</sub> which is a bacterial homolog which is extracted from *Aquifex aeolicus*'s complex of substrate LeuT and two Na<sup>+</sup> ions (PDB code: 2A65, Resolution: 1.65 Å) [23].



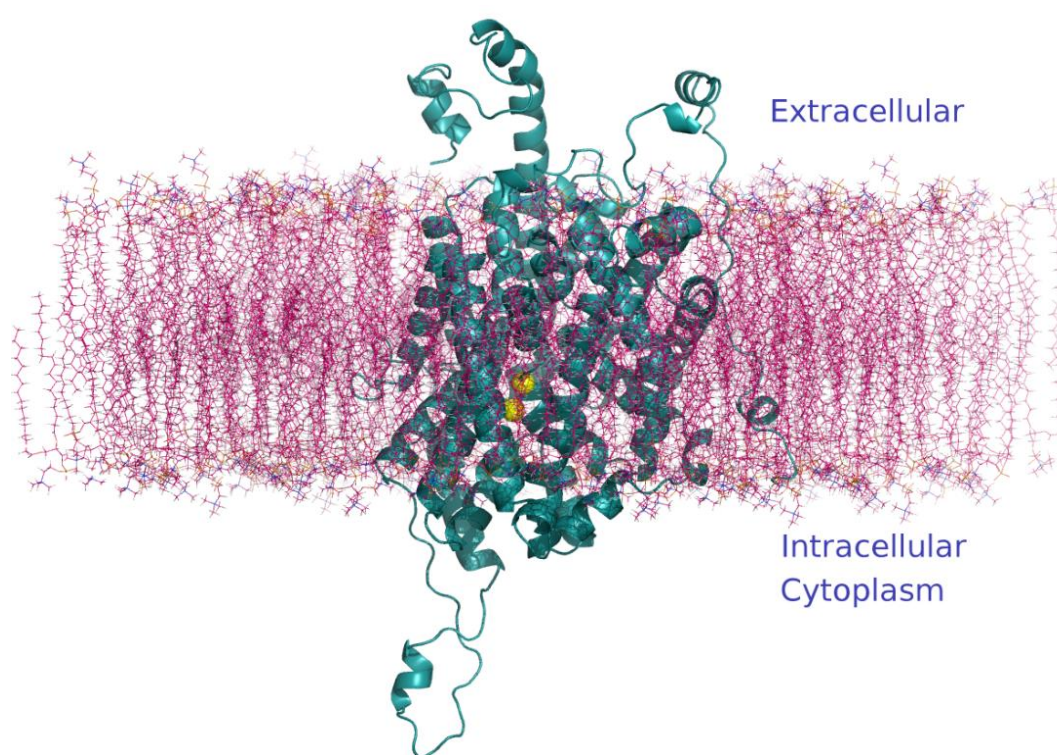
**Figure 3.3.1.** Initial structural model of human DAT which is represented as cylindrical helices in gray, with two Na<sup>+</sup> ions in cyan.

The new three-dimensional (3D) structural model of human DAT is obtained with homology modeling, via two different template structures, which are bacterial homolog of DAT leucine transporter (LeuT<sub>Aa</sub>) and the protein DAT of rat in the thesis of Gizem Tatar [133]. We have used that 3D structure of DAT as our initial structure for MD simulations shown in Figure 3.3.1. In this chapter we examined the 'DAT' model system preparation stages for Molecular Dynamics (MD) simulations, simulation details and how it behave in the membrane without dopamine.



### 3.3.1. System Preparation for MD

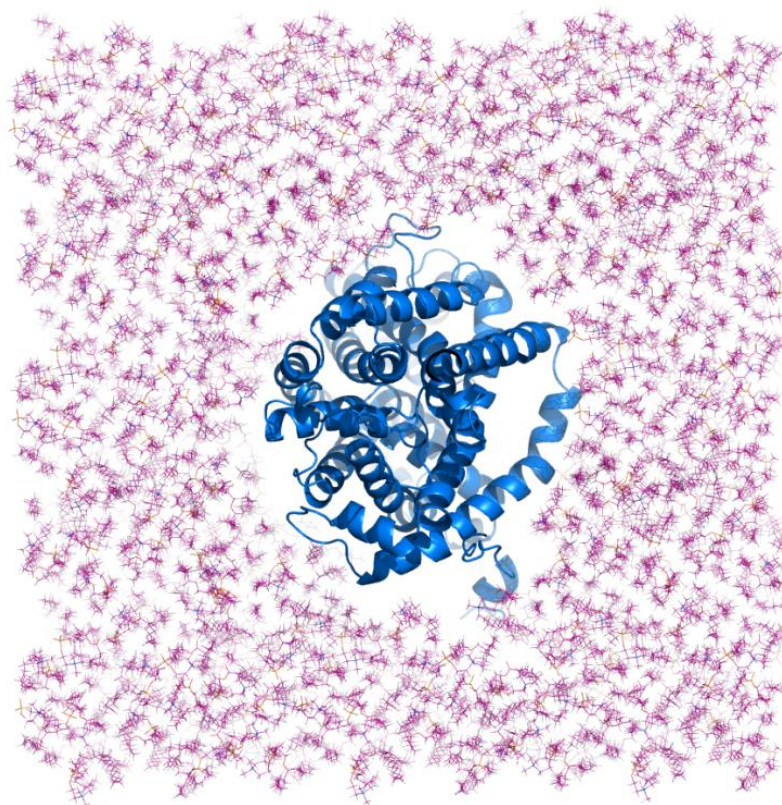
The initial DAT model was put into a preequilibrated double-layered palmitoyl-oleoyl-phosphatidylcholine (POPC) cell membrane to simulate the actual physiological environment. The POPC bilayer was generated by using the Membrane Plug-in v1.1 of VMD software and cell membrane has been generated at the direction of z-axis with a constant thickness. DAT protein is embedded in the membrane according to its hydrophobic part. Its relative orientation in the lipid bilayer was determined by referring the similar orientation of the LeuT<sub>Aa</sub> structure [20,82-84,23] shown in Figure 3.3.2.



**Figure 3.3.2.** The human DAT model in the cell membrane represented as a cyan cartoon and two  $Na^+$  ions represented as a yellow spheres.

Direction of the x and y dimensions of the cell membrane have been determined according to the same direction of protein's x and y dimensions. The distance between min and max coordinates in the x direction is found to be 73Å, distance between two farthest atoms in the protein. The same way, the distance between min and max coordinates in the y direction is found to be 99Å. Accordingly, the protein's dimensions in the x direction and y direction are determined to be 73Å and 99Å. The

membrane's dimensions in this directions are set to  $120\text{\AA} \times 120\text{\AA}$ , in order to avoid the any interaction between the protein and its own image in the periodic box at this direction. For alignment of the membrane and the protein, the membrane's center of mass was chosen as the origin and it is combined with the protein-water system. In the next step, a room is made for the DAT in the membrane layer as shown in Figure 3.3.3. Cut-off distance between protein and lipid is usually set  $0.8\text{\AA}$ - $1.6\text{\AA}$ . By that way, overlap between the protein and any lipid molecules is avoided.



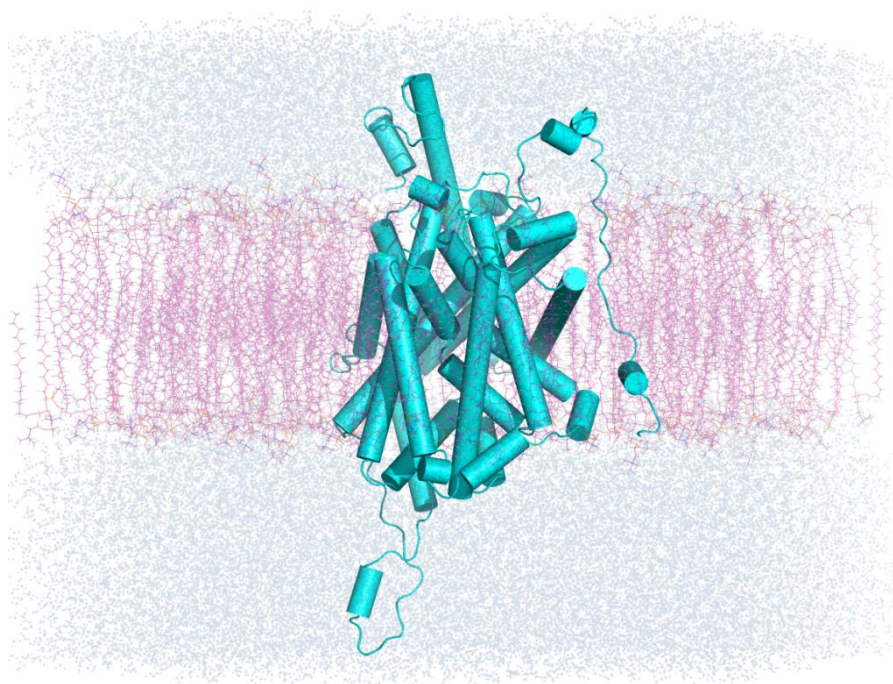
**Figure 3.3.3** The position of the DAT model in a room which is made for DAT in the cell membrane.

After the protein is embedded in the cell membrane whole system was solvated. The distance between min and max coordinates in the z direction is found to be  $75\text{\AA}$  distance between two farthest atoms in the protein. TIP3W water molecules with a thickness of around  $12\text{\AA}$  at both directions of z-axis are added to the cell membrane and protein. The dimension of the system at this direction is set to  $100\text{\AA}$ . You can see in Figure 3.3.4. the final situation of the system along with cell membrane and

water molecules at the x direction. The protein's dimensions at x,y and z directions, approximate cell dimensions and dimensions of the system is given in following Table 3.2.

**Table 3.2.** The DAT, cell membrane and system dimensions.

<b>Protein Dimension xyz (Å)</b>	<b>Cell Membrane xy (Å)</b>	<b>Box Dimensions xyz (Å)</b>
73×99×75	120×120	120×120×100



**Figure 3.3.4** Initial structural model of human DAT in the physiological environment used for MD simulations. DAT protein is represented as cylindrical helices in cyan, water molecules are shown in blue and lipid molecules are indicated as sticks in pink.

2  $Na^+$  ions were added with a concentration of 0,154 mol/L by Autoionize Plugin v1.2 of VMD to make the total net charge of the system equal to zero.

### 3.3.2 Simulation Details and Production MD run

A series of energy minimizations and MD simulations were performed by using Nanoscale Molecular Dynamics (NAMD) software package. At the first preparation stage, only lipid molecules are allowed to be mobile, protein is fixed. The system was run 10000 steps of energy minimization under these conditions and later MD simulation of 0.5 ns was performed. Next, water molecules and the cell membrane are allowed to move freely and the harmonic constraints have been imposed on the protein. Similar to the first stage, the system under these conditions is exposed to a 1000 step minimization followed by an MD simulation of 0.5 ns. The protein released along with surrounding molecules is exposed to an MD simulation of 0.5 ns, at the third preparation stage. After a detailed preparation stage an MD simulation of 200 ns for the whole system have been performed. The simulation details are tabulated in Table 3.3.

**Table 3.3** DAT simulation system details.

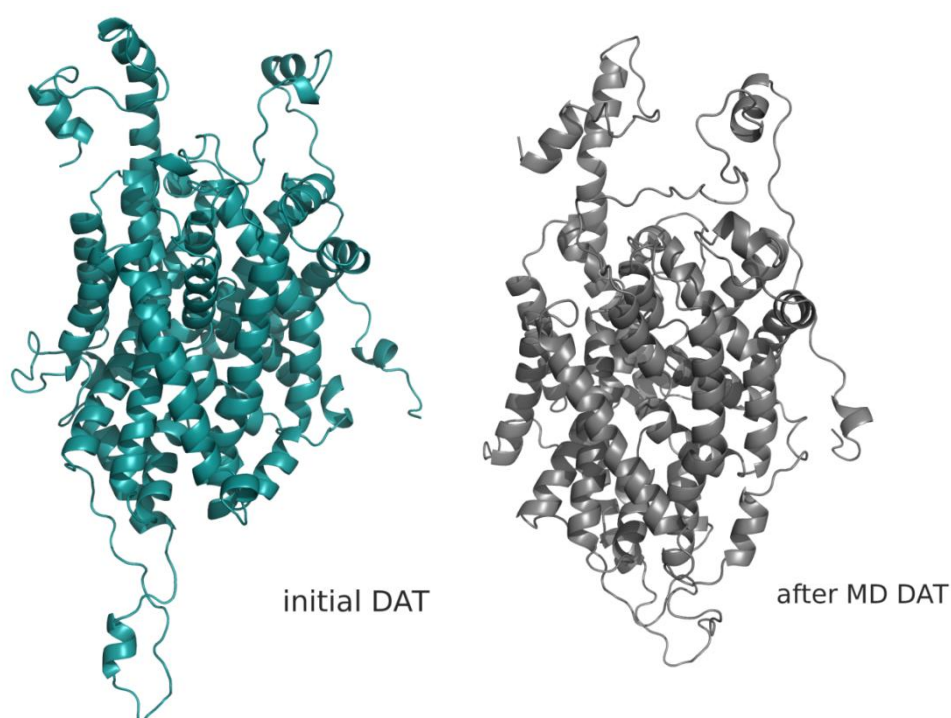
<b>Simulation Length (ns)</b>	<b>Final System Size xyz (Å)</b>	<b>Number of Water Molecules</b>	<b>Number of Lipids</b>	<b>Number of Ions</b>	<b>Total Number of Atoms</b>
200	125×125×120	33.882	43.952	2	155.293

CHARMM22 force field for protein and CHARMM27 force field for lipids were used for the interaction potentials. Temperature of the simulation was set to 310K and the pressure was kept at 1 bar by Berendsen weak-coupling approach (Berendsen *et al.*, 1984). The simulation space partitioning parameter cutoff was set to 12 Å. The other simulation space partitioning parameter ‘pairlistdist’ which is distance between pairs for inclusion in pair lists was set to 13.5 Å. PME (Particle-Mesh Ewald) method was used for long-range electrostatic interactions. The ‘timestep’ parameter was set to 2.0 *fs*. The ‘nonbondedFreq’ which is timesteps between two nonbonded evaluation was set to 1 and the ‘fullElectFrequency’ parameter which is distance between pairs for inclusion in pair lists was set to 2. ‘useGroupPressure’, ‘useFlexibleCell’ and ‘useConstantArea’, which are the pressure control parameters, were set to yes.

The ‘restartfreq’ which is the frequency of restart file generation, the ‘dcdfreq’ which is the timesteps between writing coordinates to trajectory file and the ‘xstfreq’ which shows how often to append state to XST file were all set to 1000 (every 2 *ps*). The ‘outputEnergies’ which is the timesteps between energy output and the ‘outputPressure’ which is the timesteps between pressure output were set to 50.

### 3.3.3. Analysis

In this part of the study, MD is applied to DAT ’s initial model to see what would differ structurally after MD simulation and later to investigate the effects of these differences on the binding properties with dopamine.

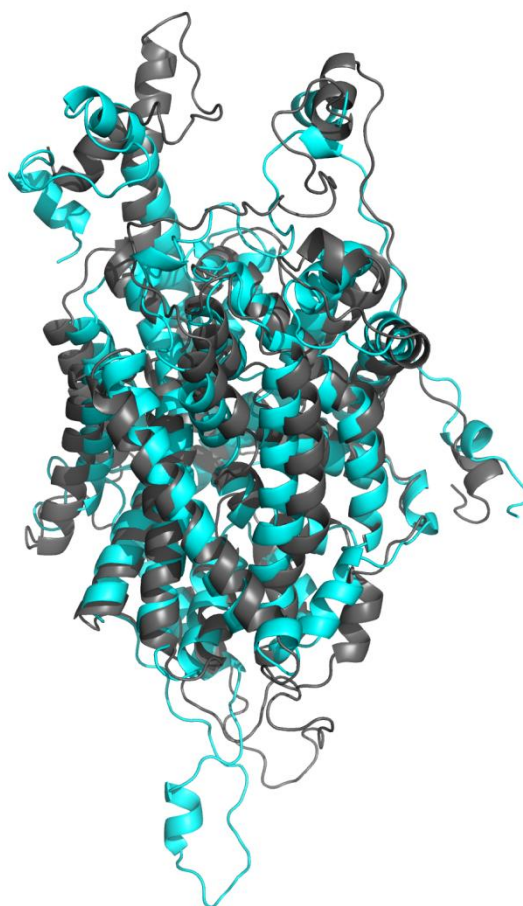


**Figure 3.3.5.** Left one initial structural model of human DAT which is represented as cartoon in cyan. Right one after molecular dynamics simulation structural model of human DAT which is represented as cartoon in gray.

As explained in detail in the previous section, the new three-dimensional (3D) structural model of human DAT is obtained with homology modeling, via two

different template structures, which are bacterial homolog of DAT leucine transporter (LeuT<sub>Aa</sub>) and the protein DAT of rat. We have used that 3D structure of DAT as our initial structure for MD simulations shown in Figure 3.3.5. A series of energy minimization and MD simulations of 200 ns have been performed and you can see the resultant DAT model shown in Figure 3.3.5.

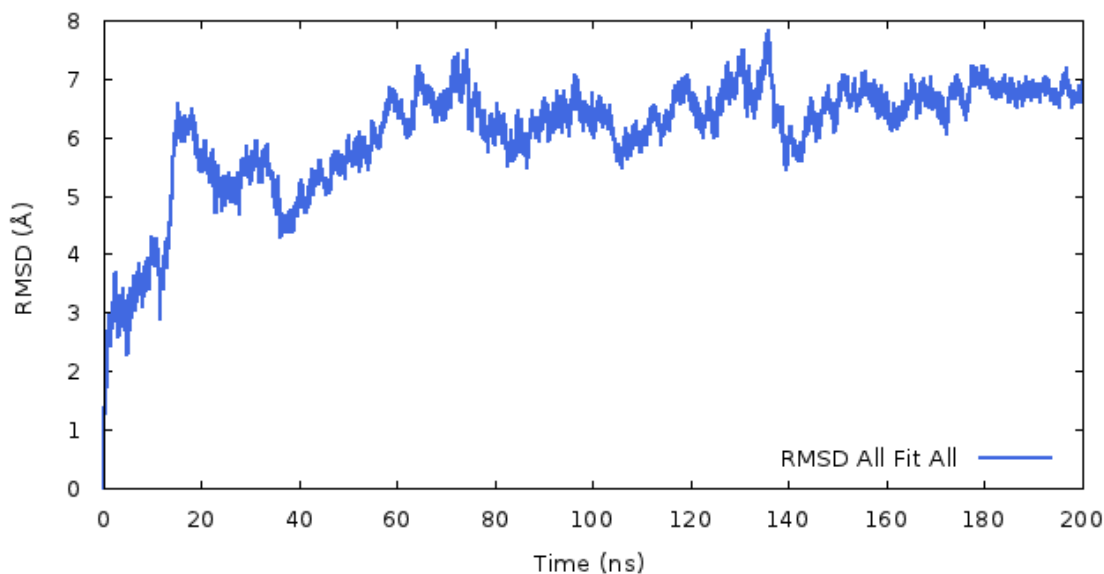
The structure alignment performed in VMD for these initial DAT and after MD simulation DAT model is shown in Figure 3.3.6. The RMSD value of these before-after models was calculated as 7.586 Å for  $C_{\alpha}$  atoms. This RMSD value indicates that DAT 's structure have undergone some variations during the Molecular Dynamics.



**Figure 3.3.6.** Structural model of human DAT after molecular dynamics which is represented as cartoon in gray and initial structural model of human DAT which is represented as cartoon in cyan, structural alignment.

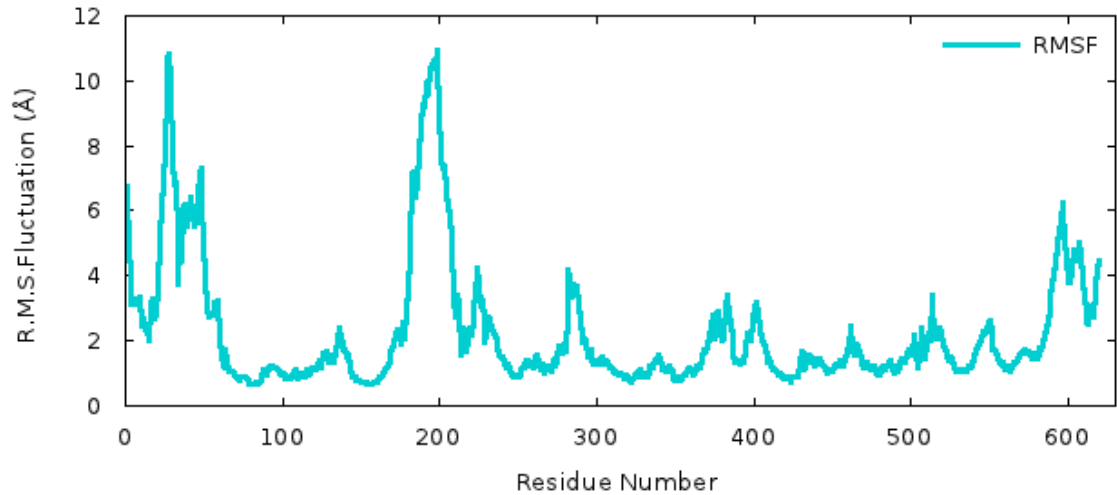
The RMSD of the DAT model along the trajectory, which is calculated after aligning the  $C_{\alpha}$  atoms of each snapshot with the initial frame, is plotted in Figure 3.3.7. The

RMSD plot shows the extent of deviation from the initial conformation and the conformational changes throughout the trajectory. The RMSD values have been calculated according to the all protein. Whole protein structure is aligned to its initial frame first, and then the RMSD value is calculated. Simulation reach equilibrium at 60-70 ns at a value of  $\sim 7$  Å, showing the stability of the simulation with small fluctuations.



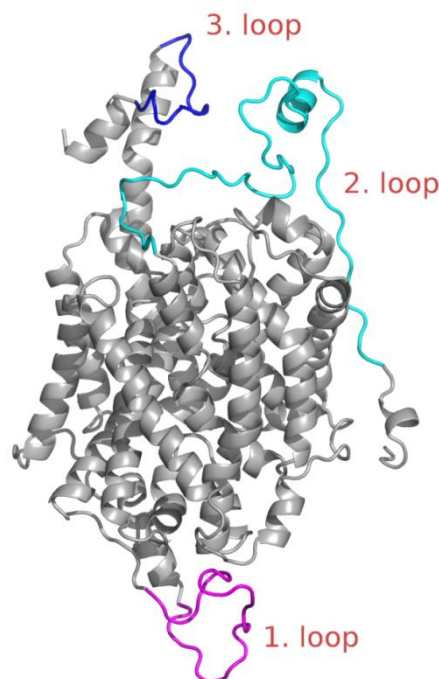
**Figure 3.3.7.** RMSD values which were obtained from 200 ns MD simulations for DAT model.

The best way to numerically express the protein's mobility along the simulation is to generate the RMSF profile (root mean square of the average fluctuations). RMSF are calculated from the production phase of the trajectory and calculations are carried out over the conformations aligned to the average structures of the simulations using only  $C_{\alpha}$  atoms. DAT's RMSF profile, which is obtained from MD simulation, shown in Figure 3.3.8.



**Figure 3.3.8.** RMSF profile of DAT model.

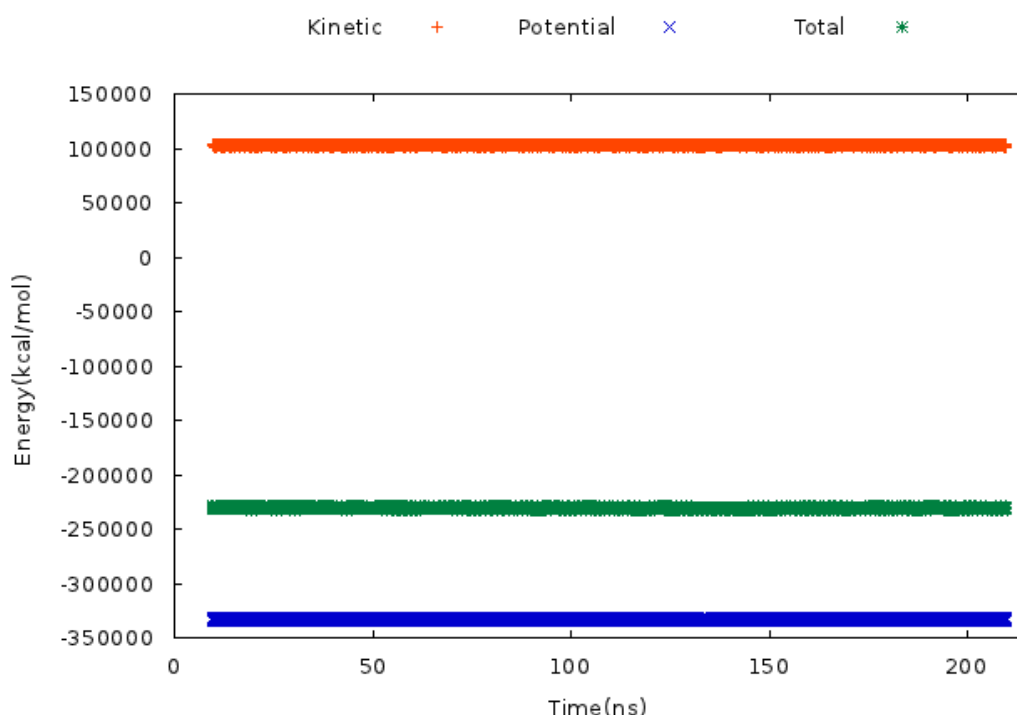
According to these profile, the highest mobility of the protein is observed at the intracellular loop and between residue 180-205. The second most mobile region is detected at extracellular loop and between residue 12-65. After 2<sup>nd</sup> loop, the third highly mobile region is detected at extracellular loop and between residue 595-610, facing outside the cell. The mobile regions are also shown on the structure of DAT model in Figure 3.3.9.



**Figure 3.3.9.** The positions of the most mobile regions on the structure of DAT model. First loop is shown in magenta, second loop is shown in cyan and third loop is illustrated in blue.



Kinetic, potential and total energy values fluctuates around an average value throughout the simulation. Simulation kinetic energy value is about 100.000 kcal/mol, potential energy value is about -350.000 kcal/mol, total energy value is -250.000 kcal/mol and seen that fluctuate the around this values. Energy values of DAT model which is obtained from MD simulation, shown in Figure 3.3.10. Total energy average value is detected as -230.759 kcal/mol, this value necessary to when compare the DAT model and DAT-dopamine complex model and important in determining the binding energy.



**Figure 3.3.10.** Kinetic, potential and total energy values of DAT model, which is obtained from MD simulations.

### 3.3.3.1. Comparison of the Helix Regions

The 3-D molecular structure in detail is not known for any transporter protein but experimental studies of the topology of the 5-HT transporter [85], an electron density projection map of the NhaA [86], and a detailed topology analysis of NhaA [87], all support the assumption that the secondary transporter proteins have 12 membrane spanning domains. These helices are important for determining the binding pocket for agonist molecules and proximity of certain conserved residues within

neighboring TM domains [88-90]. Figure 3.3.11 shows the results of DAT's experimental cDNA clone analysis [91] and in the following Table 3.4 the corresponding residue intervals for alpha helices obtained experimentally are tabulated.

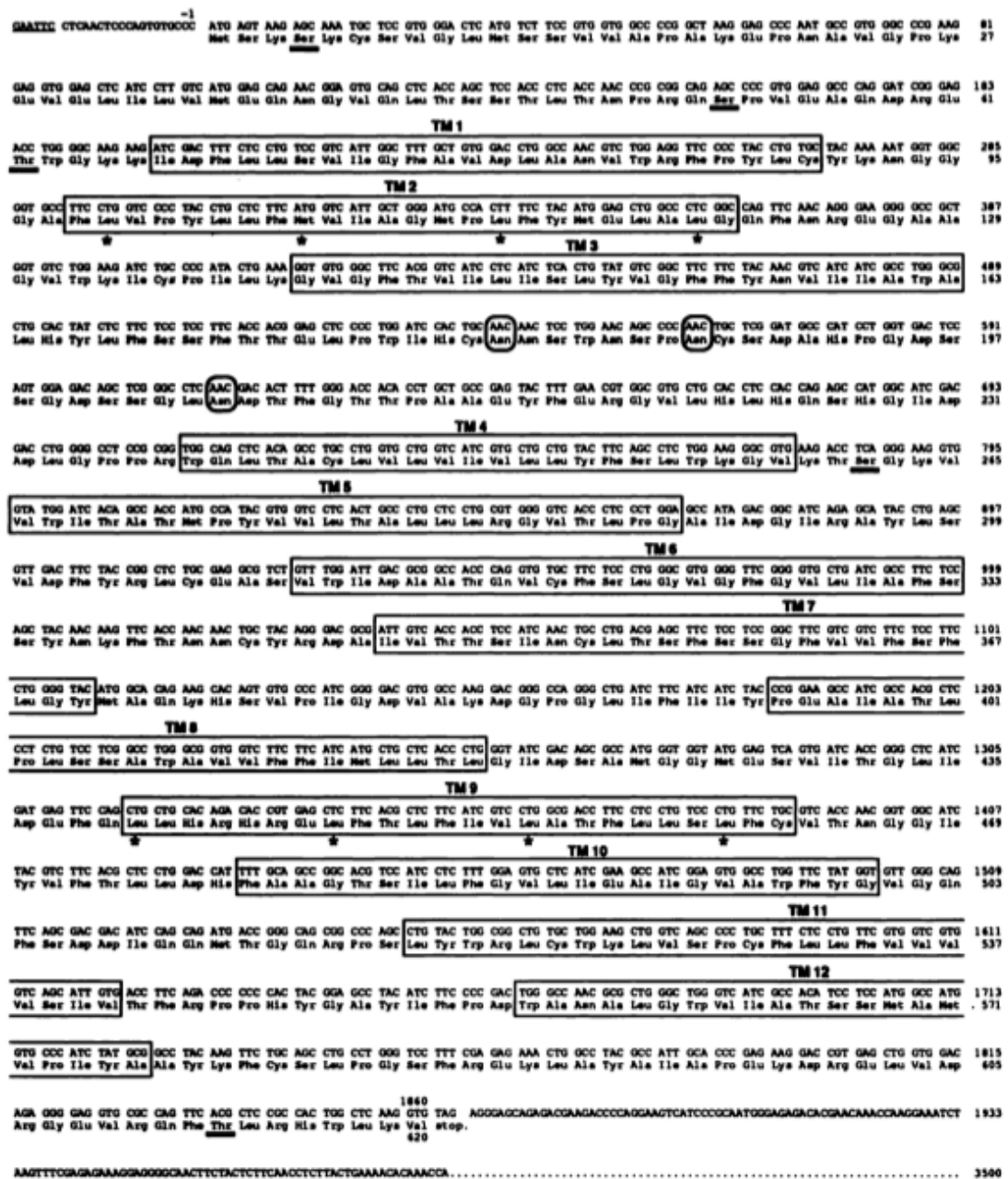


Figure 3.3.11. The human DAT cDNA clone amino acid sequences. Boxed regions indicate 12 TMH domains [91].

**Table 3.4.** Start and end points of TMHs detected in the experimental studies of human dopamine transporter (DAT).

<b>TMH number</b>	<b>Amino acid sequence positions</b>
<b>1</b>	67-90
<b>2</b>	98-122
<b>3</b>	140-163
<b>4</b>	238-259
<b>5</b>	266-289
<b>6</b>	310-333
<b>7</b>	347-370
<b>8</b>	395-418
<b>9</b>	440-463
<b>10</b>	478-500
<b>11</b>	518-541
<b>12</b>	556-576

In our study, detected computationally 24 TMH (alpha helix) on the initial DAT model by using VMD program shown in Table 3.5. Secondary structure is computed by the program STRIDE which uses an heuristic algorithm in VMD.

**Table 3.5.** Start and end points of transmembrane helices (TMHs) of initial DAT model detected computationally by using VMD program.

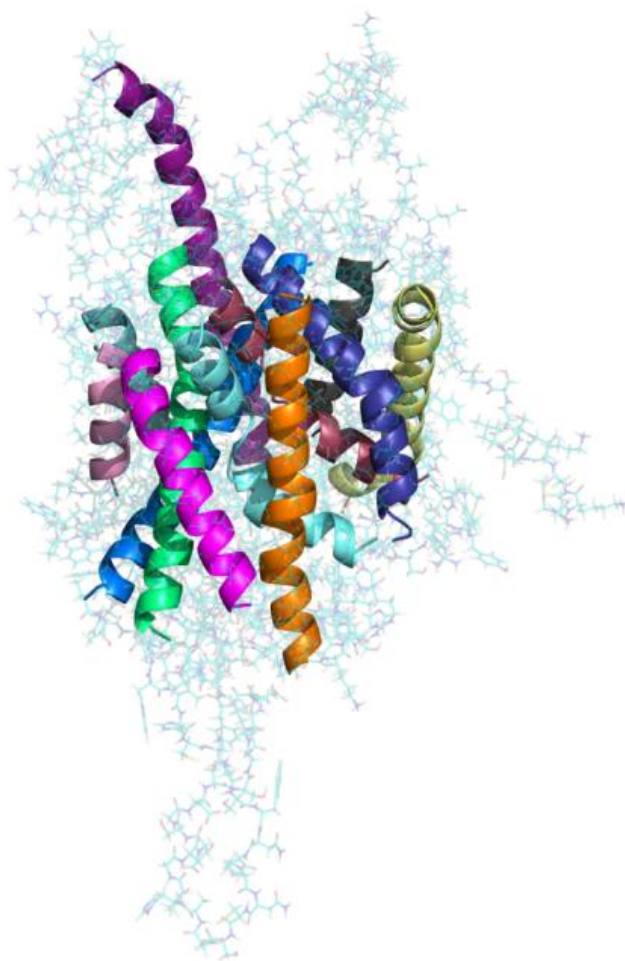
<b>TMH number</b>	<b>Amino acid sequence positions</b>	<b>TMH number</b>	<b>Amino acid sequence positions</b>
<b>1</b>	6-10	<b>13</b>	328-335
<b>2</b>	28-34	<b>14</b>	342-373
<b>3</b>	66-77	<b>15</b>	376-384
<b>4</b>	80-93	<b>16</b>	387-400
<b>5</b>	96-124	<b>17</b>	404-438
<b>6</b>	137-172	<b>18</b>	442-457
<b>7</b>	194-199	<b>19</b>	467-479
<b>8</b>	206-221	<b>20</b>	481-497
<b>9</b>	240-253	<b>21</b>	501-509
<b>10</b>	258-281	<b>22</b>	518-550
<b>11</b>	290-298	<b>23</b>	553-594
<b>12</b>	308-322	<b>24</b>	611-618

The table you see above, shows that 24 TMH region which are determined computationally, but when we compared to this regions and experimental data [85-90], is identified the 12 transmembrane helices region is shown in Table 3.6. As can be seen in the next sections, analysis of initial DAT model – ligand binding area definitions are based on these 12 regions.

**Table 3.6.** The positions of the aminoacid sequence of the transmembrane helix regions were detected in the initial DAT model corresponding to experimental studies.

<b>TMH number</b>	<b>Amino acid sequence positions</b>
<b>1a</b>	66-74
<b>1b</b>	80-93
<b>2</b>	96-124
<b>3</b>	137-172
<b>4</b>	240-253
<b>5</b>	258-281
<b>6a</b>	308-322
<b>6b</b>	328-335
<b>7</b>	342-373
<b>8</b>	404-438
<b>9</b>	442-457
<b>10</b>	481-497
<b>11</b>	518-550
<b>12</b>	553-594

When we compared the table including 12 TMHs which are computationally identified and the table involving 12 TMHs which are determined in experimental studies, we can see these regions are approximately similar. The reason of this little differences comes from the structural analysis tools of the softwares due to using different explanations of the secondary structures. 3D structure of initial DAT model 12 TMH shown in Figure 3.3.12.



**Figure 3.3.12.** Representation of the initial DAT model 12 alpha helices. Cyan represents TMH1a-TMH1b, deep blue TMH2, marine blue TMH3, pink TMH4, magenta TMH5, raspberry TMH6a-TMH6b, orange TMH7, green TMH8, teal TMH9, black TMH10, pale-yellow TMH11, deep-purple TMH12.

After molecular dynamics simulation DAT model study, we detected 22 TMH (alpha helix) computationally by using VMD program (used by STRIDE secondary structure codes). Aminoacid residue positions of these helices are shown in Table 3.7.

**Table 3.7.** Start and end points of transmembrane helices (TMHs) of after MD DAT model detected computationally by using VMD program.

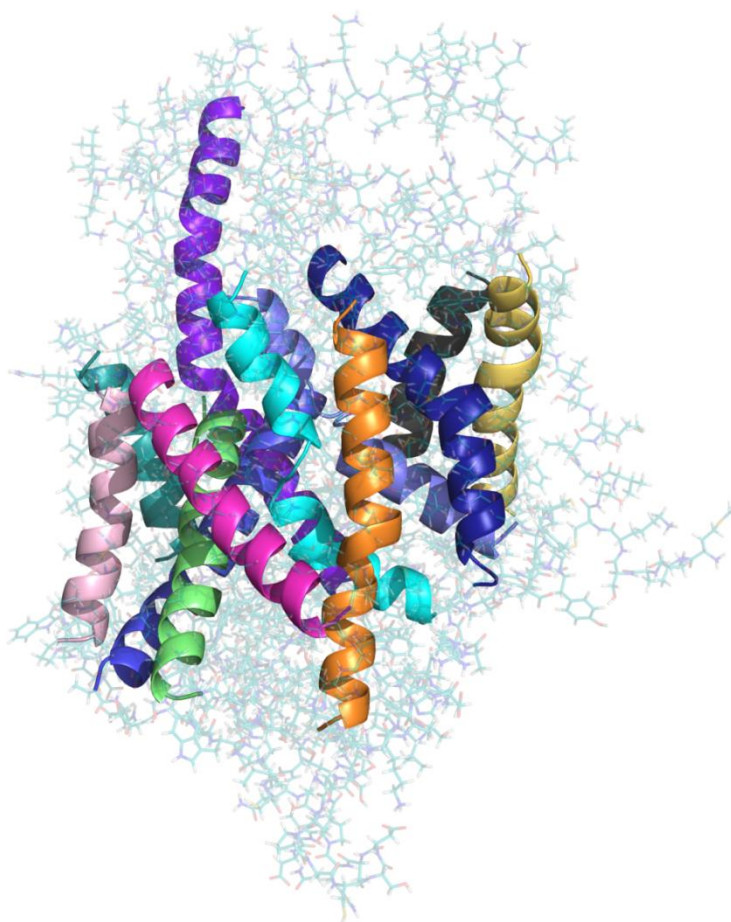
<b>TMH number</b>	<b>Amino acid sequence positions</b>	<b>TMH number</b>	<b>Amino acid sequence positions</b>
<b>1</b>	6-11	<b>12</b>	328-335
<b>2</b>	66-74	<b>13</b>	344-372
<b>3</b>	80-92	<b>14</b>	392-399
<b>4</b>	96-124	<b>15</b>	404-428
<b>5</b>	129-134	<b>16</b>	432-438
<b>6</b>	143-172	<b>17</b>	471-480
<b>7</b>	215-219	<b>18</b>	482-498
<b>8</b>	235-253	<b>29</b>	518-541
<b>9</b>	259-282	<b>20</b>	543-549
<b>10</b>	291-298	<b>21</b>	553-594
<b>11</b>	308-322	<b>22</b>	611-618

The table you see above, shows that 22 TMH region which are determined computationally, but when we compared to these regions and experimental data [85-90], corresponding 12 transmembrane helices are shown in Table 3.8.

**Table 3.8.** The positions of amino acid sequence of transmembrane helices obtained in the after MD simulation DAT model corresponding to experimental studies.

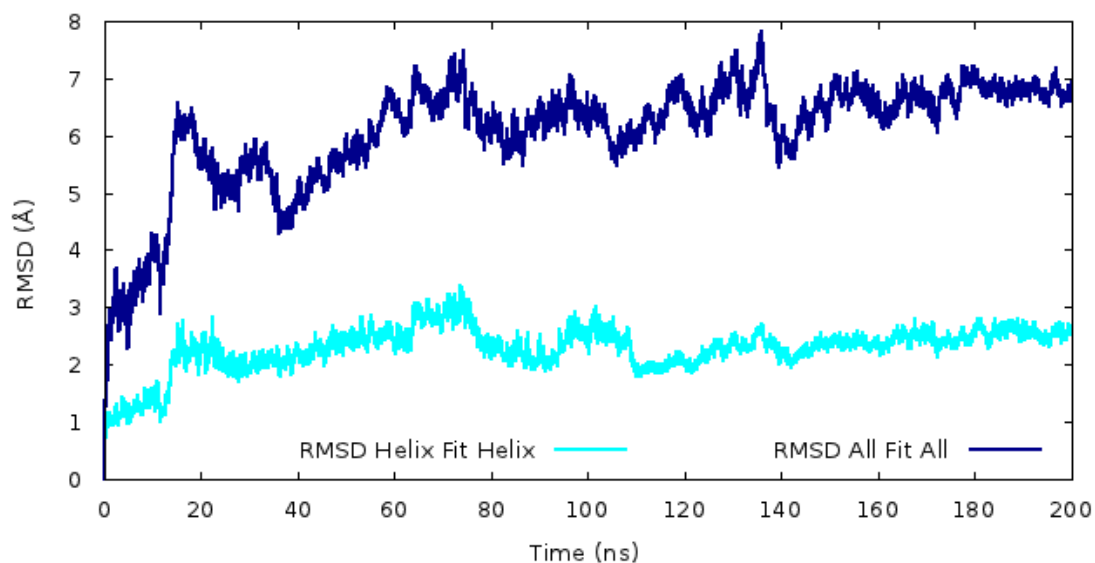
<b>TMH number</b>	<b>Amino acid sequence positions</b>
<b>1a</b>	66-74
<b>1b</b>	80-92
<b>2</b>	96-124
<b>3</b>	143-172
<b>4</b>	235-253
<b>5</b>	259-282
<b>6a</b>	308-322
<b>6b</b>	328-335
<b>7</b>	344-372
<b>8</b>	404-428
<b>9</b>	442-458
<b>10</b>	482-498
<b>11</b>	518-541
<b>12</b>	553-594

3D structure of after MD simulation DAT model 12 TMH shown in Figure 3.3.13.



**Figure 3.3.13.** Representation of the after MD simulation DAT model 12 alpha helices. Cyan TMH1a-TMH1b, deep blue TMH2, marine blue TMH3, pink TMH4, magenta TMH5, raspberry TMH6a-TMH6b, orange TMH7, green TMH8, teal TMH9, black TMH10, pale-yellow TMH11, deep-purple TMH12.

When compared the 24 TMH (alpha helix) regions that are computationally detected on initial DAT model and 22 TMH (alpha helix) regions that are computationally detected on after MD simulation DAT model, have some differences, such as loss of two helices. However, compared to the entire structure, we can see that in fact the most stable regions the helix regions. It can also be observed RMSD chart shown in Figure 3.3.14., that displacements in the helix regions are quite less with respect to the overall structure.

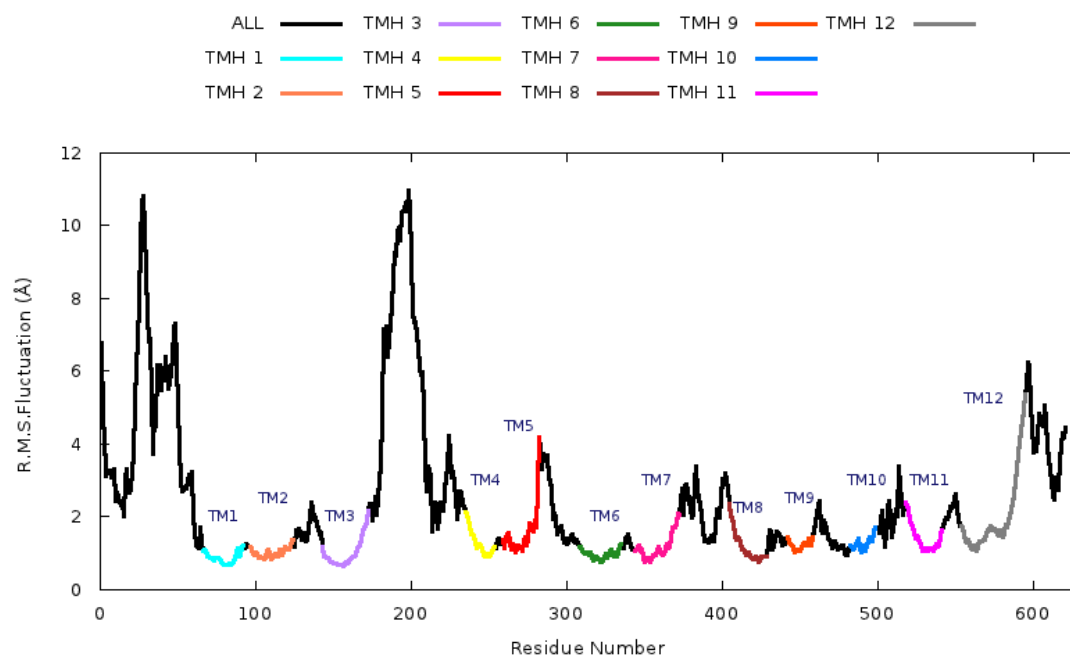


**Figure 3.3.14.** Root Mean Square Deviation values which were obtained from 200 ns MD simulations for all structure and helix regions.

According to these profile, the highest stability of the protein is observed at the helix region and we can say that a, longer simulation can be performed to see more mobility on these helix regions which are affecting the binding site.

In the same way, when we generated the RMSF (root mean square of the average fluctuations) profile for helix regions. RMSF graph numerically expresses the helices mobility along the simulation as shown in Figure 3.3.15.

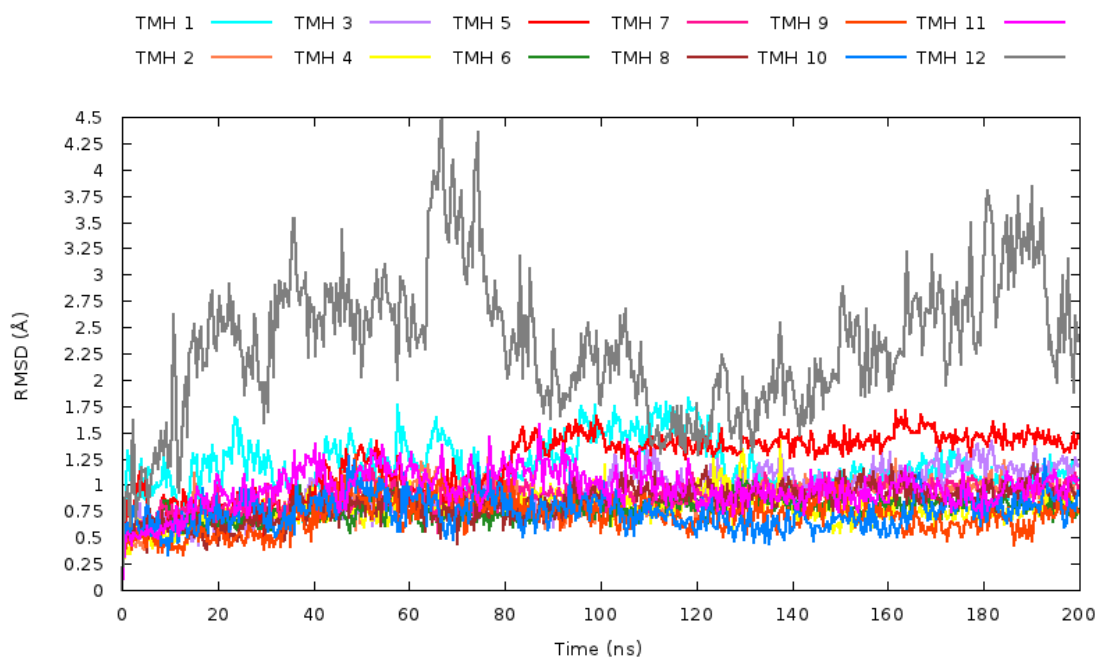




**Figure 3.3.15.** RMSF about the average position plotted for residues which were obtained from 200 ns MD simulations for all structure and helix regions.

According to these RMSF profile, between the protein helices the highest mobility is observed at the TMH12 region which constitutes residues 550-595. TMH5 is the second mobile helix region between the residues 260-280. Other helices fluctuation values are less than the fluctuation values of TMH5 and TMH12. The fluctuation values of TMH1, TMH2, TMH6, TMH9 and TMH10 are approximate similar. According to these results, highly mobile residues between the helices are belong to TMH5 and TMH12. These residues have the highest fluctuation values in these helices.

To clearly observe the contribution of each helix separately to the RMSD values during the MD simulations RMSD graphs in Figure 3.3.16. was created.



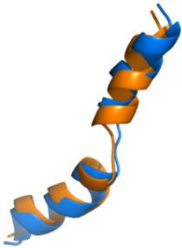
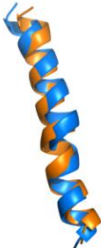
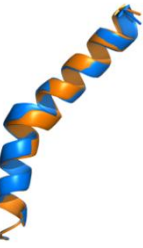

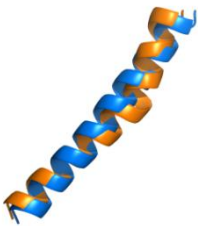
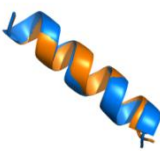

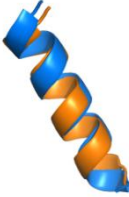
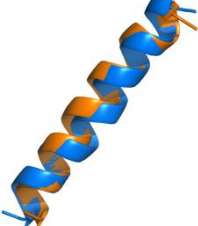
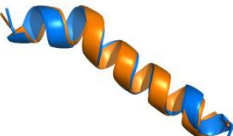
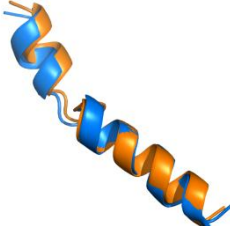
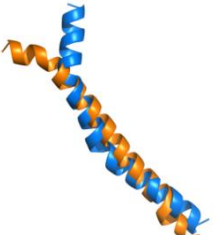
**Figure 3.3.16.** RMSD values which were obtained from 200 ns MD simulations for all helix regions on DAT model.

The RMSD plot shows the extent of deviation from the initial conformation of helices and the conformational changes throughout the trajectory. The RMSD values have been calculated according to the helix regions. Whole helix structures are aligned to their initial frame first, and then the RMSD value is calculated.

When we look at the RMSD profile of structure, we see that values are proportional to the RMSF profile of structures. Among all transmembrane helices, the most mobile ones are the twelfth and the fifth helices (TMH12 and TMH5). Most of the helices achieve equilibrium at 20-60 ns with a value of  $\sim 1$  Å. They remain stable during the simulation, but the biggest helix TMH12 is fluctuating. The second mobile helix TMH5 achieve equilibrium at 20-80 ns at a value of  $\sim 1.5$  Å.

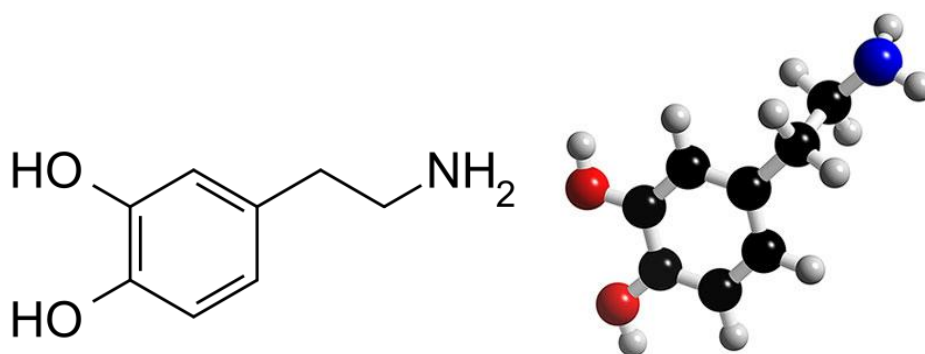
After the analysis of RMSD and RMSF profiles, you can see the internal individual structural differences of all 12 TMH in the same direction represented in Table 3.9.

**Table 3.9.** Comparison of the initial and after MD simulation DAT helices structures and RMSD values.

RMSD Value	Aligning of Initial and Final	RMSD Value	Aligning of Initial and Final
TMH1 1,801 Å		TMH7 1,272 Å	
TMH2 0,900 Å		TMH8 0,913 Å	
TMH3 1,402 Å		TMH9 0,525 Å	
TMH4 1,374 Å		TMH10 1,235 Å	
TMH5 1,525 Å		TMH11 1,489 Å	
TMH6 0,742 Å		TMH12 4,500 Å	

### 3.4. Molecular Dynamics (MD) Simulations of Dopamine

The dynamic properties of protein-ligand (DAT-dopamine) interactions are described via MD simulations in the next chapter. A well known molecule, dopamine, which is shown in Figure 3.4.1., is a symporter and is impossible to pass the membrane without dopamine transporter and ions. In this chapter we embedded the dopamine in the membrane, to see how it behaves in the membrane without dopamine transporter.



**Figure 3.4.1.** Molecular model and 3D structure of neurotransmitter dopamine.

#### 3.4.1. Creating Topology File for Dopamine

To create a PSF structure file for dopamine, a CHARMM forcefield topology file which contains all of the information about the structure is needed. Thus a list of residue names can be converted into a complete PSF file [92]. When presented with a nonstandard group, the first step is to find out exactly which parameters are already known, and which will be needed to develop.

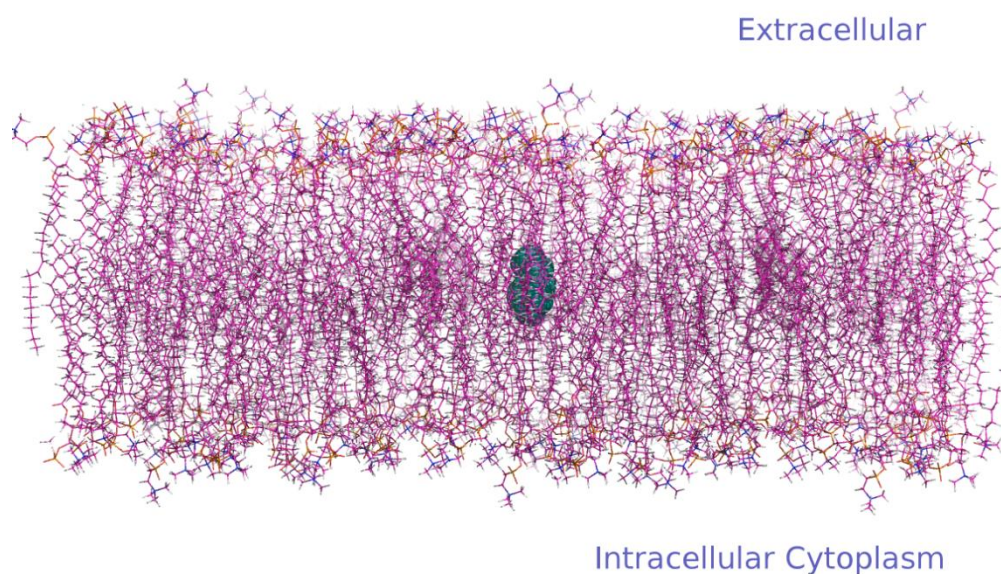
To do this, we will integrate two pre-existing topology file entries p-ethylphenol and ethylammonium. We have used the `top_all36_cgenff.inp` topology file. The topology file specifies the partial charge of each atom and the connectivity of the atoms. We will then use this topology file while creating the `.psf` and `.pdb` files for our simulations.

Below is the final topology file entry for the dopamine ligand. The dopamine parameters appearing in it were created by combining a regular p-ethylphenol entry (with some additions and moldings) with a ethylammonium entry (with some additions and moldings). When merging the two residues into one, at the place where you connect the groups you will have to delete atoms and alter the charges [93].

ATOM CG	CG2R61	0.00	GROUP		
			ATOM HH	HGP1	0.42
GROUP			ATOM CZ	CG2R61	0.11
ATOM CD1	CG2R61	-0.115	ATOM OH	OG311	-0.53
ATOM HD1	HGR61	0.115			
			GROUP		
GROUP			ATOM HB2	HGA2	0.09
ATOM CD2	CG2R61	-0.115	ATOM CB	CG321	-0.18
ATOM HD2	HGR61	0.115	ATOM HB1	HGA2	0.09
GROUP			GROUP		
ATOM CE1	CG2R61	0.11	ATOM HZ2	HGP2	0.33
ATOM OH1	OG311	-0.53	ATOM CA	CG324	0.21
ATOM HH1	HGP1	0.42	ATOM NZ	NG3P3	-0.30
			ATOM HZ3	HGP2	0.33
GROUP			ATOM HA1	HGA2	0.05
ATOM CE2	CG2R61	-0.115	ATOM HA2	HGA2	0.05
ATOM HE	HGR61	0.115	ATOM HZ1	HGP2	0.33

### 3.4.2. System Preparation for MD

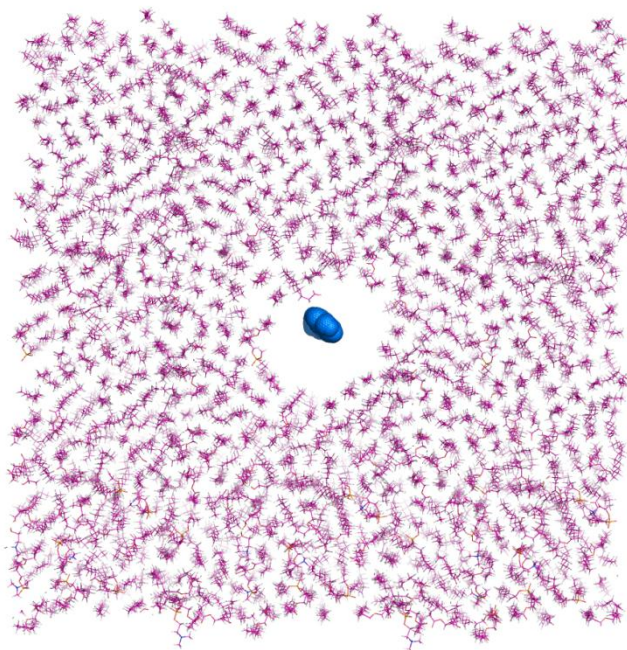
The dopamine was put into a preequilibrated double-layered (POPC) cell membrane to simulate the actual physiological environment. The POPC bilayer was generated by using the Membrane Plug-in v1.1 of VMD software and cell membrane has been generated at the direction of z-axis with a constant thickness. Dopamine is embedded in the membrane according to membrane centre as shown in Figure 3.4.2.



**Figure 3.4.2.** The neurotransmitter dopamine in the cell membrane represented as a cyan dots.

Direction of the x and y dimensions of the dopamine smaller than direction of the x and y dimensions of the dopamine transporter but we created the membrane according to DAT 's dimension to make a comparison between the two system.

The dopamine's dimensions in the x direction and y direction are determined to be 10 Å and 7 Å. The membrane's dimensions in this directions are set to 120 Å × 120 Å like a DAT's dimesions. For alignment of the membrane and the dopamine, the membrane's center of mass translated to the origin and it is combined with the dopamine-water system. The next step, a room is made for the dopamine in the membrane layer is shown in Figure 3.4.3., cut-off distance between molecule and lipid is usually set 0.8 Å-1.6 Å. This way, overlap between the protein and any lipid molecules is avoided.

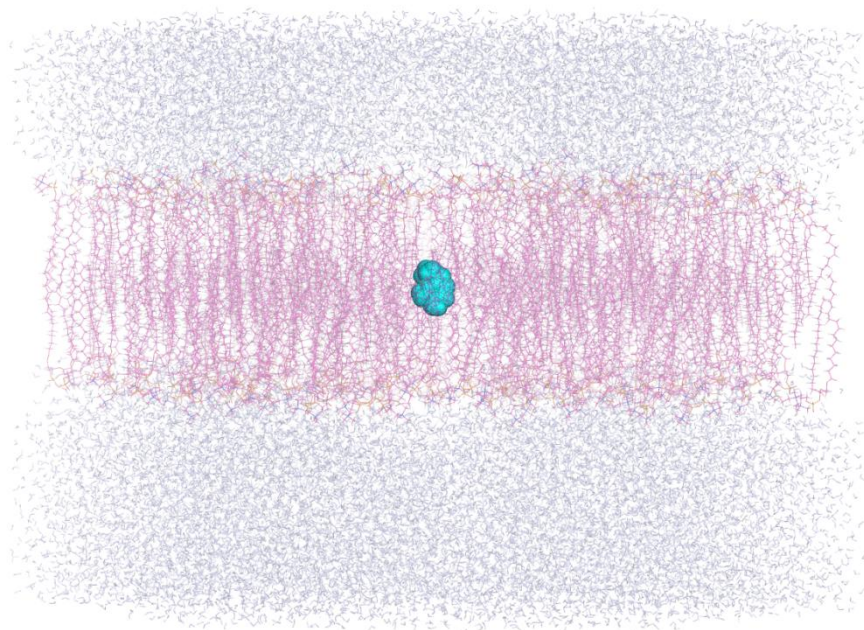


**Figure 3.4.3** The position of the Dopamine in the cell membrane.

After the dopamine is embedded in the cell membrane it's solvated by water molecules at each side of lipid bilayer. The distance between min and max coordinates in the z direction is found to be 14 Å distance between two farthest atoms in the molecule. TIP3W water molecules with a thickness of around 35 Å at both directions of z-axis are added to the cell membrane and dopamine. The dimension of the system at this direction is set to 100 Å for having the same dimensions of the DAT model. You can see in Figure 3.4.4. the final situation of the system along with cell membrane and water molecules at the x direction. The dopamine's dimensions at x, y and z directions, approximate cell dimensions and dimensions of the system is given in following Table 3.10.

**Table 3.10.** The dopamine, cell membrane and system dimensions.

<b>Dopamine Dimension</b> <b>xyz</b> <b>(Å)</b>	<b>Cell Membrane</b> <b>xy</b> <b>(Å)</b>	<b>Box Dimensions</b> <b>xyz</b> <b>(Å)</b>
10×7×14	120×120	120×120×100



**Figure 3.4.4** Neurotransmitter dopamine in the physiological environment used for MD simulations. Dopamine molecule is represented as dots in cyan, water molecules are shown in blue and lipid molecules are indicated as sticks in pink.

1  $Na^+$  and 8  $Cl^-$  ions were added with a concentration of 0,154 mol/L by Autoionize Plugin v1.2 of VMD to make the total net charge of the system equal to zero.

### 3.4.3 Simulation Details and Production MD run

A series of energy minimizations and MD simulations were carried out by NAMD software package. At the first preparation stage, only lipid molecules are allowed to be mobile, dopamine is fixed. The system was run 50000 steps of minimization under these conditions and later to an MD simulation of 0.5 ns. Next, water molecules and the cell membrane are allowed to move freely and the harmonic constraints have been imposed on the dopamine. Similar to the first stage, the system under these conditions is exposed to a 1000 step minimization followed by an MD simulation of 0.5 ns. The dopamine released along with surrounding molecules is exposed to a MD simulation of 0.5 ns, at the third preparation stage. After a detailed



preparation stage an MD simulations of 15 ns for the whole system have been performed. The simulation details are summarized in Table 3.11.

**Table 3.11** Dopamine simulation system details.

Simulation Length (ns)	Final System Size xyz (Å)	Number of Water Molecules	Number of Lipids	Number of Ions	Total Number of Atoms
15	125×125×120	35.164	52.129	9	158.100

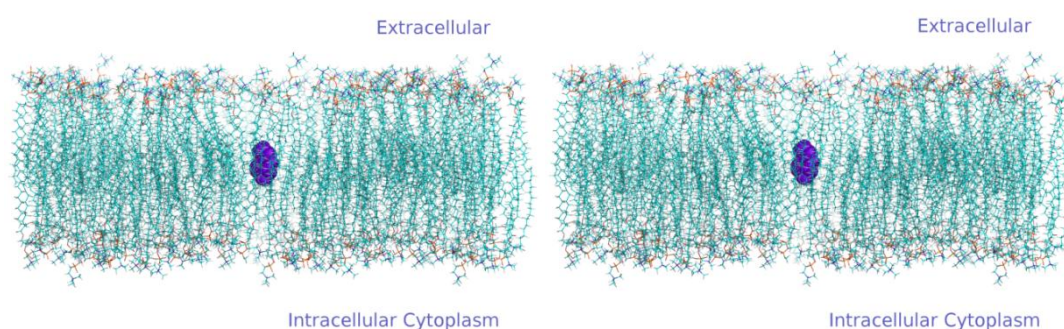
CHARMM22 force field for protein, CHARMM27 force field for lipids and the topology file which is we defined for dopamine were used for the interaction potentials. Temperature of the simulation was set to 310K and the pressure was kept at 1 bar by Berendsen weak-coupling approach [97]. The simulation space partitioning parameter cutoff which is local interaction distance common to both electrostatic and van der Waals calculations was set to 12 Å. The other simulation space partitioning parameter ‘pairlistdist’ which is distance between pairs for inclusion in pair lists was set to 13.5 Å. PME (Particle-Mesh Ewald) method was used for long-range electrostatic interactions. The ‘timestep’ parameter was set to 2.0 *fs*. The ‘nonbondedFreq’ which is timesteps between nonbonded evaluation was set to 1 and the ‘fullElectFrequency’ parameter which is distance between pairs for inclusion in pair lists was set to 2. ‘useGroupPressure’, ‘useFlexibleCell’ and ‘useConstantArea’, which are the pressure control parameters, were set to yes. The ‘restartfreq’ which is the frequency of restart file generation, the ‘dcdfreq’ which is the timesteps between writing coordinates to trajectory file and the ‘xstfreq’ which shows how often to append state to XST file were all set to 1000 (every 2 *ps*). The ‘outputEnergies’ which is the timesteps between energy output and the ‘outputPressure’ which is the timesteps between pressure output were set to 50.

#### 3.4.4. Analysis

As mentioned before, dopamine is a symporter and is impossible to pass the membrane without dopamine transporter and ions. According to the previous study of electrophysiology and radiolabeled dopamine, its system very similar to the most widely accepted monamine transporter and DAT need to two or more molecules to

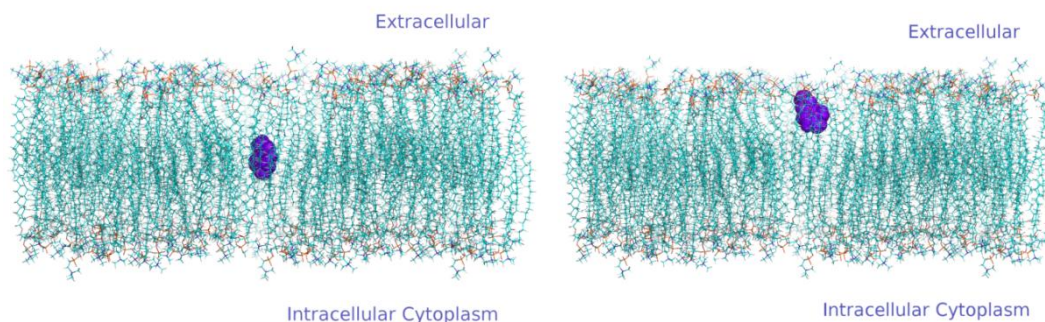
bear the dopamine. The direction of movement is from the high to low direction of ion concentration [13,94-96].

We embedded the dopamine in the membrane, to see how it behaves in the membrane without dopamine transporter and for compare its behavior with as it should be realistic form. After placement of the dopamine in the centre of membrane, it is seen that dopamine moving step by step. Seven different snapshots taken during the 15 ns simulation to follow the movement of dopamine.



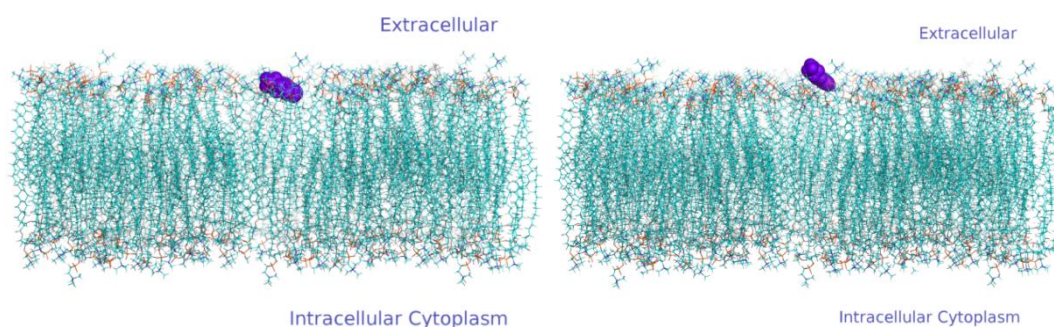
**Figure 3.4.5** First (left one) and second (right one) snapshots of dopamine in the membrane. Dopamine molecule is represented as dots in purple.

The first snapshot is taken after placing the dopamine into the membrane. In this phase, dopamine coordinates are found to be, x direction  $-0.315 \text{ \AA}$ , y direction  $0.486 \text{ \AA}$  and z direction  $0.213 \text{ \AA}$ . The second snapshot is taken the melting lipid tails part which is the first preparation stage and only lipid molecules are allowed to be mobile, dopamine is fixed. As expected, dopamine did not show any movement shown in Figure 3.4.5 and its coordinates are found to be same the first snapshot.



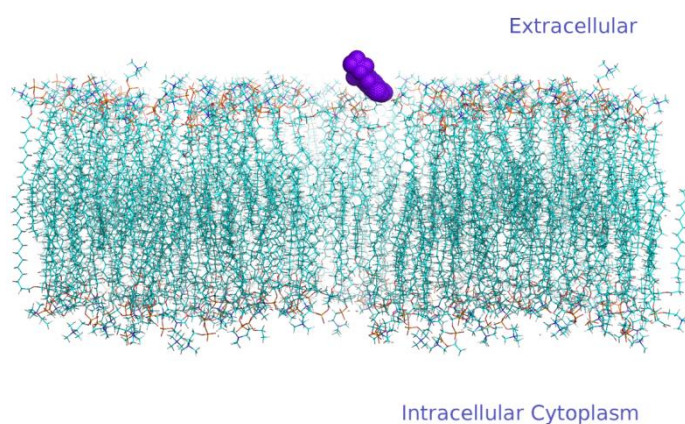
**Figure 3.4.6** Third (left one) and fourth (right one) snapshots of dopamine in the membrane. Dopamine molecule is represented as dots in purple.

In minimization and equilibration phase the third snapshot is taken, in which water molecules and the cell membrane are allowed to move freely and the harmonic constraints have been imposed on the dopamine. In this phase, dopamine coordinates are found to be, x direction  $-0.643 \text{ \AA}$ , y direction  $0.161 \text{ \AA}$  and z direction  $0.210 \text{ \AA}$ . Dopamine undergoes a little displacement. Next, the fourth snapshot is taken the equilibration with dopamine phase which is the dopamine released along with surrounding molecules. Its coordinates are found to be, x direction  $3.013 \text{ \AA}$ , y direction  $1.957 \text{ \AA}$  and z direction  $12.489 \text{ \AA}$  in this phase. Totally, in the first 1.5 ns, the dopamine moved by  $3 \text{ \AA}$  in the negative x-direction and  $2 \text{ \AA}$  in the y-direction while it moved  $12 \text{ \AA}$  in z-direction. The displacement curve started to increase as shown in Figure 3.4.6.



**Figure 3.4.7** Fifth (left one) and sixth (right one) snapshots of dopamine in the membrane. Dopamine molecule is represented as dots in purple.

After a detailed preparation stage of MD simulations, we started production runs and fifth, sixth and seventh snapshots are taken the different timesteps of production phases. In fifth snapshot which is taken from the timestep is 4 ns , dopamine coordinates are found to be, x direction 4.907 Å, y direction 13.063 Å and z direction 22.348 Å. Dopamine shows a the big displacement and it moved by approximate 5 Å in the x-direction and 13 Å in the y-direction while it moved 22.5 Å in z-direction with respect to initial coordinates. Next the sixth snapshot, dopamine showed less displacement and its coordinates are found to be, x direction 4.874 Å, y direction 15.521 Å and z direction 22.662 Å shown in Figure 3.4.7.

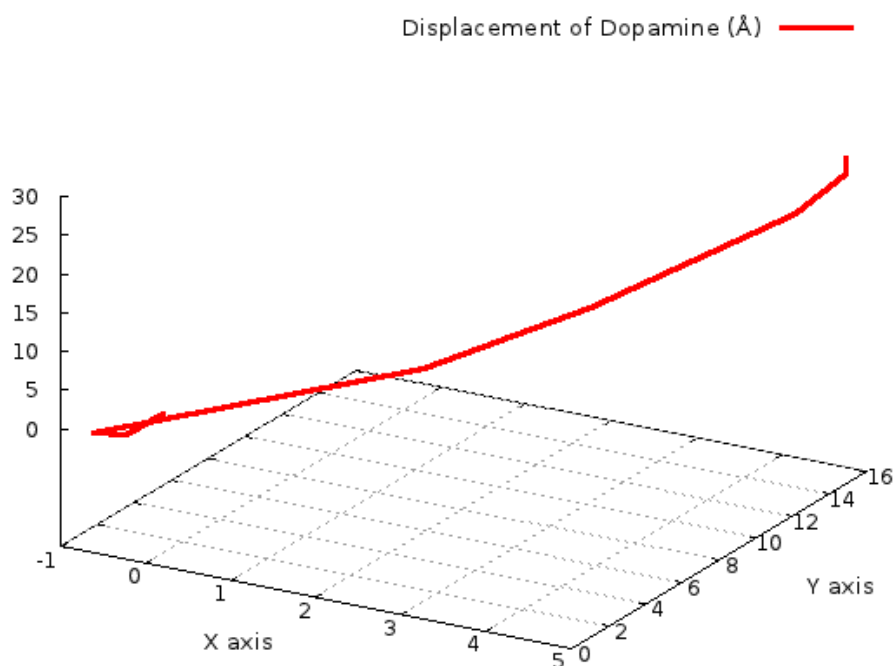


**Figure 3.4.8** Seventh snapshots of dopamine in the membrane. Dopamine molecule is represented as dots in purple.

Finally, the last snapshot seventh which is taken from the timestep is 15 ns, dopamine was completely out of the lipid molecules as shown in Figure 3.4.7. In this phase, dopamine coordinates are found to be, x direction 26.161 Å, y direction -9.660 Å and z direction 27.999 Å. Dopamine shows a big displacement again and it moved by approximate 26 Å in the x-direction and 9 Å in the y-direction while it moved 28 Å in z-direction also with respect to initial coordinates.

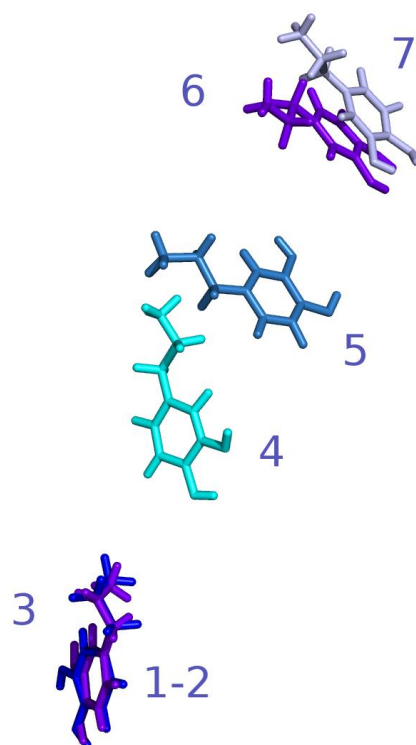
The RMSD of the Dopamine model along the trajectory, which is calculated after aligning the  $C_{\alpha}$  atoms of each snapshot to the initial frame. The RMSD values have been calculated according to the dopamine. Dopamine structure is aligned to its initial frame first, and then the RMSD value is calculated and its detected 1.506 Å.

Displacement was defined as the total change of location of the center of mass of the alpha carbon atoms of the ligand in x, y and z coordinates. The initial coordinates of the dopamine, was chosen as the reference point. Displacement values start at 0 Å and report motion of the dopamine atom with respect to the initial coordinates of this atom. Dopamine total displacement in x-, y-, z- directions was about 26 Å as shown in Figure 3.4.9, red curve.



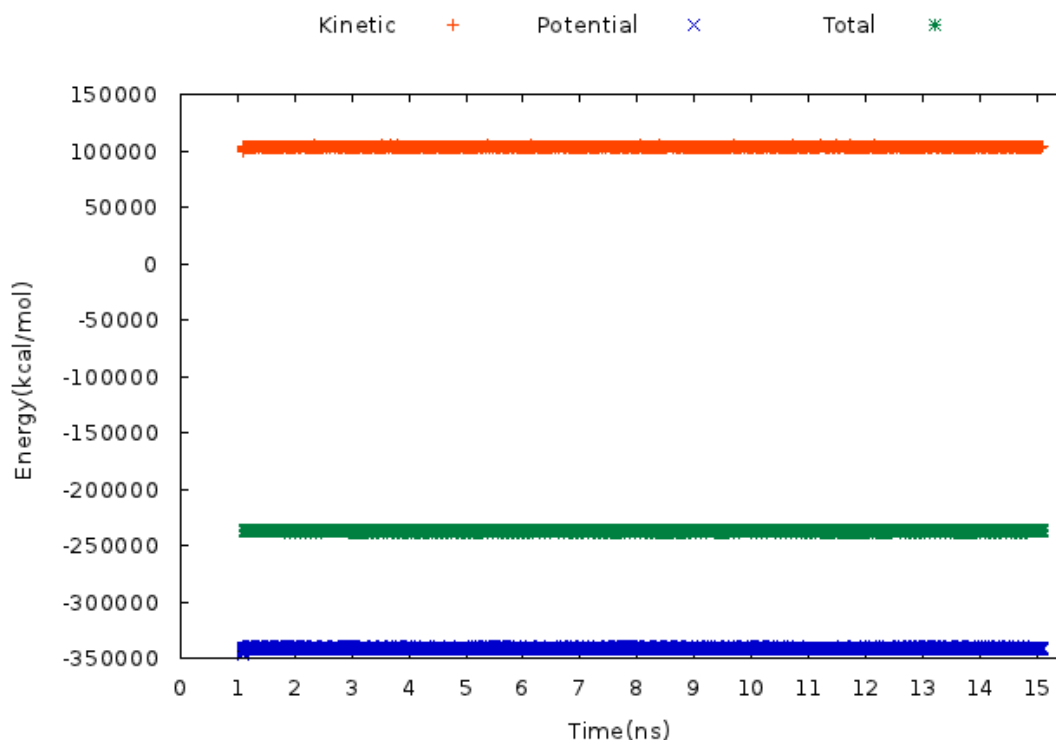
**Figure 3.4.9** The displacement of the dopamine in the 15 ns MD simulations for Dopamine model.

As mentioned before, dopamine went out from membrane as expected. Dopamine moves 14.5 ns of the total of simulation. You can see above in Figure 3.4.9 and Figure 3.4.10 moves gradually with a total displacement of 26 Å.



**Figure 3.4.10** Movement of dopamine ligand, step by step in the membrane.

Kinetic, potential and total energy values fluctuates around an average throughout the simulation. Simulation kinetic energy value is about 100.000 kcal/mol, potential energy value is about -350.000 kcal/mol, total energy value is -250.000 kcal/mol. Energy values of Dopamine model which is obtained from MD simulation, shown in Figure 3.4.11. Total energy average value is detected -237.368 kcal/mol, this value can be used to compare the DAT model and DAT-dopamine complex model and important in determining the binding energy.



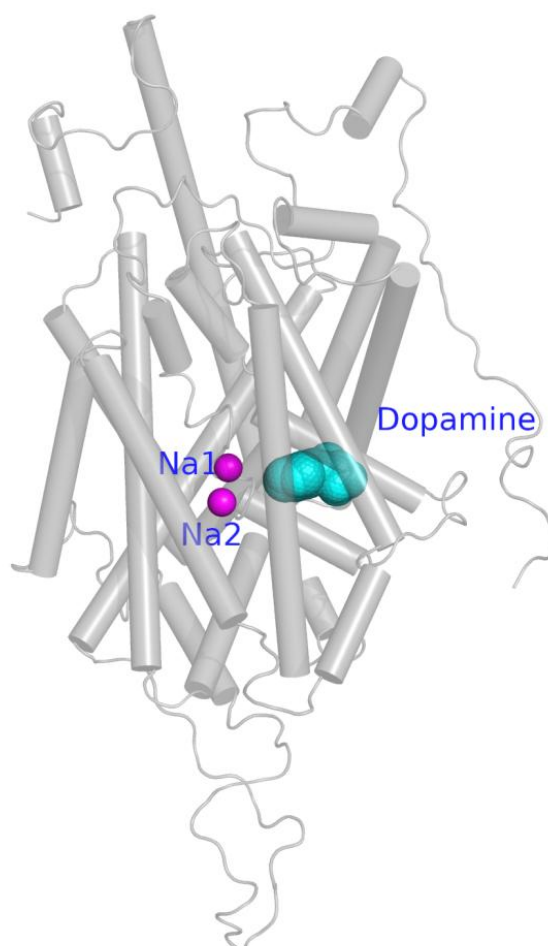
**Figure 3.4.11.** Kinetic, potential and total energy values of Dopamine model, which is obtained from MD simulations.

### 3.5. Molecular Dynamics (MD) Simulations of DAT-Dopamine Complex

The dopamine transporter (DAT), transports dopamine across the membrane which is located on the plasma membrane of nerve terminals. By taking into synaptic dopamine ligand into neurons, it plays a critical role in maintaining dopamine homeostasis and in terminating dopamine neurotransmission in the central nervous system [98-100]. The reuptake mechanism of dopamine is  $Na^+$  and  $Cl^-$  dependent, and follows a sequence of events where one dopamine molecule or two sodium ions initially bind to the dopamine transporter protein, followed by binding of one chloride ion to the transporter [32]. The inwardly directed  $Na^+$  gradient provides energy for an inward movement of dopamine molecule against a concentration gradient [33]. The transporter require  $Na^+$  ion accessing of dopamine and the first

step initiating the uptake cycle is thought to be the identification of dopamine molecule as a reversible binding interaction with the dopamine transporter [101].

How dopamine transporter (DAT) interacts with  $Na^+$  and dopamine, and goes through the cell membrane is described above according to previous studies. In our study, we placed the dopamine and dopamine transporter in the membrane, complex form of dopamine and DAT, which is created by molecular docking shown in Figure 3.5.1. 2  $Na^+$  and 5  $Cl^-$  ions are embedded into the membrane with complex structure, to make the total net charge of the system equal to zero. In this chapter we examined the ‘DAT-dopamine complex’ model system preparation stages for Molecular Dynamics (MD) simulations, simulation details and how it behave in the membrane with dopamine.



**Figure 3.5.1.** Structural model of human DAT and dopamine complex. DAT is represented as cylindrical helices in gray, dopamine shown in cyan dots with two  $Na^+$  ions in magenta.



### 3.5.1 Molecular Docking of Dopamine Transporter and Dopamine

As explained detailed in the following chapter, in the molecular modeling field, the process of docking a ligand to a binding site consists in mimicking the natural course of interaction of the ligand and its receptor via a lowest energy pathway.

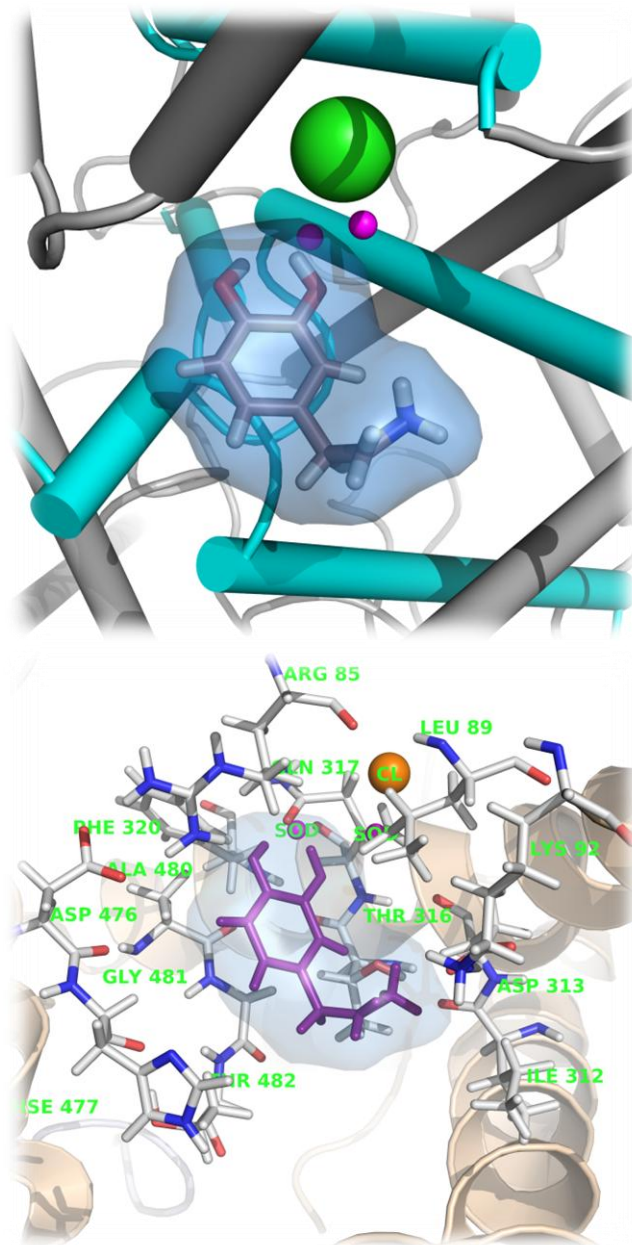
Based on the structural model of DAT which is obtained in this study and is taken from DAT model production phase, the binding mode of dopamine with DAT was explored through molecular docking by using the Autodock 4.0 program.

Firstly ligand and receptor's coordinate files which include informations for AutoGrid and AutoDock are prepared. For making docking calculation fastly, precalculated gridmaps which are created by AutoGrid used in Autodock. A grid map consists of a three dimensional lattice of regularly spaced points, surrounding (either entirely or partly) and centered on some region of interest of the macromolecule. In our study, the grid size was set to be  $70 \times 70 \times 70$  and the grid space default value was  $0.375 \text{ \AA}$ . After AutoGrid calculation, we created the a docking parameter file that specifies the files and parameters for the docking calculation. AutoDockTools may be used to generate the docking parameter file, as described below, which typically has the extension "dpf". We have chosen the Lamarckian genetic algorithm (LGA) search methods. In grid box minimized ligands were randomly placed. Docking parameters were as follow: torsion step is 50, torsional degrees of freedom 3, number of enery evaluations 2500000 and run number of 100. After docking process, Autodock gives a log file which include the coordinates for each docked configuration along with information on clustering and interaction energies.

Binding energy of the ligand to the active site is the most important result from a docking process .For choosing the best inhibitor this binding energy value can be compared between different compounds. In our study, after the docking process with AutoDock 4.0 program, is determined the best pose of dopamine based on binding

energies. The dopamine transporter and dopamine have -5.73 kcal/mol binding energies in this phase.

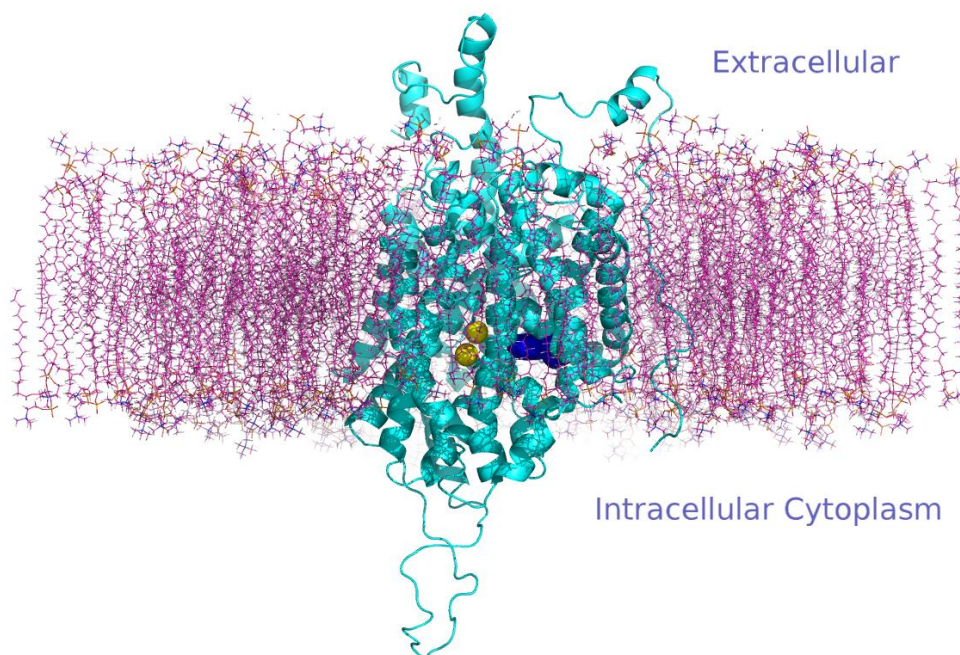
The dopamine-binding site in our human DAT structure was made by unwound regions of helices 1, 6 and 10, which was close to the sites of  $Na^+$  and  $Cl^-$  -binding, as seen in Figure 3.5.2. The residues around the activesite, that can have important roles in binding, are Arg 85, Leu 89, Lys 92, Ile 312, Asp 313, Thr 316, Gln 317, Phe 320, Asp 476, Hse 477, Ala 480, Gly 481 and Thr 482.



**Figure 3.5.2.** Figure above is typical structure of the DAT-dopamine binding complex, snapshottaken from after Autodock. Viewing the dopamine molecule (shown as ball-and-stick) in the complex model. Only helix part of the DAT is shown as cylindrical helices, two Na ions shown as dots in magenta and Cl ions shown as dots in green. Helices 1, 6 and 10 are represented in cyan to indicate the relative position of dopamine in DAT. Figure below one shows that dopamine in the binding site interacts basicly with residues of TMH 1,6 and 10. Residues from DAT within 5 Å of dopamine are labeled and shown in stick style, while dopamin is shown in purple stick.

### 3.5.2. System Preparation for MD

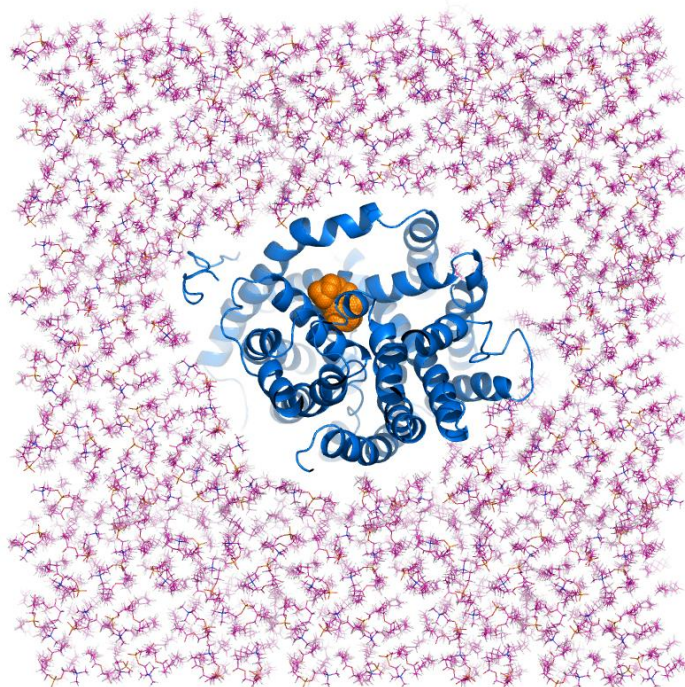
DAT-dopamine complex structure is embedded in the membrane according to its hydrophobic part shown in Figure 3.5.3. It's relative orientation in the lipid bilayer was determined by referring the similar orientation of the LeuT<sub>Aa</sub> structure [31,35].



**Figure 3.5.3.** The human DAT and dopamine complex model in the cell membrane. DAT is represented as a cyan cartoon, dopamine as a blue dot, and two  $Na^+$  ions as yellow spheres.

Direction of the x and y dimensions of the cell membrane have been determined according to the same direction of protein's x and y dimensions. The distance between min and max coordinates in the x direction is found to be 73 Å distance between two farthest atoms in the protein. The same way, the distance between min and max coordinates in the y direction is found to be 99 Å distance between two farthest atoms in the protein. Accordingly, the protein's dimensions in the x direction and y direction are determined to be 73 Å and 99 Å. The membrane's dimensions in these directions are set to 120 Å × 120 Å, in order to avoid any interaction between the protein and its own image in the periodic box at this direction. For

alignment of the membrane and the protein, the membrane's center of mass translated to the origin and it is combined with the protein-water system. The next step, a room is made for the DAT in the membrane layer is shown in Figure 3.5.4., cut-off distance between protein and lipid is usually set 0.8 Å-1.6 Å. This way, overlap between the protein and any lipid molecules is avoided.

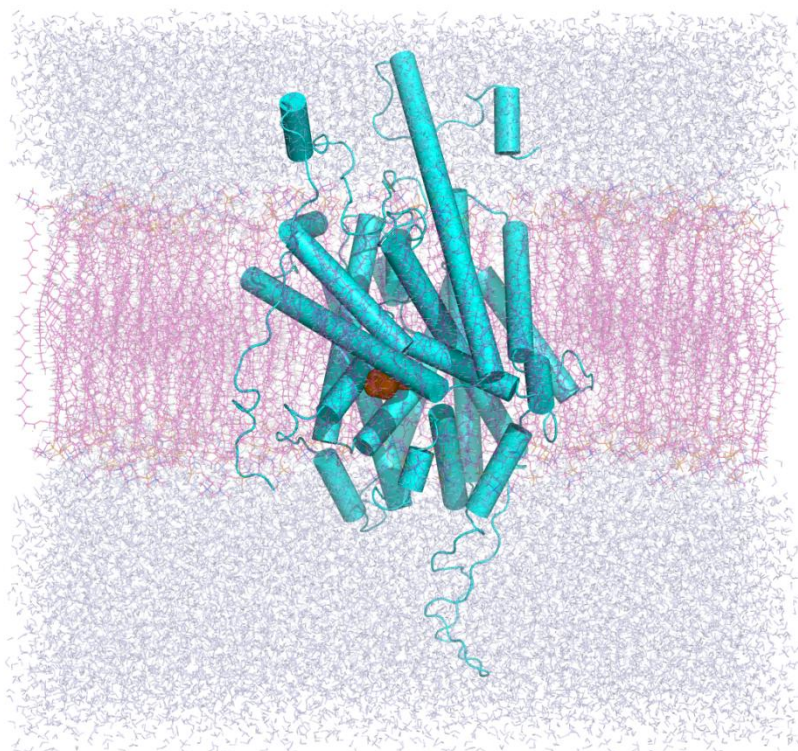


**Figure 3.5.4** The position of the DAT-dopamine complex model in the cell membrane.

After the complex model is embedded in the cell membrane it's solvated by two layers of water molecules at each side of lipid bilayer. The distance between min and max coordinates in the z direction is found to be 75 Å distance between two farthest atoms in the protein. TIP3W water molecules with a thickness of around 12 Å at both directions of z-axis are added to the cell membrane and protein. The dimension of the system at this direction is set to 100 Å. You can see in Figure 3.5.5. the final situation of the system along with cell membrane and water molecules at the x direction. The structure's dimensions at x, y and z directions, approximate cell dimensions and dimensions of the system is given in following Table 3.12.

**Table 3.12.**The DAT complex structure, cell membrane and system dimensions.

<b>Structure Dimension</b> xyz (Å)	<b>Cell Membrane</b> xy (Å)	<b>Box Dimensions</b> xyz (Å)
73×99×75	120×120	120×120×100



**Figure 3.5.5** Structural model of human DAT and dopamine complex in the physiological environment used for MD simulations. DAT protein is represented as cylindrical helices in cyan, dopamine shown in orange, water molecules are shown in blue and lipid molecules are indicated as sticks in pink.

2  $Na^+$  and 5  $Cl^-$  ions were added with a concentration of 0,154 mol/L by Autoionize Plugin v1.2 of VMD to make the total net charge of the system equal to zero.

### 3.5.3 Simulation Details and Production MD run

A series of energy minimizations and MD simulations were performed by using Nanoscale Molecular Dynamics (NAMD) software package. At the first preparation stage, only lipid molecules are allowed to be mobile, protein is fixed. The system was run 300.000 steps of minimization under these conditions and later to an MD simulation of 0.5 ns. Next, water molecules and the cell membrane are allowed to move freely and the harmonic constraints have been imposed on the protein. Similar to the first stage, the system under these conditions is exposed to a 1000 step minimization followed by an MD simulation of 0.5 ns. The protein released along with surrounding molecules is exposed to a MD simulation of 0.5 ns, at the third preparation stage. After a detailed preparation stage an MD simulations of 20 ns for the whole system have been performed. The simulation details are summarized in Table 3.13.

**Table 3.13** DAT complex simulation system details.

Simulation Length (ns)	Final System Size xyz (Å)	Number of Water Molecules	Number of Lipids	Number of Ions	Total Number of Atoms
20	125×125×120	34.310	43.684	7	156.188

CHARMM22 force field for protein, CHARMM27 force field for lipids and the topology file which is we defined for dopamine were used for the interaction potentials. Temperature of the simulation was set to 310K and the pressure was kept at 1 bar by Berendsen weak-coupling approach [97]. The simulation space partitioning parameter cutoff was set to 12 Å. The other simulation space partitioning parameter ‘pairlistdist’ which is distance between pairs for inclusion in pair lists was set to 13.5 Å. PME (Particle-Mesh Ewald) method was used for long-range electrostatic interactions. The ‘timestep’ parameter was set to 2.0 fs.

The ‘nonbondedFreq’ which is timesteps between nonbonded evaluation was set to 1 and the ‘fullElectFrequency’ parameter which is distance between pairs for inclusion

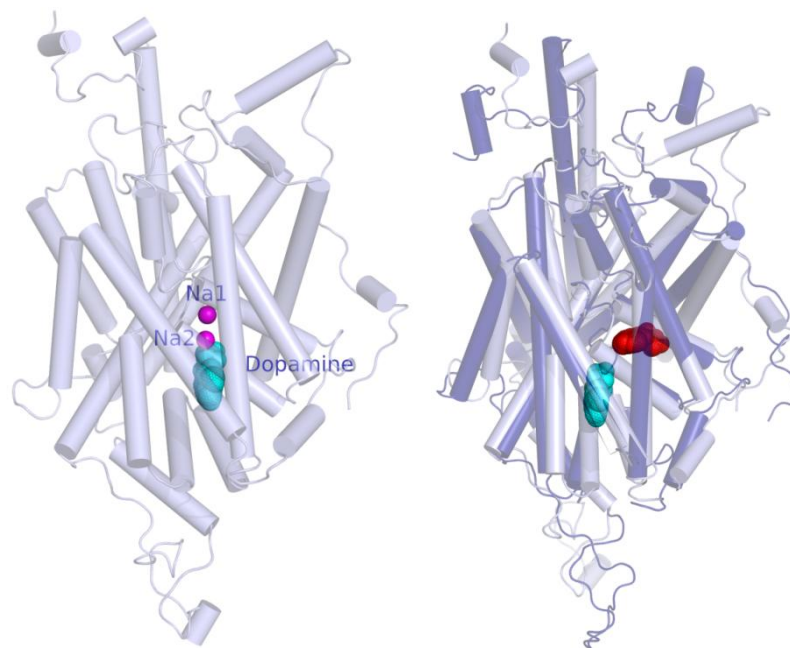
in pair lists was set to 2. 'useGroupPressure', 'useFlexibleCell' and 'useConstantArea', which are the pressure control parameters, were set to yes.

The 'restartfreq' which is the frequency of restart file generation, the 'dcdfreq' which is the timesteps between writing coordinates to trajectory file and the 'xstfreq' which shows how often to append state to XST file were all set to 1000 (every 2 *ps*). The 'outputEnergies' which is the timesteps between energy output and the 'outputPressure' which is the timesteps between pressure output were set to 50.

### **3.5.4 Analysis**

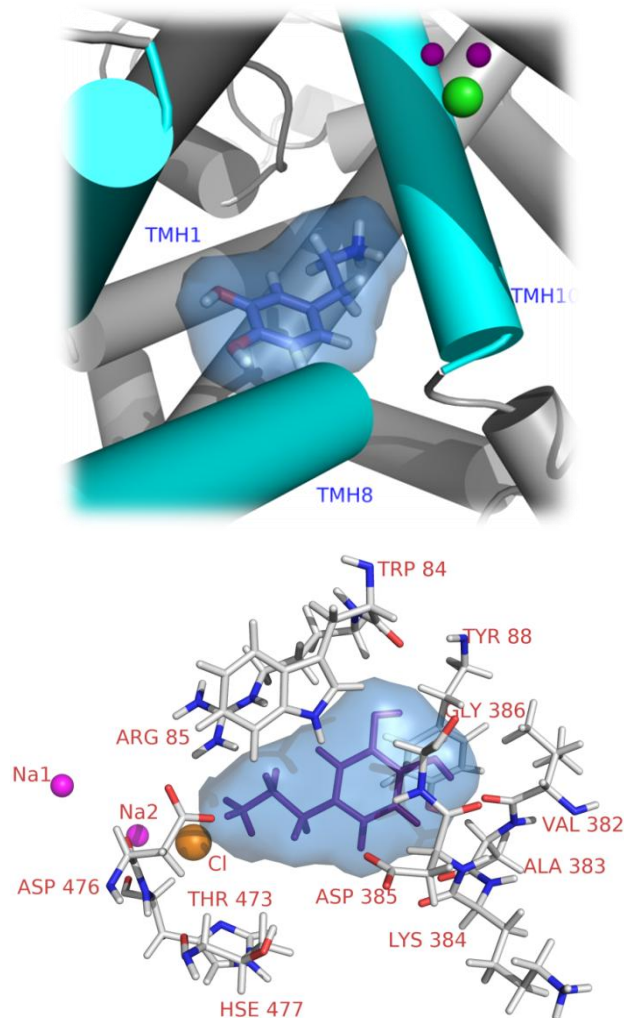
This part of the study, we placed the dopamine and dopamine transporter into the membrane, as a complex form, which is created via molecular docking, to see, when dopamine and DAT inserted into the membrane as a complex how they behave and what changes they are showing according to the initial position. The differences which will be described in detail below. The first one is difference in dopamine binding site as shown in Figure 3.5.6.





**Figure 3.5.6.** Right Figure is after molecular dynamics simulation structural model of human DAT and dopamine complex. DAT is represented as a cylindrical helices in gray, dopamine shown in cyan dots with two  $Na^+$  ions in magenta. Left Figure is structural alignment of complex structures, after and before molecular dynamics simulation and positions of dopamine. Before md simulation complex structure is represented as cylindrical helices in blue, dopamine shown in red dots, after md simulation complex model is represented as similar as in the right figure.

We can see in Figure 3.5.6, dopamine changed its position, the new dopamine-binding site in DAT was made by unwound regions of helices 1, 8 and 10 which was close to the sites of  $Na^+$  and  $Cl^-$  -binding, as seen in Figure 3.5.7. In a typical structure of the MD-simulated dopamine-DAT complex at the 20ns snapshot of the MD trajectory, dopamine was located in a totally dehydrated pocket.



**Figure 3.5.7.** Figure above is typical structure of the DAT-dopamine binding complex, snapshottaken from after MD simulation. Viewing the dopamine molecule (shown as ball-and-stick) in the complex model. Only helix part of the DAT is shown as cylindrical helices, two Na ions shown as dots in magenta and Cl ion shown as dots too in green. Helices 1, 8 and 10 are represented in cyan to indicate the relative position of dopamine in DAT. Figure below one shown that dopamine in the binding site interacts basicly with residues of TMH 1, 8 and 10. Residues from DAT within 5 Å of dopamine are labeled and shown in stick style, while dopamin is shown in purple stick.

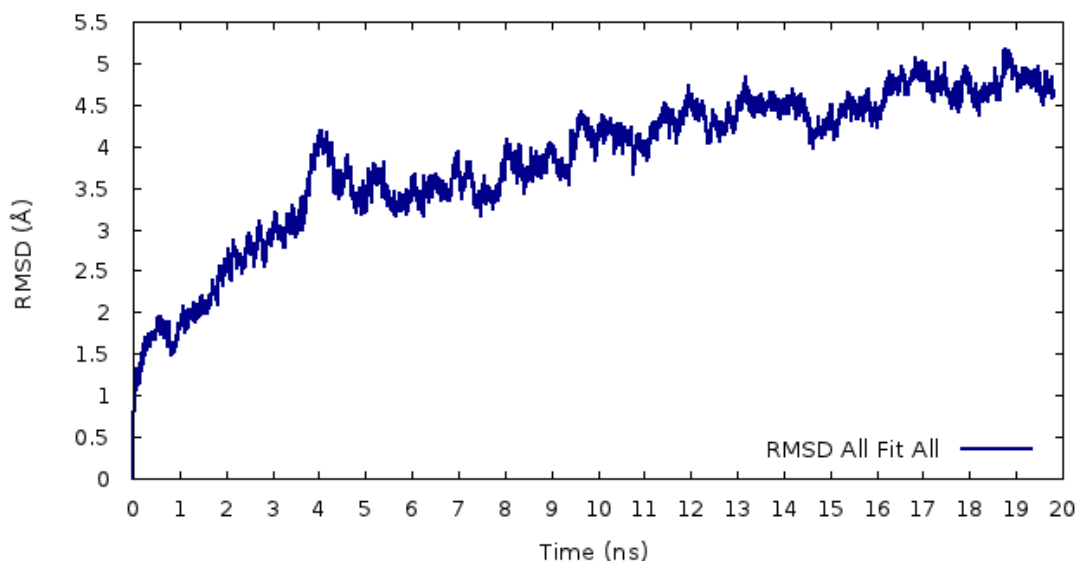
**Table 3.14.** The residues in the binding sites pertaining to the before and after MD-simulated DAT-dopamine complexes. Common residues found in these regions are shown in dark.

Before MD Simulation Binding Site Regions			After MD Simulation Binding Site Regions	
Arg 85	Gln 317	Thr 482	Thr 84	Asp 385
<b>Leu 89</b>	Phe 320		<b>Arg 85</b>	Gly 386
<b>Lys 92</b>	<b>Asp 476</b>		Tyr88	Thr 473
<b>Ile 312</b>	<b>Hse 477</b>		Val 382	<b>Asp 476</b>
<b>Asp 313</b>	Ala 480		Ala 383	<b>Hse 477</b>
<b>Thr 316</b>	Gly 481		Lys 384	

The residues around the active site, that can have important roles in binding, are shown in Table 3.14. As seen in the above table Arg 85, Asp 476 and Hse 477 are the common residues in interaction with dopamine, before and after Molecular Dynamics simulations. According to the commonality of binding residues, we can say that MD simulation affected binding of DAT-dopamine and changed the binding site.

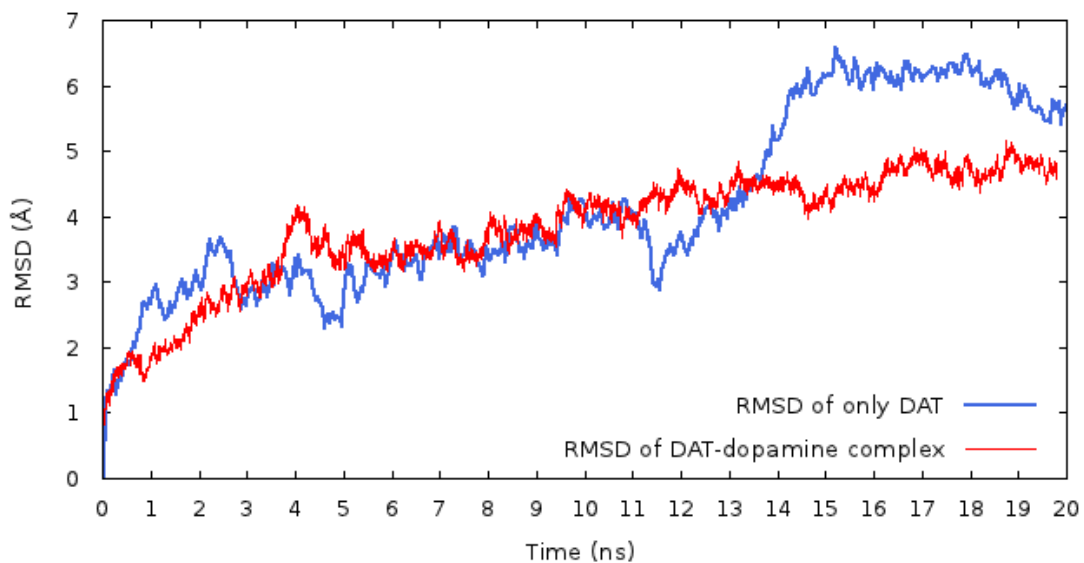
More interestingly, Arg 85 and Asp 476 make strong interactions with the ion. The minimum distance between the charged side chains of this pair of residues, with the ion was  $<3 \text{ \AA}$  at most of the snapshots. These dynamic changes reveal that the Na<sup>+</sup>-bound DAT was stabilized by the binding of dopamine.

The RMSD of the DAT-dopamine complex model along the trajectory, which is calculated after aligning the  $C_{\alpha}$  atoms of each snapshot to the initial frame, is plotted in Figure 3.5.8. The RMSD plot shows the extent of deviation from the initial conformation and the conformational changes throughout the trajectory. The RMSD values have been calculated according to the all complex structure. Whole complex structure is aligned to its initial frame first, and then the RMSD value is calculated.



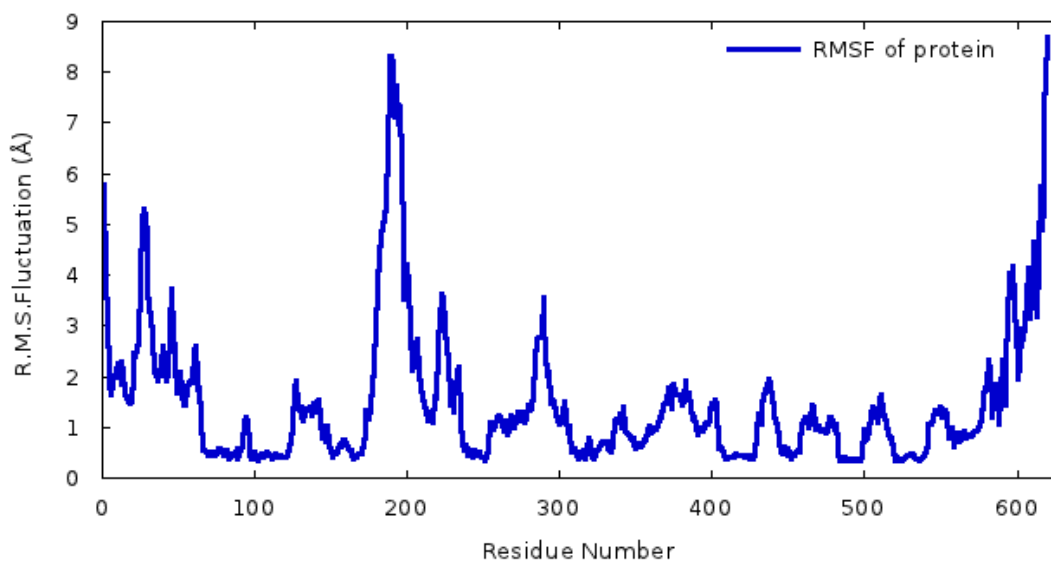
**Figure 3.5.8.** RMSD values which were obtained from 20 ns MD simulations for DAT-dopamine complex model.

As described in previous sections DAT model after a detailed preparation stage an MD simulations of 200 ns for the whole system have been performed. For the complex model an MD simulation of 20 ns for the whole system have been performed. For comparison DAT and DAT+dopamine simulations, initial 20 ns part of DAT simulation, extracted from 200 ns MD trajectory, is considered. The dynamic behavior of the DAT-dopamine complex and DAT have been monitored by the  $C_{\alpha}$  RMSD changes shown in Figure 3.5.9. As shown in Figure 3.5.9, during the first 3 ns and 13 ns to 20 ns of the MD simulation,  $C_{\alpha}$  RMSD change of DAT dopamine complex was smaller than that of the corresponding DAT structure without dopamine.



**Figure 3.5.9** Plots of the  $C_{\alpha}$  RMSD in the simulated DAT and DAT-dopamine structures versus the simulation time (nanoseconds).

The best way to numerically express the protein's mobility along the simulation is to generate the RMSFs profile as mentioned before. RMSF are calculated from the production phase of the trajectory and calculations are carried out over the conformations aligned to the average structures of the simulations using only  $C_{\alpha}$  atoms. DAT's RMSF profile, which is obtained from MD simulation, shown in Figure 3.5.10.

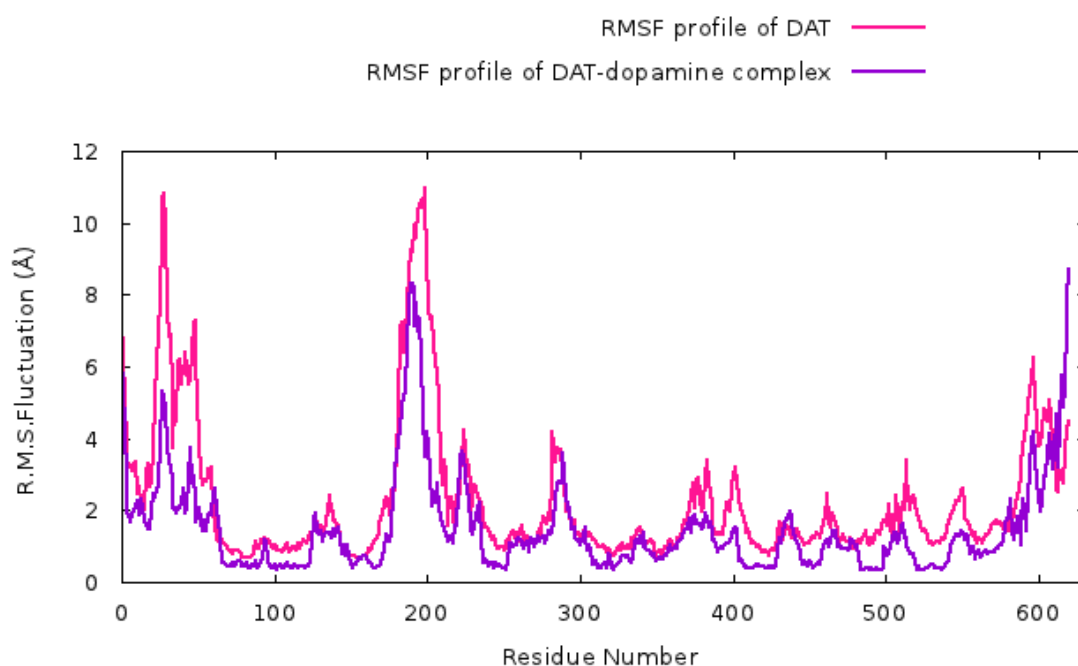


**Figure 3.5.10** RMSD about the average position plotted for  $C_{\alpha}$  atoms of residues for MD result.

According to these profile, the highest mobility of the protein is observed at the extracellular loop and between residue 585-620, facing outside the cell. The second mobile region is detected at intracellular loop and between residue 180-205. After 2.loop, the third highly mobile region is detected at extracellular loop and between residue 1-65.

When looking the RMSF profile of DAT without dopamine simulations on previous section, changing of loop regions can be observed. This indicates that running of MD simulation together with dopamine effects on DAT protein's conformational dynamics.

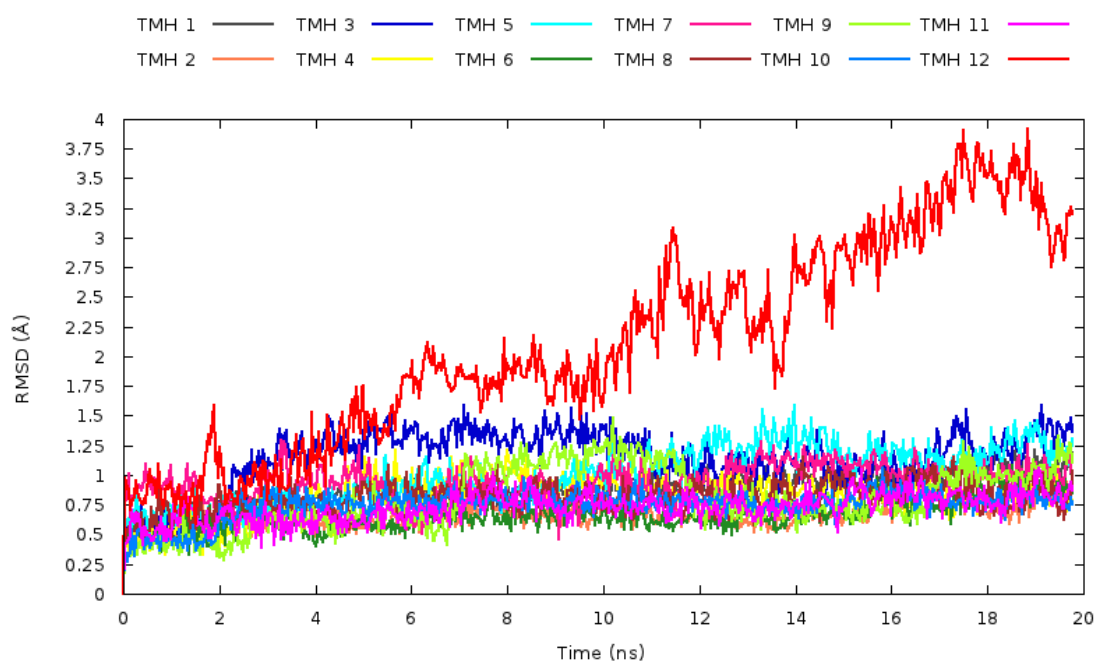
As chart of DAT and DAT-dopamine complex RMSD profile, in the same way, when we generated the RMSF profile for DAT and DAT-dopamine complex in the same chart, it can be observed that change in DAT dopamine complex was much smaller than that of the corresponding DAT structure without dopamine. There is a  $\sim 2.5$  Å difference between two MD simulated model shown in Figure 3.5.11.



**Figure 3.5.11** RMSF about the average position plotted for residues which were obtained from 200 ns MD simulations of only DAT for all structure and 20 ns MD simulations of DAT with dopamine.

According to these RMSF profile, mobility is observed in the approximately same regions but in different amounts. Highest mobile region is observed at the intracellular loop and between residue 180-205, in DAT model but complex model highest mobility is observed at the extracellular loop and between residue 585-620. The second mobile region is detected at extracellular loop and between residue 12-65 in DAT model but complex model's second mobile region is detected at intracellular loop and between residue 180-205. Likewise the third highly mobile region is detected at extracellular loop and between residue 595-610, facing outside the cell for DAT model and at extracellular loop and between residue 1-65 for complex model.

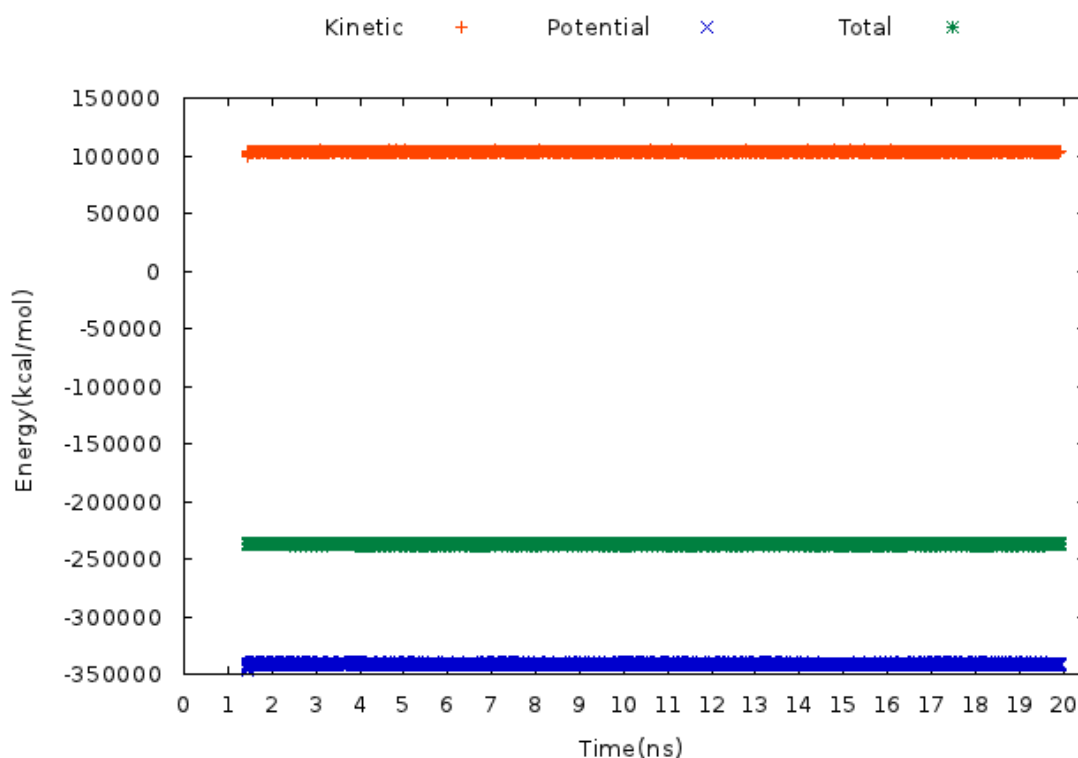
During molecular dynamics simulations to see clearly what changes on the helices in detail, RMSD charts were created. They contain the RMSD values of separately helices as shown in Figure 3.5.12



**Figure 3.5.12** Root Mean Square Deviation values which were obtained from 20 ns MD simulations for all helix regions on DAT-dopamine complex model.

When we look at the RMSD profile of structure, we see that values are proportional to the RMSF profile of structures. Among all transmembrane helices, the most mobile ones are the twelfth, the fifth and thirteenth helices (TMH12, TMH5, TMH3). Most of the helices reach equilibrium at 2-3 ns at a value of  $\sim 1$  Å. However, the biggest helix TMH12 is fluctuating through the simulation. The helices TMH1, TMH8 and TMH10 which binding with dopamine, are remain stable with respect to TMH12, TMH5 and TMH3 can be observed.

Kinetic, potential and total energy fluctuates around averages throughout the simulation. Simulation kinetic energy value is about 100.000 kcal/mol, potential energy value is about -350.000 kcal/mol, total energy value is -250.000 kcal/mol and seen that fluctuate the around this values. Energy values of DAT-dopamine complex model which is obtained from 20 ns MD simulation, shown in Figure 3.5.13. Total energy average value is detected -234.019 kcal/mol, this value necessary to compare the DAT model and DAT-dopamine complex model and important in determining the binding energy.



**Figure 3.5.13.** Kinetic, potential and total energy values of DAT-dopamine complex model, which is obtained from MD simulations.



## Chapter 4

### Clustering Analysis

#### 4.1 Clustering Analysis Methodology

In this part of the study, we used Molecular Dynamics simulation results which are explained in previous chapters. A representative set of different structures can be selected among the large number of conformations generated by MD simulations for subsequent analysis using the cluster analysis. Cluster analysis groups conformations according to a similarity of measure, which is RMSD in this case.

Procedures of cluster analysis requires a similarity matrix in which each element represents the structural difference between a pair of conformations. Matrix of similarity is constructed by measuring the distance between frames using the (RMSD):

$$RMSD = \sqrt{\frac{\sum_{i=1}^N d_i^2}{N}} \quad (4.1)$$

where  $N$  is the number of atoms over which the RMSD is measured and  $d_i$  is the distance between the coordinates of atom  $i$  in the two structures, when they are superimposed [102].

In this work, k-means clustering method that is part of the *kclus*t module of Multiscale Modeling Tools for Structural Biology (MMTSB) Tool Set [103] is used to reduce the conformational space and identify a few distinct clusters or conformational states that are generated during the simulation. k-means, which is a high-performance clustering algorithm, starts by randomly choosing groups of frames from the MD trajectory, each of which is assigned to its own cluster. It is then iterated over all other frames. Each frame is assigned to the cluster whose centroid is closest; the centroid for this cluster is then recomputed. The iterative procedure continues until all frames are assigned to their clusters. The clusters and the centroids are updated after each iteration step. The number of clusters is a parameter which depends on the cutoff value of RMSD (cluster radius); as RMSD cutoff increases less number of clusters are found by the algorithm. After all these calculations, the conformation, which is closest to the centroid, is selected as the representative snapshot of that cluster.

## 4.2 Clustering Results of MD Trajectory Snapshots

In this part, we made clustering according to overall structure and according to binding site. We used for this process DAT model snapshots taken from 200 ns MD trajectories. The program used for cluster analysis is the *kclus*t script.

As mentioned before, in the clustering of the conformations k-means clustering method was used. This method uses an algorithm that goes through the MD trajectory and locates clusters of conformations that are the same by grouping them together using RMSD as the similarity measure. From this it creates centroids (cluster center) describing each cluster and then gives an RMSD for every structure in the trajectory with respect to each identified centroid. An average structure for each cluster centroid is produced. However, this is not quite physical since it is just a mathematical average rather than a real-visited conformation, it meaningful one. The structure that is nearest to the centroid is a more physically relevant to the structure of the centroid, which is called the cluster best member (BM). Therefore, these best members are used for the analysis.

To understand the extent of conformational change, all simulations of DAT model is merged and clustered at different RMSD thresholds. MD snapshots are clustered according to the binding-site residues and the overall structure in order to get distinct conformations. These binding-site residues used in clustering analysis were determined previously according to experimental and computational studies taking place in the literature. After that we used these conformations in docking studies to investigate the relation between conformational changes and the binding sites.

The total length of the simulation for DAT model is 200 ns that produce 100000 snapshots. This 100000 snapshots is strided 1000 frame data to clustering analysis for each cluster proces. For first cluster proces which is determined according to overall structure of DAT, cluster radius 1.9, 2.5 and 3.0 were used. Second cluster proces is based on binding-site residues which are chosen as; Asp 79, Val 152, Tyr 156, Phe 76, Ala 77, Asp 79, Ser 149, Ser 422, Phe 320, Ser 321, Ala 423, Leu 322, Gly 323, Phe 326, Val 328 and Gly 426 [108-117,13,100,23]. For the latter case cluster radius 3.0, 2.0 and 1.3 were used. In general the smaller cluster radius values produce more clusters, often unmanageable and insignificantly different from each other. In our studies, distinguishable clusters are obtained with a threshold of 3.00 Å RMSD in the first case. For second cluster process, cluster radius 1.3 gave better results. An overview of the clusters formed and their details are given in Table 4.1 and Table 4.2.

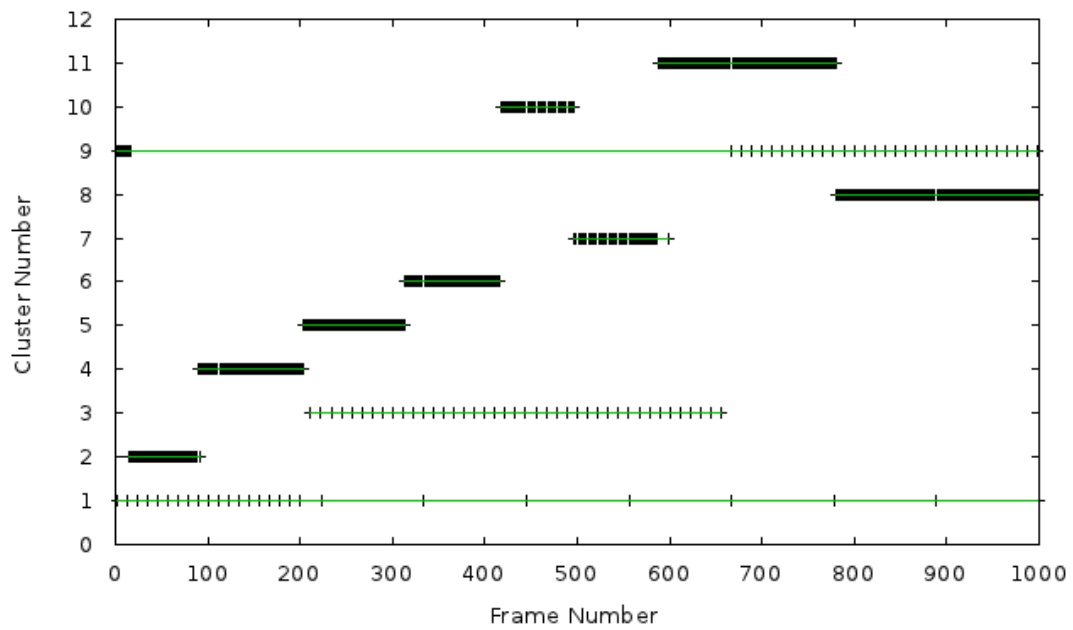
**Table 4.1** Cluster members and best members (BM) resulting from cluster radius of 3.0 Å with overall structural considerations.

	<b>Cluster #</b>	<b>RMSD from Cluster Centroid (Å)</b>	<b>BM Snapshot #</b>	<b>No. Of Members</b>
All Structure (RMSD Threshold : 3Å)	1	1.3376	7	28
	2	1.6603	150	68
	3	1.561	40	41
	4	1.5639	234	102
	5	1.4339	343	99
	6	1.423	439	93
	7	1.2786	578	82
	8	1.4519	914	198
	9	1.5243	90	44
	10	1.4296	509	72
	11	1.5916	726	173

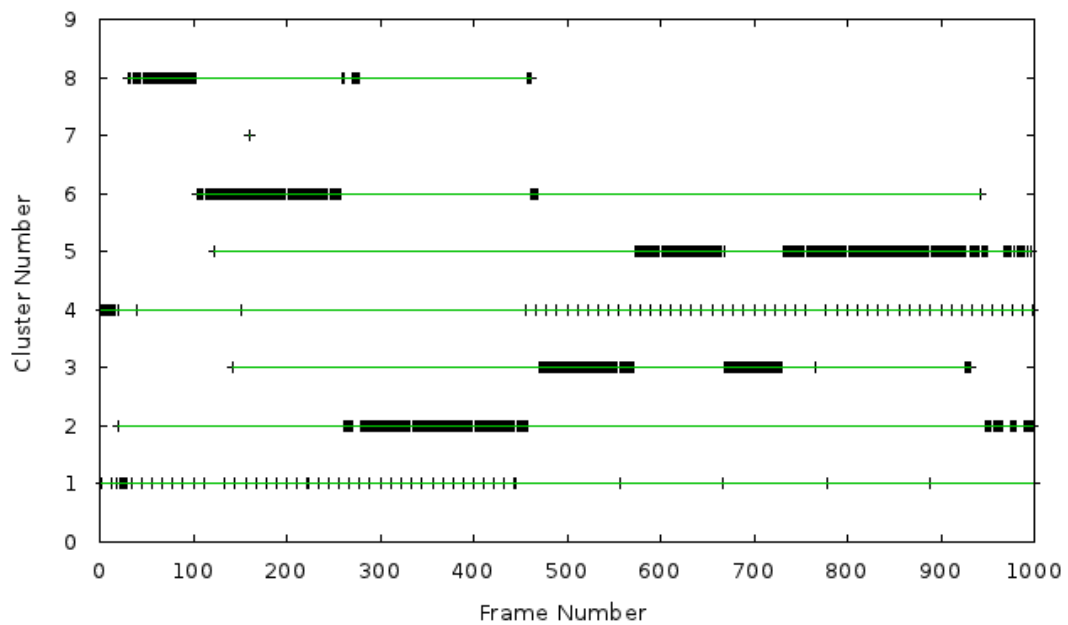
**Table 4.2** Cluster members and best members (BM) resulting from cluster radius of 1.3 Å when binding-site is taken as reference.

	Cluster #	RMSD from Cluster Centroid (Å)	BM Snapshot #	No. Of Members
Binding Site (RMSD Threshold : 1.3Å)	1	0.597	27	59
	2	0.6652	498	198
	3	0.6149	708	157
	4	0.6243	81	67
	5	0.6135	892	294
	6	0.7074	266	145
	7	0.000	243	1
	8	0.601	165	79

A more detailed picture of cluster evolution as a function of time is given in Figure 4.1 and Figure 4.2. In these figures, the cluster conformations are given in the order of their appearance in the trajectory. Figure 4.1 shows the cluster evolution in time for the DAT model clustering with respect to overall structural radii of 3.0 Å. Figure 4.2 shows the cluster evolution in time for the DAT model clustering with respect to binding-site regions with cluster radii of 1.3 Å. The number of clusters are eleven and eight for the respective cases. The clustering approach extracts unique conformational states sampled throughout the time span of the simulations. As seen, a cluster could have members at different times of the trajectory, which may indicate the dynamic equilibrium between the conformational states.

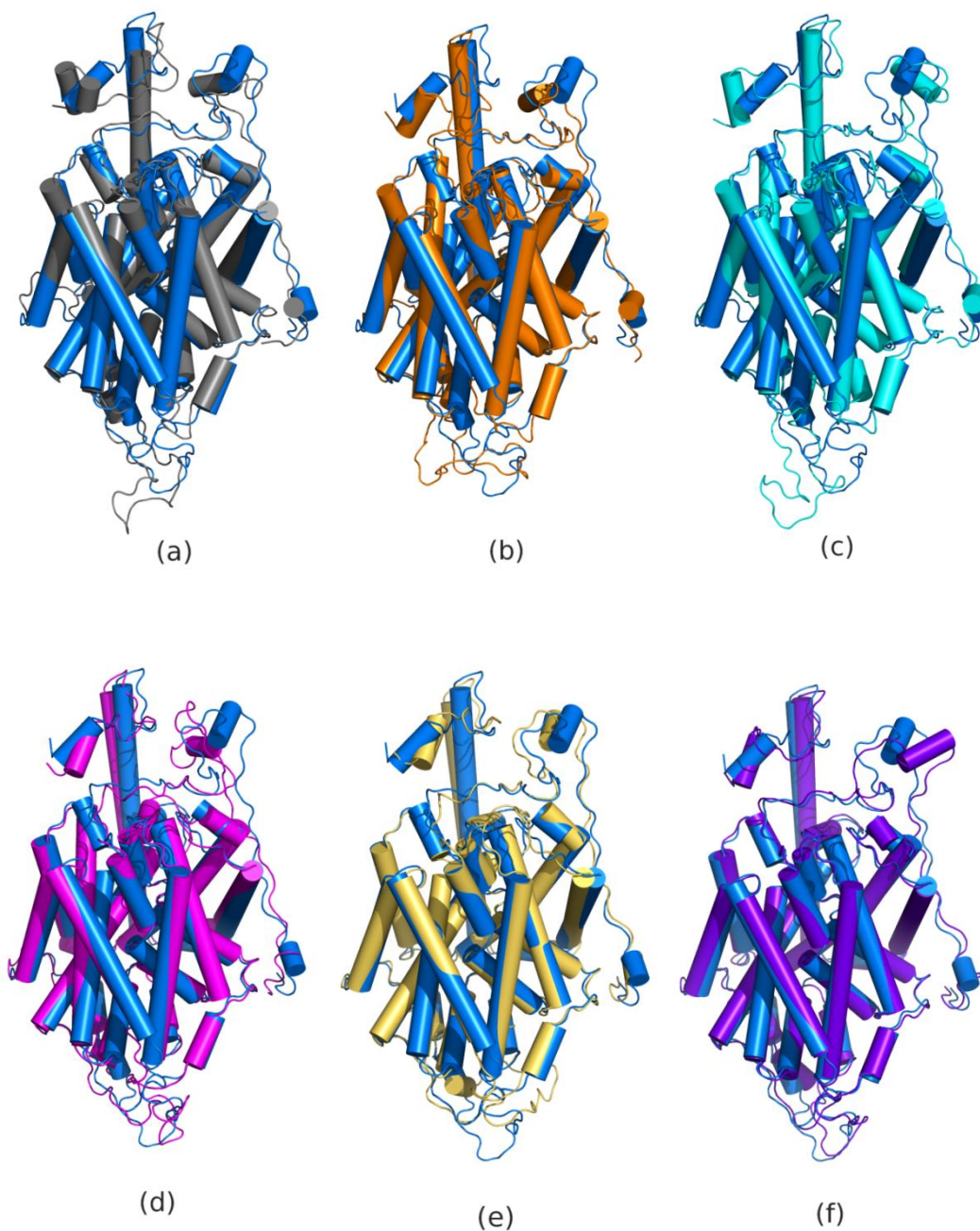


**Figure 4.1** Clustering of the simulation according to all structural information using a RMSD threshold of 3.00 Å.

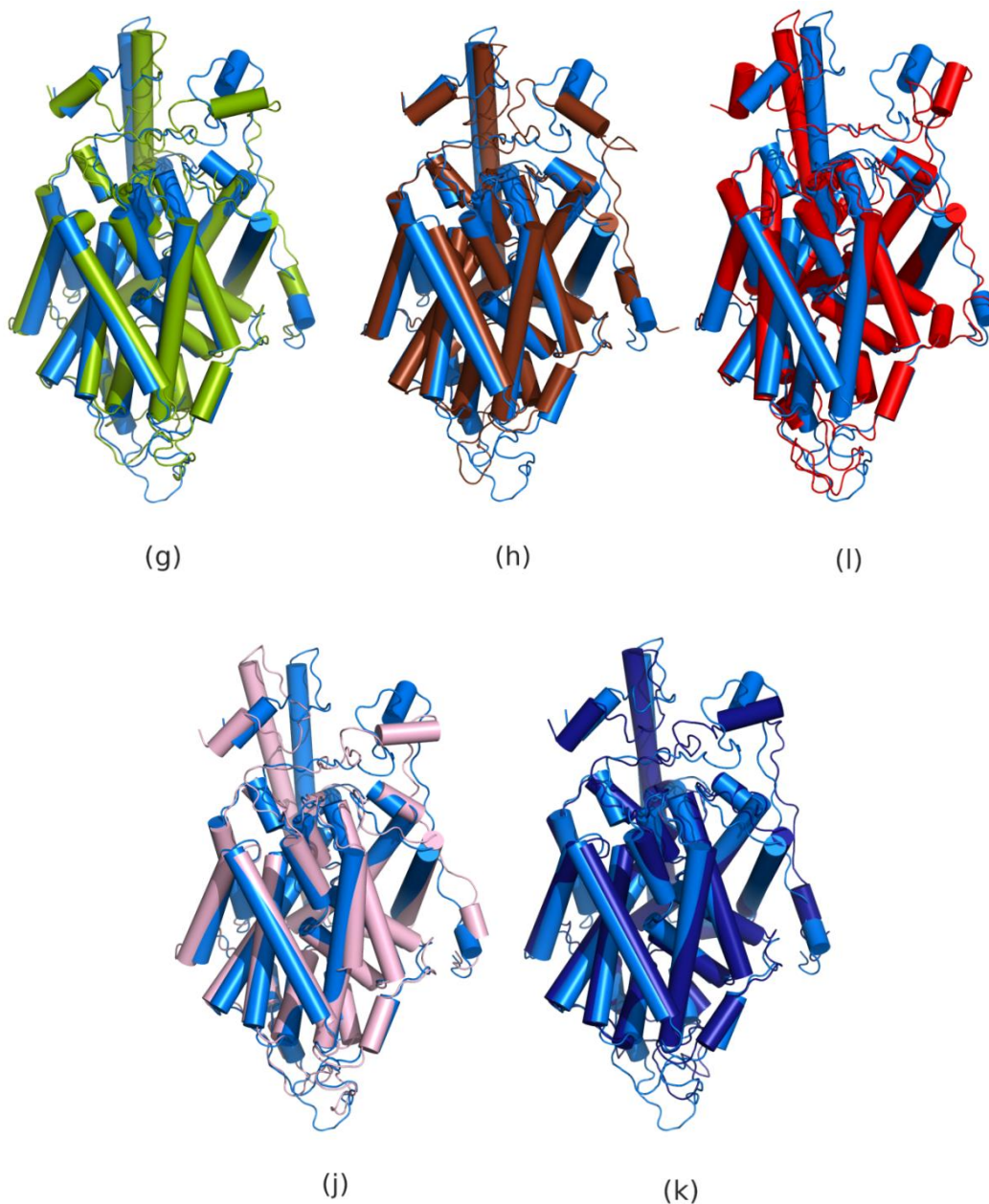


**Figure 4.2** Clustering of the simulation according to binding site region using a RMSD threshold of 1.3 Å.

The cluster best members of the clustering with respect to all structure formed with a cluster radii of 3.00 Å and clustering with respect to binding-site formed with a cluster radii of 1.3 Å are examined in detail. The representative members of first clustering according to overall structure, are presented as cartoon in Figure 4.3. Each member was aligned with respect to the initial structure of DAT. As shown in Figure 4.3, the clustering profile reveals eleven clusters.



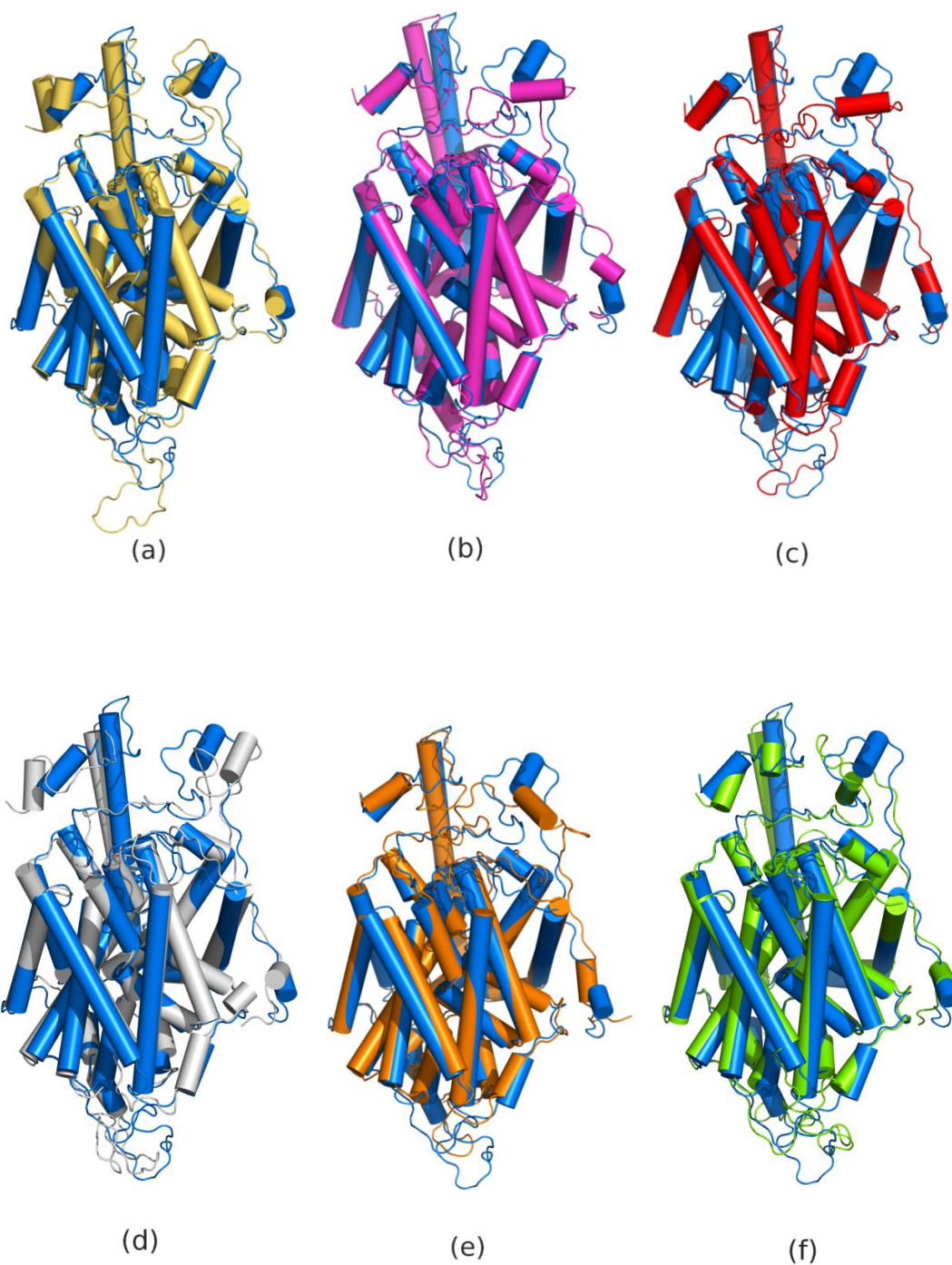
**Figure 4.3**



**Figure 4.3 cont.** The best representative members of the first clustering process, clusters are aligned on initial structure. Initial structure represented as a cartoon in blue and representative from (a) gray: Cluster1; (b) orange: Cluster2 ; (c) cyan: Cluster3; (d) magenta: Cluster4; (e) yellow: Cluster5; (f) purple: Cluster6; (g) green: Cluster7; (h) brown: Cluster8; (i) red: Cluster9; (j) light pink: Cluster10; (k) dark blue: Cluster11.

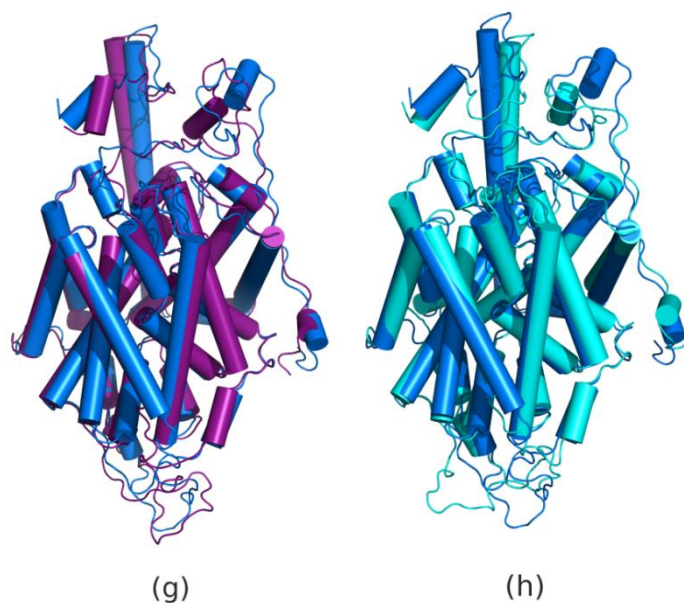
The representative members of second clustering which is determined according to binding site regions, are presented as cartoon in Figure 4.4. They are also aligned

with respect to the initial structure of DAT. As shown in Figure 4.4, the clustering profile reveals eight clusters in this case.



**Figure 4.4**





**Figure 4.4 cont.** The best representative members of the second cluster process, clusters are aligned on initial structure. Initial structure represented as a cartoon in blue and representative from (a) yellow: Cluster1; (b) pink: Cluster2 ; (c) red: Cluster3; (d) gray: Cluster4; (e) orange: Cluster5; (f) green: Cluster6; (g) purple: Cluster7; (h) cyan: Cluster8.

The positions of the most mobile regions on the structure of DAT model are defined in Chapter 3, Figure 3.3.9. When we examined the alignment results of clustering with respect to the initial structure, we observed that most mobile regions belong to 2. loop, 3. loop and 1. loop respectively.

When we compare the cluster results with the results of MD, we also observed that differences in clusters are based more on the loop regions than the helix regions. This means that the conformational changes observed during the simulation, causing the cluster variations, are mainly resulting from the more flexible loops in the structure. Likewise, when we examine the RMSD analysis results in chapter 3, DAT structure undergoes small fluctuations, that mean not very large movements of structural parts. While the helix parts are stable (fluctuating less), overall small fluctuation seemed to be the cause of transport mechanism. Helix regions stability also supports that the structure of human DAT is evolutionary protected.

Furthermore, when compare changes on the helix regions TM12, TM5, TM1 and TM3 have more differences than others for two cases. How the differences on these helix regions affected the binding of dopamine were examined in following chapters.

After two different clustering proces, we have obtained 11 from the initial case and 8 from the latter case. Totally 19 different conformations of DAT model were obtained. These 19 different conformations were used for docking analysis in order to understand the binding variations.

## Chapter 5

### Docking Analysis

As mentioned above chapters, dopamine transporter (DAT), transports dopamine across the membrane which is located on the plasma membrane of nerve terminals. To explain the transport properties, the pathway and different binding sites, we used a DAT model and its different conformations which are obtained from clustering as mentioned previous chapter.

Dopamine, norepinephrine, and serotonin, as well as amino acids (glycine,  $\gamma$ -aminobutyric acid and proline) are biogenic amines [19]. The transporters for the biogenic amine, dopamine, is DAT. That is why understanding the dynamics of the molecule particular interest because it is targeted by many drugs, including the widely abused psychostimulants cocaine and amphetamine as well as antidepressants [96,26].

The reuptake mechanism of dopamine is  $Na^+$  and  $Cl^-$  dependent, and follows a sequence of events where one dopamine molecule or two sodium ions initially bind to the dopamine transporter protein, followed by binding of one chloride ion to the transporter [32]. The inwardly directed  $Na^+$  gradient provides energy for an inward movement of dopamine molecule against a concentration gradient [33].

In this thesis, to study the mechanism of dopamine translocation to the intracellular side we used different conformations of a DAT model which are obtained from clustering analysis from a dynamic data as explained in previous chapter. To explore the pathway and different binding sites we have performed binding analysis. For the binding analysis of DAT and dopamine we have used a docking software, AutoDock 4.0. The dopamine-binding modes have been

determined through the calculation of binding free energies. We shown that there is a remarkable agreement between the identities of the key residues in the translocation mechanism we obtained from our simulations and experimental data in the literature.

## 5.1 Methodology

AutoDock 4 is a free software available under the GNU General Public License. It computes the interaction energies of different poses of the ligand in the molecule. Furthermore, it allows side chains in the macromolecule to be flexible, as well as allowing for ligand flexibility. Autodock 4.0 uses a free-energy scoring function created from a linear regression analysis, the AMBER force field, and a large set of diverse protein-ligand complexes with known inhibition constants. The searching algorithms include simulated annealing and a genetic algorithm. We have used AutoDock 4.0 program during all docking process analysis for different conformations of DAT and dopamine. The stages of AutoDock 4.0 used here were as follows;

### 1. Preparing Coordinates

We started with creating the ligand and receptor coordinate files to include the information needed by AutoGrid and AutoDock. These coordinate files are created in an AutoDock-specific coordinate file format, termed PDBQT, which include spartial charges, atom types, polar hydrogen atoms and information on the articulation of flexible molecules. PDBQT files also include information on the torsional degrees of freedom [125].

### 2 . AutoGrid Calculation

AutoDock requires pre-calculated grid maps, one for each atom type present in the ligand being docked. This helps to make the docking calculations fast. These maps are calculated by AutoGrid. A grid map consists of a three dimensional lattice of regularly spaced points, surrounding (either entirely or partly) and centered on some region of interest of the macromolecule. In our study, the grid size was set to be  $70 \times 70 \times 70$  and the grid space was the default value of  $0.375 \text{ \AA}$ .

### 3. Docking with AutoDock

In this step, we created a docking parameter file that specifies the input, output files and parameters for the docking calculation. AutoDockTools may be used to generate the docking parameter file, as described below, which typically has the extension “dpf”. We have chosen the Lamarckian genetic algorithm (LGA) search methods. Minimized ligands were randomly placed inside the grid box, and the docking process initiated with a quaternion and torsion step is 50, torsional degrees of freedom 3, number of energy evaluations 2500000 and run number of 100.

At the end of a docking simulation, AutoDock writes the coordinates for each docked conformation to the docking log file, along with information on clustering and interaction energies (binding free energy of the protein-ligand complex).

## **5.2 Results and Discussion**

As explained before, the results are presented from the clustering DAT model according to overall structure and according to binding site snapshots taken from 200 ns MD trajectories.

After two different clustering proces, we have obtained totally 19 different conformations of DAT model. These 19 different conformations are used for binding analysis.

Firstly docking was performed on the different conformations of DAT model which are obtained from clustering analysis according to the overall structure. Dopamine was docked with DAT to compute the binding energy, binding site and how connections they have.

Generally researchers need to identify binding-site residues on a protein, in the research on protein active sites. The strategy is to find a protein structure and its partner from the Protein Data Bank (PDB) and calculate binding-site residues based on the complex structure. However, according to Hu et al. since a protein may participate in multiple interactions, the binding-site residues calculated based on one complex structure usually do not reveal all binding sites on a protein [117]. In connection with this view, in our study we obtained several different conformations of DAT before the docking with dopamine process.

### **5.2.1 Binding Energies For Different Conformations of DAT Clustered With Respect to Overall Structure**

After the first clustering analysis which is described in detail in Chapter 4, we have obtained 11 different conformations of DAT which corresponds to several snapshots taken from 200 ns MD trajectories. Each of these conformations, docking proces stages are applied and docked with dopamine ligand. 100 runs for dopamine

were performed for each subcluster. Binding energies obtained from these analysis were tabulated in Table 5.1.

**Table 5.1** Docking results for DAT model subclusters (radius of 3.0 Å) - dopamine with AutoDock 4.0

<b>Cluster (RMSD Threshold : 3Å)</b>	<b>Rank</b>	<b>Sub-Rank</b>	<b>Run</b>	<b>Binding Energy(kcal/mol)</b>	<b>Reference RMSD (Å)</b>
<b>Subcluster 1</b>	1	1	86	-5.76	21.45
<b>Subcluster 2</b>	1	1	28	-7.00	15.61
<b>Subcluster 3</b>	1	1	18	-5.89	23.18
<b>Subcluster 4</b>	1	1	77	-7.00	7.25
<b>Subcluster 5</b>	1	1	89	-6.68	9.55
<b>Subcluster 6</b>	1	1	27	-5.79	16.54
<b>Subcluster 7</b>	1	1	55	-6.10	26.25
<b>Subcluster 8</b>	1	1	14	-6.30	26.52
<b>Subcluster 9</b>	1	1	57	-6.54	23.24
<b>Subcluster 10</b>	1	1	20	-6.16	13.06
<b>Subcluster 11</b>	1	1	86	-6.09	12.54

As seen in Table 5.1, after the docking process with AutoDock 4.0, the binding energies and RMSD values for each run were obtained. The results are classified in ranks and also each run is divided into sub-ranks. Each docking run gives the best poses based on binding energies. For the natural ligand dopamine, subcluster 2 the run number 28 which belongs to rank 1 and also sub-rank 1, is the best pose with binding energy -7.00 kcal/mol. It has 15.61 Å RMSD value. In addition, subcluster 4 the run number 77 which belongs to rank 1 and also sub-rank 1, is another best pose with binding energy -7.00 kcal/mol, and it has 7.25 Å RMSD value.

At the beginning of docking process, we placed the dopamine ligand at the center of the DAT molecule for all subclusters. The values of binding energy is obtained between -5.76 and -7.00 as we can see Table 5.1 but reference RMSD values are different from each other. For example, subcluster 2 and subcluster 4

showed the same lowest binding energy value of -7.00 kcal/mol while one of them has 15.61 Å and other one has 7.25 Å RMSD. Therefore, we can say that dopamin is connected to different regions of the dopamine transporter in the same study.

According to the experimental studies conducted previously with the DAT-dopamine complex the binding energy value was also found as -7.4 kcal/mol [118]. When we compare this score to our computational docking study, we can see that subcluster-2 and subcluster-4 scores of first cluster process, show quite close confirming a good agreement.

In the protein functional site analysis, identifying the binding-site residues on a protein is the main procedure. Only comparing the binding energy is not enough, to explore the complex binding affinities of protein and ligand. For this reason we determined the binding site residues for dopamine in DAT model which is obtained from first cluster process.

### **5.2.2 Binding Site Residues and Interactions in DAT model Subclusters (Radius of 3.0 Å) with Dopamine**

After the docking the DAT model subcluster conformations clustered according to the overall structure with dopamine, the binding site residues are obtained and they are shown in Table 5.2. As seen in the table, the common residues in the 11 subclusters are Gly386, Asp385, Glu 126, Asp 476, Phe472, Thr473, Trp84, Arg85 and Tyr88.

As explained in detail in the previous chapter, we identified the 12 transmembrane helices and these helices are important in maintaining the three dimensional structure and the pocket for agonist binding. Docking results of dopamine and DAT model 11 different conformations show that binding site residues commonly belong to TMH1, TMH3, TMH8, TMH6, TMH10, TMH9 and TMH4.



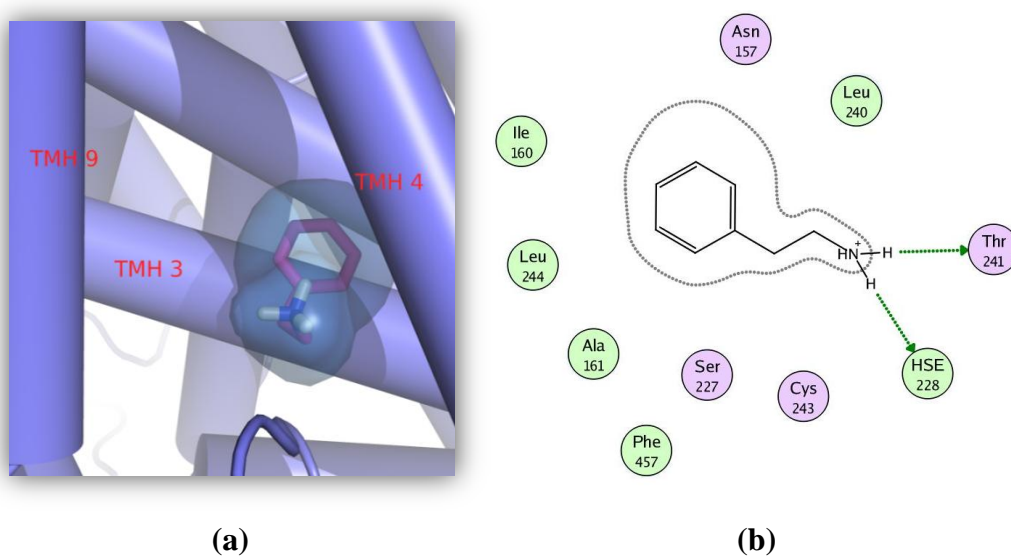
**Table 5.2** Binding site residues of the DAT model subclusters (radius of 3.0 Å)

Subclusters	Binding Site Residues					
at1	Cys243 Asn157	Leu244 Ala161	Thr241 Leu240	Ser227 Gly229	Ile160 Phe457	Hse228
at2	Asp476 Pro387	Trp84 Gly386	Hse477 Tyr88	Arg85	Asp385	
at3	Ile435 Arg445	Glu428 Leu255	Val259 Hse442	Leu251 Trp256	Glu446 Ser254	Tyr252
at4	Trp84 Gly386	Arg85 Tyr88	Asp385	Thr473	Phe472	Asp476
at5	Pro387 Phe472	Gly386 Thr473	Asp385 Tyr88	Asp476	Trp84	Arg85
at6	Val471 Trp162	Tyr470 Gly386	Ile469 Phe217	Asp385 Phe472	Thr473	Val221
at7	Gly127 Glu126	Ile431 Arg606	Gly433 Leu434	Gly437	Val430	Arg60
at8	Gly130 Ala128	Tyr578 Glu126	Glu437 Leu434	Gly127	Pro50	Val131
at9	Tyr335 Asp436	Arg125 Gly433	Glu61 Glu126	Arg60 Trp256	Thr432	Ile435
at10	Ile148 Thr144	Gly325 Gly487	Ile484 Glu491	Ile330 Glu117	Val488 Val141	Val145
at11	Trp162 Ile469	Glu218 Tyr470	Thr473	Val471	Phe472	Phe217

Docking results of the dopamine and different 11 conformations of DAT which is obtained from first cluster explained in detail, especially the important interactions between dopamine and the binding site residues of DAT.

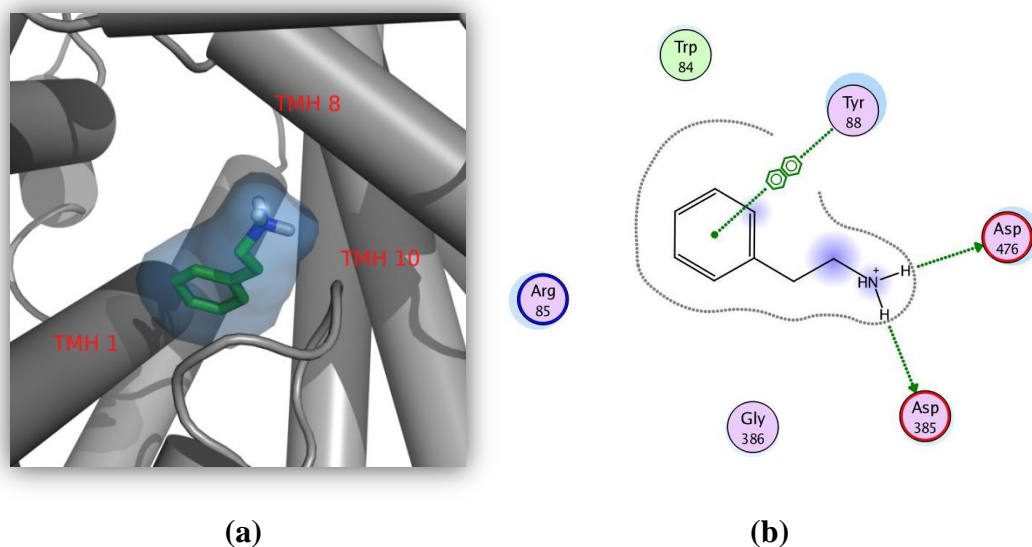
Figure 5.1 shows DAT (subcluster at1)-dopamine complex snapshot which was taken from docking studies. The conformation of subcluster at1 of DAT and dopamine made up an unwound region. Dopamine interacted with transmembrane helices 4, 3 and 9 of DAT, as seen in Figure 5.1 (a). Dopamine is shown as ball-and-stick, while DAT's helices are shown as cylindrical in all figures. 2D representation of dopamine in the binding site is displayed in Figure 5.1 (b). Only the residues of DAT within the 5 Å length from dopamine is shown. The residues around the active site,

that can have important roles in binding are, Leu244, Ile160, Hse228, Ala161, Leu240 and Phe457. They are hydrophobic residues and all colored with a green interior. In addition to these, Asn 157, Thr 241, Ser 227 and Cys 243 are the other active site residues, which are polar and colored in light purple. As shown in Figure 5.1. (b), there are hydrogen bonding interactions between the side chain of dopamine and DAT's residues of Thr241 and Hse228. They are drawn with an arrow head to denote the direction of the hydrogen bond.



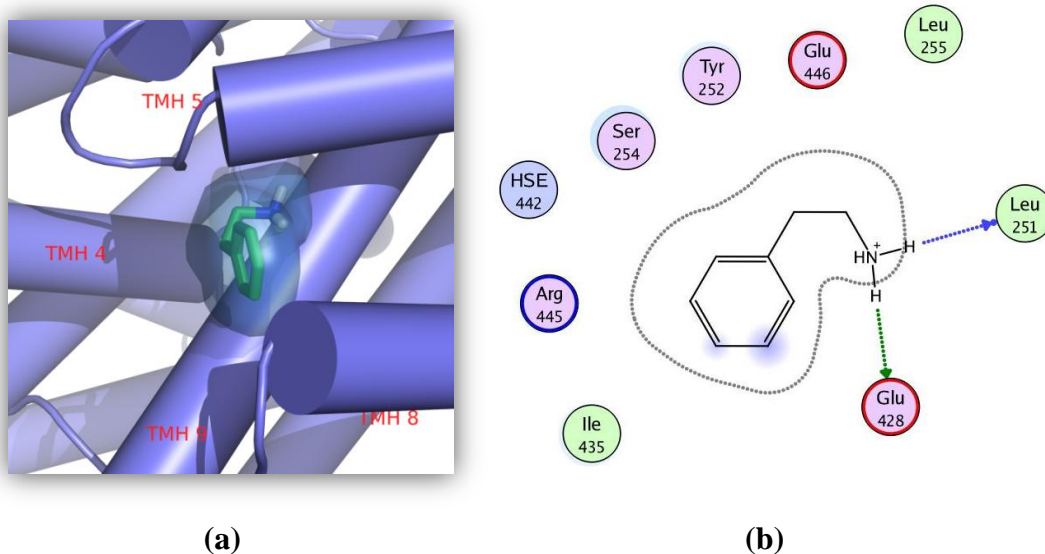
**Figure 5.1.** A snapshot taken from docking studies of DAT (subcluster at1)-dopamine binding complex (a) and 2D representation of the atomic interactions between the DAT and dopamine (b).

The dopamine-binding site, which is resulted from docking of subcluster at2, was made up of unwound regions of transmembrane helices 1, 8 and 10, as seen in Figure 5.2 (a). The residues around the active site are; Trp84 is hydrophobic residue and colored with a green interior whereas Tyr88, Arg85, Asp476, Asp385 and Gly386 are polar residues and colored in light purple. Basic residues are further annotated by a blue interior ring, and acidic residues with a red ring. As shown in Figure 5.2. (b), there are important interactions; that are hydrogen bonding interactions between the side chain of dopamine and DAT's residues of Asp476 and Asp385. On the other hand, Tyr88 interacts with the aromatic ring of dopamine.



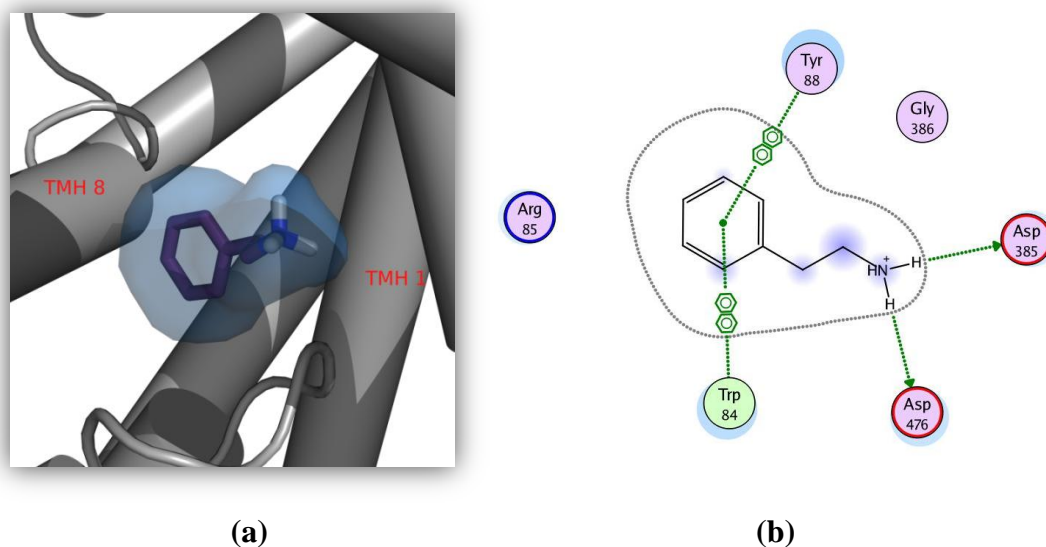
**Figure 5.2** A snapshot taken from docking studies of the DAT (subcluster at2)-dopamine binding complex (a). 2D representation of the atomic interactions between the DAT and dopamine (b).

DAT subcluster at3 and dopamine complex snapshot which was taken from docking studies is shown in Figure 5.3. The conformation of subcluster at3 of DAT and dopamine made up an unwound region. Dopamine interacted with transmembrane helices 4, 5, 8 and 9, as seen in Figure 5.3 (a). In Figure 5.3 (b), residues from DAT within 5 Å of dopamine are labeled and show as 2D representation of the atomic interactions between the DAT and dopamine. Leu255, Leu251 and Ile 435 residues have important roles in binding. They are hydrophobic residues and all colored with a green interior. In addition Glu446, Glu428, Tyr252, Ser254 and Arg445 are polar residues and colored in light purple. Also Arg445 is basic residue and further annotated by a blue interior ring, and Glu446 and Glu428 are acidic residues and shown with a red ring. As shown in Figure 5.3., there are hydrogen bonding interactions between the side chain of dopamine and DAT's residues of Glu428 and Leu251. They are drawn with an arrowhead and when the hydrogen bond is formed with the residue side chain, the arrow is drawn in green. Hydrogen bonds to the residue backbone are drawn in blue, with an additional dot drawn at the residue attachment point.



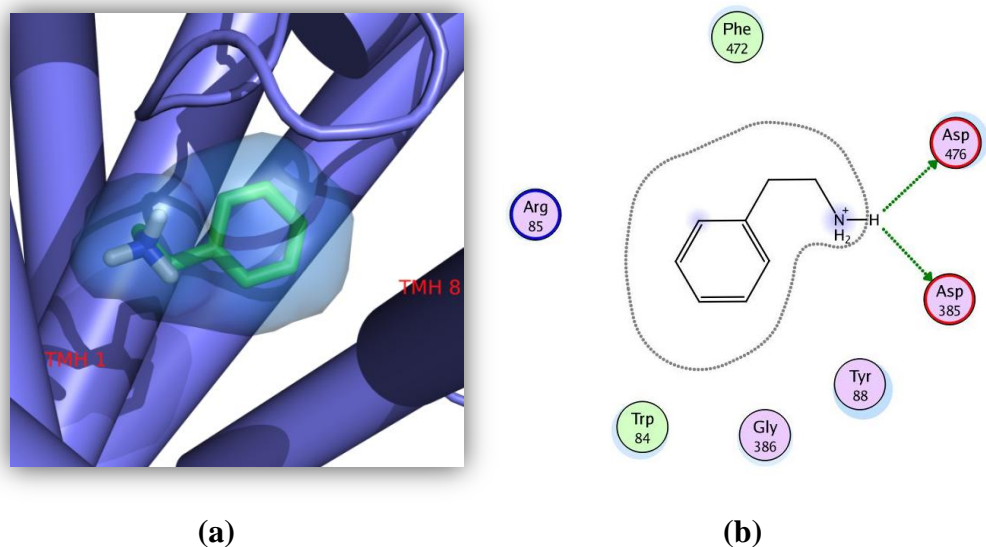
**Figure 5.3** A snapshot taken from docking studies of the DAT (subcluster at3)-dopamine binding complex (a). 2D representation of the atomic interactions between the DAT and dopamine (b).

Figure 5.4 shows DAT structure of the result of subcluster at4 and dopamine complex snapshot which was taken from docking studies. Dopamine interacted with TMH 1 and 8, as seen in Figure 5.4 (a). As shown in Figure 5.4 (b), Trp84 is hydrophobic residue and colored with a green interior, while Asp385, Gly386, Tyr88, Asp476 and Arg85 are polar residues and colored in light purple. Also Arg85 is basic residue and further annotated by a blue interior ring. The other active site residues which are Asp476 and Asp385 are acidic residues and shown with a red ring and they are hydrogen bonding interactions between the side chain of dopamine. Tyr88 and Trp84 interacts with the aromatic ring of dopamine.



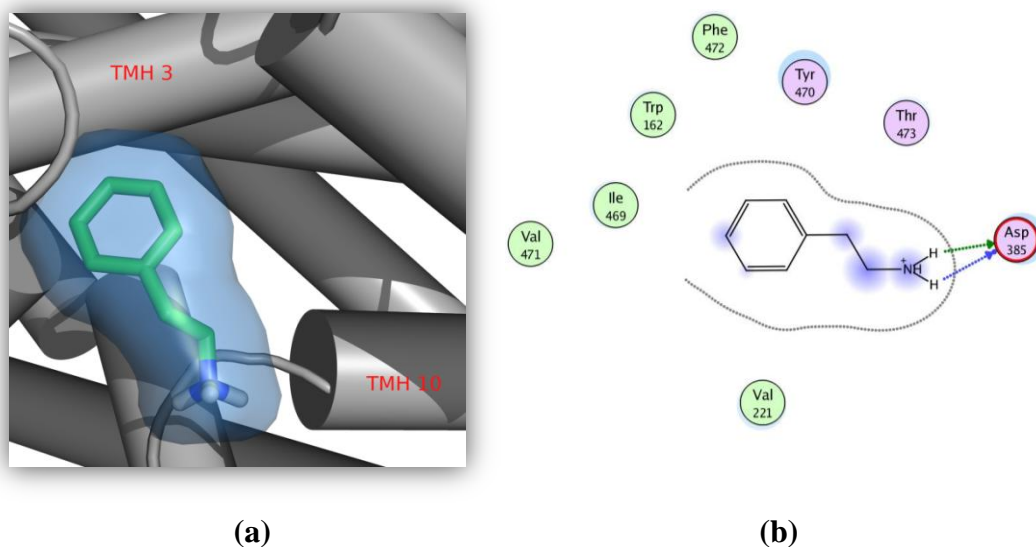
**Figure 5.4.** A snapshot taken from docking studies of the DAT (subcluster at4)-dopamine binding complex (a). 2D representation of the atomic interactions between the DAT and dopamine (b).

The dopamine-binding site in our structure which is result of subcluster at5, was made by unwound regions of transmembrane helices 1 and 8 similar to subcluster at4, as seen in Figure 5.5 (a). 2D representation of dopamine in the binding site is displayed in Figure 5.5 (b). Only the residues of DAT within the 5 Å length from dopamine is shown. Trp84 and Phe472 are hydrophobic residues whereas Asp385, Gly386, Tyr88, Asp476 and Arg85 are polar residues. Also Arg85 is basic residue and further annotated by a blue interior ring. Asp476 and Asp385 are acidic residues and shown with a red ring, while they are hydrogen bonding interactions between the side chain of dopamine.



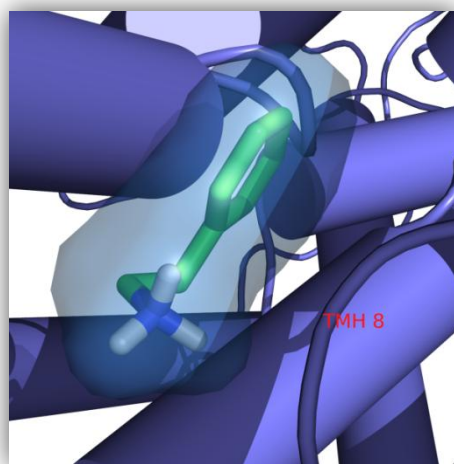
**Figure 5.5.** A snapshot taken from docking studies of the DAT (subcluster at5)-dopamine binding complex (a). 2D representation of the atomic interactions between the DAT and dopamine (b).

As shown in Figure 5.6, there are important helices and interactions with residues in the active site of DAT (subcluster at6). Dopamine interacted with transmembrane helices 10 and 3, as seen in Figure 5.6.(a). Phe472, Trp162, Ile469, Val471 and Val221 are hydrophobic whereas Tyr470, Thr473 and Asp385 are polar residues. As shown in Figure 5.6.(b), there are hydrogen bonding interactions between the side chain of dopamine and Asp386 residue.

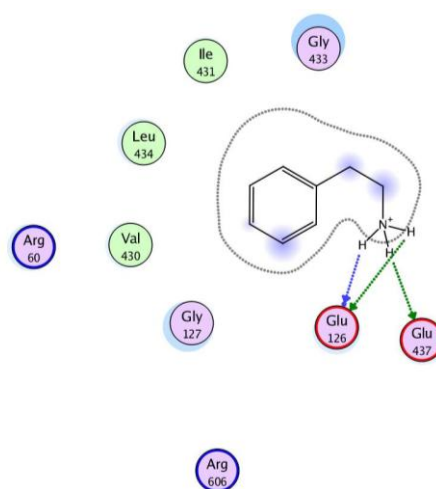


**Figure 5.6.** A snapshot taken from docking studies of the DAT (subcluster at6)-dopamine binding complex (a). 2D representation of the atomic interactions between the DAT and dopamine (b).

Dopamine interacted with only transmembrane helices 8 of DAT structure (subcluster at7), as seen in Figure 5.7.(a). In Figure 5.7.(b) the residues around 5Å proximity within the active site of DAT (subcluster at7) are shown. Ile431, Leu434 and Val430 residues are hydrophobic whereas Gly433, Gly127, Glu126, Glu437 and Arg606 residues are polar. Also Arg60 and Arg606 are basic residue and further annotated by a blue interior ring, and Glu437 and Glu126 are acidic residues and shown with a red ring. In addition to these, there are hydrogen bonding interactions between the side chain of dopamine and DAT's residues of Glu437 and Glu126, they are drawn with an arrowhead to denote the direction of the hydrogen bond.



(a)

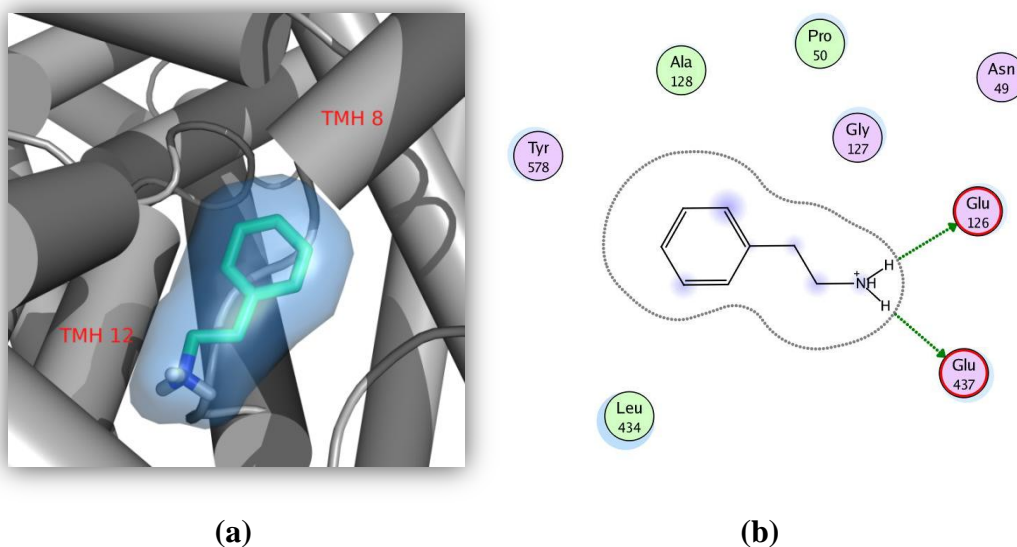


(b)

**Figure 5.7.** A snapshot taken from docking studies of the DAT (subcluster at7)-dopamine binding complex (a). 2D representation of the atomic interactions between the DAT and dopamine (b).

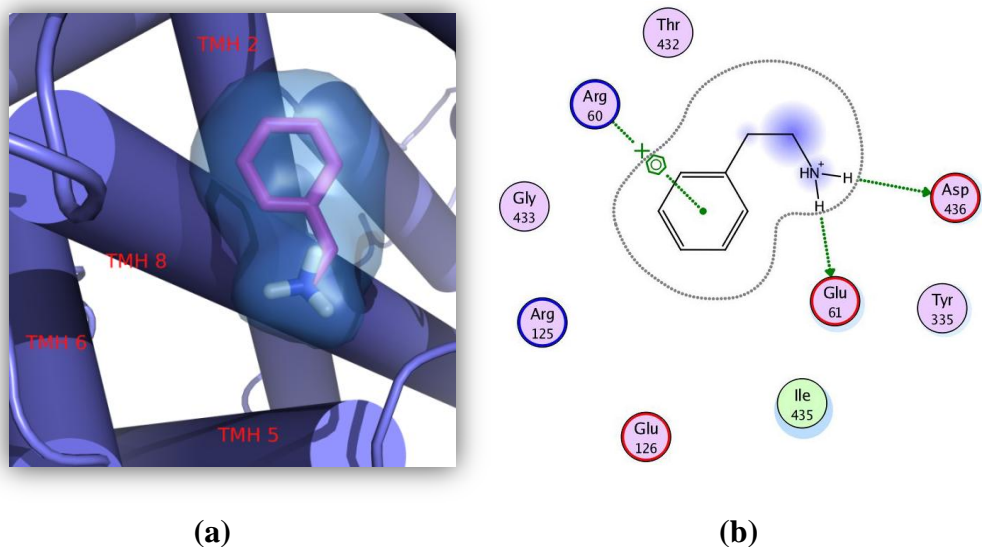
Transmembrane helices 12 and 8 are important for dopamine when binding with DAT (subcluster at8), as seen in Figure 5.8.(a). Ala128, Pro50 and Leu434 are hydrophobic residues. Among these residues, Asn49, Gly127, Glu126, Glu437 and Tyr578 are polar. Glu437 and Glu126 are acidic residues and shown with a red ring and that are hydrogen bonding interactions between the side chain of dopamine, as shown in Figure 5.8.(b).





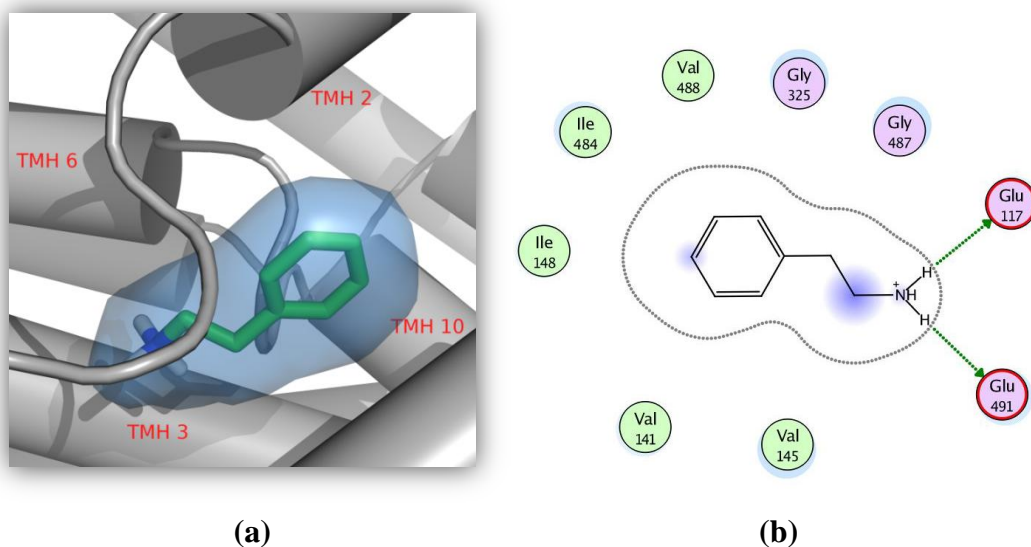
**Figure 5.8.** A snapshot taken from docking studies of the DAT (subcluster at8)-dopamine binding complex (a). 2D representation of the atomic interactions between the DAT and dopamine (b).

DAT subcluster at9 and dopamine complex snapshot which was taken from docking studies is shown in Figure 5.9. The conformation of subcluster at9 of DAT and dopamine made up an unwound region. Dopamine interacted with TMH 2, 5, 6 and 8, as seen in Figure 5.9.(a). In Figure 5.9.(b), residues from DAT within 5 Å of dopamine are labeled and show as 2D representation of the atomic interactions between the DAT and dopamine. Ile435 is hydrophobic residue and Thr432, Arg60, Gly433, Arg125, Glu126, Glu61, Tyr335 and Asp436 are polar residues. Basic residues are further annotated by a blue interior ring, and acidic residues with a red ring. As shown in Figure 5.9.(b), there are hydrogen bonding interactions between the side chain of dopamine and DAT's residues of Asp436 and Glu61 whereas Arg60 interacts with the aromatic ring of dopamine.



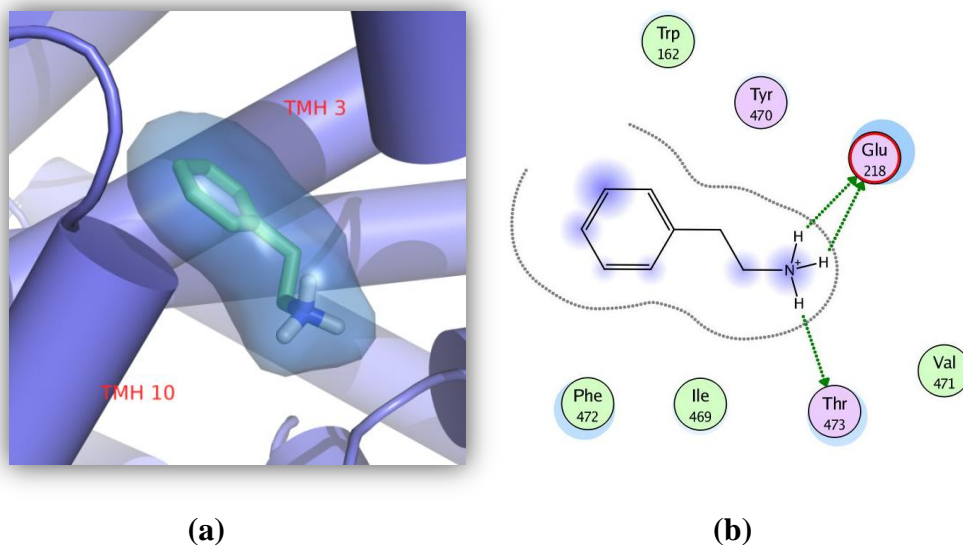
**Figure 5.9.** A snapshot taken from docking studies of the DAT (subcluster at9)-dopamine binding complex (a). 2D representation of the atomic interactions between the DAT and dopamine (b).

Figure 5.10 shows DAT structure of the result of subcluster at10 and dopamine complex snapshot which was taken from docking studies. The dopamine-binding site in our structure of the result of subcluster at10, was made by unwound regions of transmembrane helices 2, 3, 6 and 10, as seen in Figure 5.10.(a). As shown in Figure 5.10 (b), Ile484, Ile148, Val141, Val145 and Val488 residues are hydrophobic and colored with a green interior. In addition to these Glu385, Glu487, Glu117 and Glu491 are polar residues and colored in light purple. There are hydrogen bonding interactions between the side chain of dopamine and Glu117 and Glu491 residues also they are acidic and shown with a red ring.



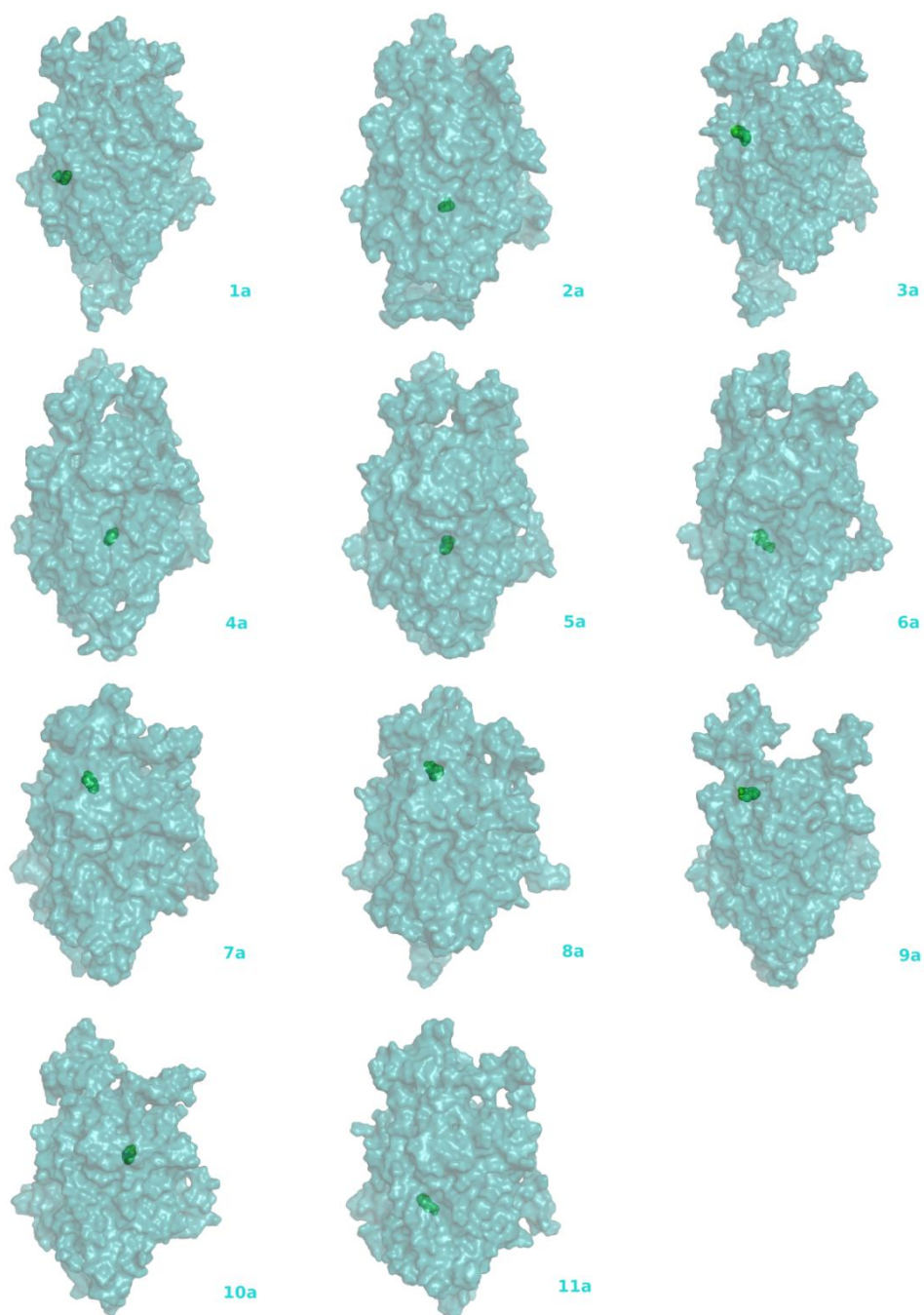
**Figure 5.10.** A snapshot taken from docking studies of the DAT (subcluster at10)-dopamine binding complex (a). 2D representation of the atomic interactions between the DAT and dopamine (b).

Dopamine interacted with TMH 3 and 10 of DAT structure (subcluster at11), as seen in Figure 5.11.(a). In Figure 5.11.(b) the residues around 5Å proximity within the active site of DAT (subcluster at11) are shown. The residues around the active site, that can have important roles in binding are Trp162, Phe472, Ile469 and Val471. They are hydrophobic residues and colored with a green interior whereas Tyr470, Glu218 and Thr473 are the other active site residues, which are polar and colored in light purple. Also Glu218 is acidic residue and shown with a red ring. As shown in Figure 5.11.(b), there are hydrogen bonding interactions between the side chain of dopamine and DAT's residues of Glu218 and Thr473 and they are drawn with an arrowhead to denote the direction of the hydrogen bond.



**Figure 5.11.** A snapshot taken from docking studies of the DAT (subcluster at11)-dopamine binding complex (a). 2D representation of the atomic interactions between the DAT and dopamine (b).

You can see from the above figures, and explanations, docking results of dopamine and DAT model subclusters clustering of 200 ns simulation according to the overall structure using a RMSD threshold of 3 Å, have been analyzed. As shown in these analyzes, dopamin contacted with variously helices and residues in different conformations of DAT thereby it forms different binding sites. In the following sections they will be examined in detail in a way that these different binding sites in the protein is depicted in Figure 5.12.



**Figure 5.12.** Autodock different binding site results of dopamine and DAT model subclusters clustering of all simulations according to the overall structure using a RMSD threshold of 3 Å. Viewing the dopamine in the binding pocket. The binding pocket is represented in molecular surface format, colored with cyan. The dopamine molecule shown as dots in green, in the complex model.

All the conformations shown in Figure 5.12 were from the same angle for the aligned snapshots of the best members of the cluster.

### 5.2.3 Binding Energies For Different Conformations of DAT Clustered With Respect to Binding Site

After the second clustering process (clustering of the all simulations according to binding site region using a RMSD threshold of 1.3 Å) which is described in detail in Chapter 6, we have obtained 8 different conformations of DAT. Each of these conformations, docking proces stages are applied and docked with dopamine ligand.100 runs for dopamine were performed for each subcluster.

**Table 5.3** Docking results for DAT model subclusters (radius of 1.3 Å) - dopamine with AutoDock 4.0

Cluster (RMSD Threshold:1.3Å)	Rank	Sub-Rank	Run	Binding Energy(kcal/mol)	Reference RMSD (Å)
<b>Subcluster 1</b>	1	1	48	-6.08	9.2
<b>Subcluster 2</b>	1	1	56	-6.01	25.35
<b>Subcluster 3</b>	1	1	65	-6.28	21.95
<b>Subcluster 4</b>	1	1	27	-6.06	28.90
<b>Subcluster 5</b>	1	1	1	-6.51	6.27
<b>Subcluster 6</b>	1	1	79	-6.00	9.15
<b>Subcluster 7</b>	1	1	43	-6.57	8.94
<b>Subcluster 8</b>	1	1	86	-7.31	16.72

As seen in Table 5.3, after the docking process with AutoDock 4.0, the binding energies and RMSD values for each run were obtained. The results are classified in ranks and also each run is divided into sub-ranks. Each of docking process taken of best poses based on binding energies. For the natural ligand dopamine, subcluster 8 the run number 86 which belongs to rank 1 and also sub-rank 1, is the best pose based on binding energies (-7.31 kcal/mol) and it has 16.72 RMSD value.

At the beginning of docking process, we placed the dopamine at the center of the DAT for all 8 subclusters, as in the first docking. The values of binding energy is obtained between -6.00 and -7.31 as we can see in Table 5.3.

As observed in the first process of docking, reference RMSD values are so different from each other. For example subcluster 2 and subcluster 6 show almost the same lowest binding energy value (-6.00/-6.01 kcal/mol), however, one of them has 25.35 Å and other one has 9.15 Å. Therefore we can say that dopamin connected to different regions of the dopamine transporter.

Experimental binding energy value was calculated as -7.4 kcal/mol for DAT-dopamine complex [142], as mentioned before. When we compare this score to our computational docking study, we can see that subcluster 8 scores (-7.31 kcal/mol) of second cluster process, show quite close confirming a good agreement.

Comparing only the binding energy is not enough to explore the complex binding affinities of protein and ligand. For this reason we determined the binding site residues for dopamine in DAT model which is obtained from second cluster process as well.

#### **5.2.4 Binding Site Residues and Interactions in DAT model Subclusters (Radius of 1.3 Å) with Dopamine**

After the docking with dopamine and DAT model subcluster conformations clustered according to the experimental binding site residues using a RMSD threshold of 1.3 Å, computational binding site residues are obtained shown in Table 5.4. As seen in the following table, the common residues in the 8 subclusters are Gly386, Asp385, Asp 476, Trp84, Arg85 and Tyr88.

As explained in detail in the previous chapter, we identified the 12 transmembrane helices and these helices are important in maintaining the three dimensional structure and the pocket for agonist binding. Dopamine and DAT model 8 different conformations docking results shown that binding site residues commonly belong to TMH1, TMH3, TMH8 and TMH4.

**Table 5.4** Binding site residues of the DAT model subclusters (radius of 1.3 Å)

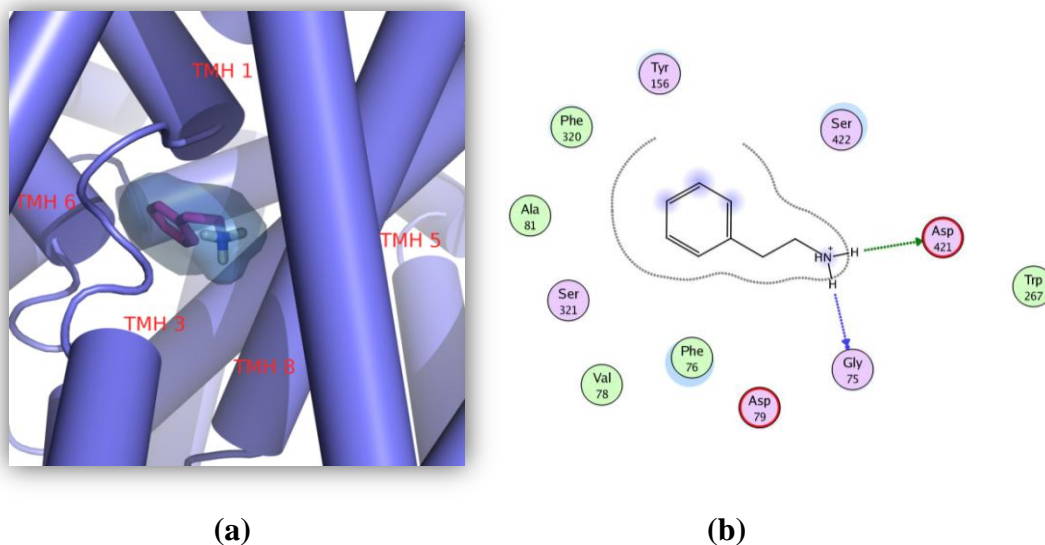
Subclusters	Binding Site Residues						
at1	Ser321	Leu418	Phe76	Gly75	Val78	Trp267	Ala81
	Phe320	Leu80	Ser422	Asp421	Tyr156	Asp79	
at2	Hse422	Lys257	Glu428	Leu255	Leu251	Ser254	
	Arg445	Glu446	Trp256	Tyr252			
at3	Val430	Gly433	Leu434	Arg606	Ala129	Ile431	
	Glu126	Pro50	Glu437	Gly127	Ala128		
at4	Gln239	Hse165	Ser169	Tyr216	Pro236	Gln239	
	Phe168	Glu174	Leu224	Hse225	Leu240		
at5	Gly386	Asp385	Arg85	Tyr88	Phe472	Ala480	
	Trp84	Asp476	Phe155				
at6	Pro387	Trp84	Asp385	Tyr88	Gly386	Asp476	
	Arg85						
at7	Trp84	Arg85	Ala480	Phe472	Tyr88	Asp476	
	Asp385	Phe155					
at8	Arg85	Trp84	Asp385	Asp476	Pro387	Lys384	
	Gly386	Tyr88	Leu389				

Dopamine and different 8 conformations of DAT which is obtained from second cluster, docking analysis results are explained in detail, especially the important interactions between the binding site residues of DAT and dopamine.

Figure 5.13 shows dopamine and DAT structure (subcluster at1), complex snapshot which was taken from docking studies. Dopamine and the conformation of subcluster at1 of DAT made up an unwound region. Dopamine interacted with TMH 1, 3, 5, 6 and 8, as seen in Figure 5.13.(a). Dopamine is shown as ball-and-stick, while DAT's helices are shown as cylindrical in all figures. 2D representation of dopamine in the binding site is displayed in Figure 5.13.(b). Only the residues of DAT within the 5 Å length from dopamine is shown. Phe320, Ala81, Val78, Phe76 and Trp267 are hydrophobic residues and all colored with a green interior. In addition to these, Ser321, Tyr156, Ser422, Asp79, Gly75 and Asp421 are polar residues and colored in light purple. Basic residues are further annotated by a blue interior ring, and acidic

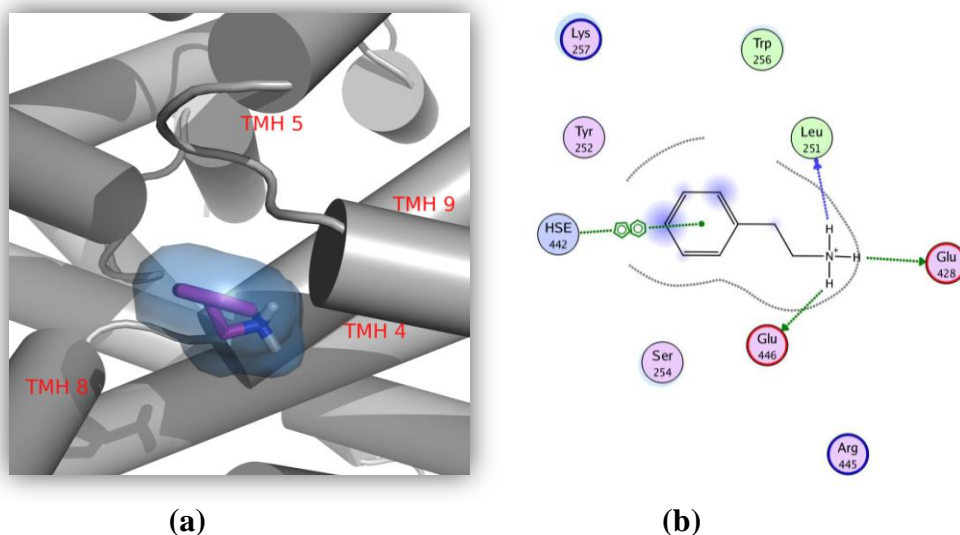


residues with a red ring. As shown in Figure 5.13.(b), there are hydrogen bonding interactions between the side chain of dopamine and DAT's residues of Gly75 and Asp421. They are drawn with an arrowhead to denote the direction of the hydrogen bond. When the hydrogen bond is formed with the residue side chain, the arrow is drawn in green. Hydrogen bonds to the residue backbone are drawn in blue, with an additional dot drawn at the residue attachment point.



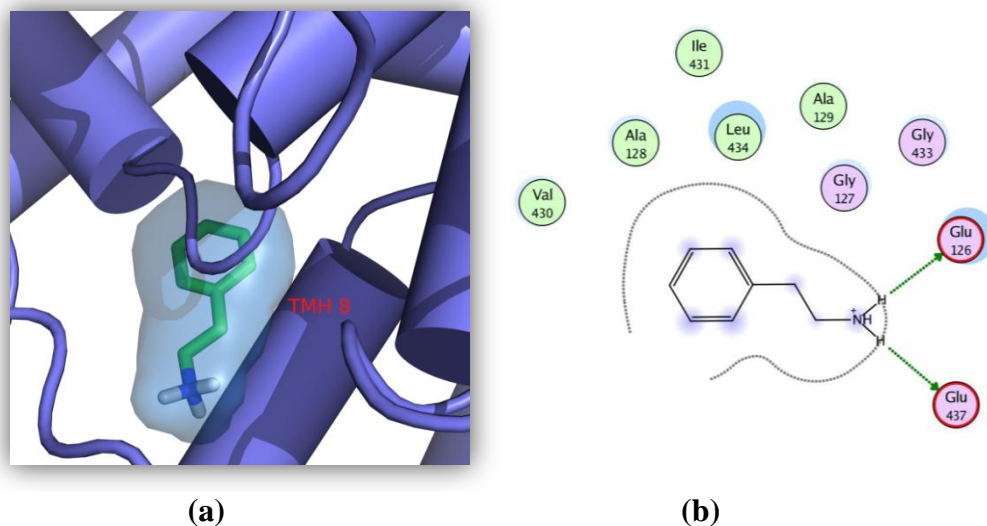
**Figure 5.13.** DAT (subcluster at1)-dopamine binding complex snapshot which is taken from docking studies (a). 2D representation of the atomic interactions between the DAT and dopamine (b).

The dopamine-binding site, which is resulted from docking of subcluster at2, was made up of unwound regions of transmembrane helices 4, 5, 9 and 8, as seen in Figure 5.14 (a). Trp256 and Leu251 residues are hydrophobic and Lys257, Tyr252, Ser254, Glu446, Glu428 and Arg445 residues are polar. Basic residues are further annotated by a blue interior ring, and acidic residues with a red ring. As shown in Figure 5.14., there are important interactions; that are hydrogen bonding interactions between the side chain of dopamine and DAT's residues of Glu446, Glu428 and Leu251 whereas Hse442 interacts with the aromatic ring of dopamine.



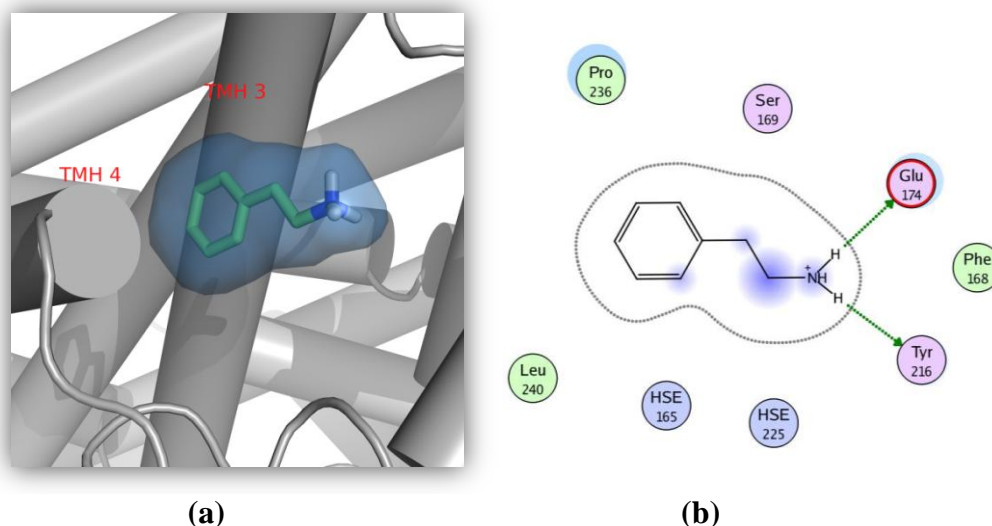
**Figure 5.14.** DAT (subcluster at2)-dopamine binding complex snapshot which is taken from docking studies (a). 2D representation of the atomic interactions between the DAT and dopamine (b).

DAT subcluster at3 and dopamine complex snapshot which was taken from docking studies is shown in Figure 5.15. The conformation of subcluster at3 of DAT and dopamine made up an unwound region. Dopamine interacted with only transmembrane helices 8, as seen in Figure 5.15.(a). In Figure 5.15 (b), residues from DAT within 5 Å of dopamine are labeled and show as 2D representation of the atomic interactions between the DAT and dopamine. Hydrophobic residues are Ala129, Leu434, Ile431, Ala128 and Val430 and all colored with a green interior. In addition to these, Gly433, Gly127, Glu126 and Glu437 are polar residues and colored in light purple. As shown in Figure 5.15., there are hydrogen bonding interactions between the side chain of dopamine and DAT's residues of Glu126 and Glu437, they are acidic residues and shown with a red ring.



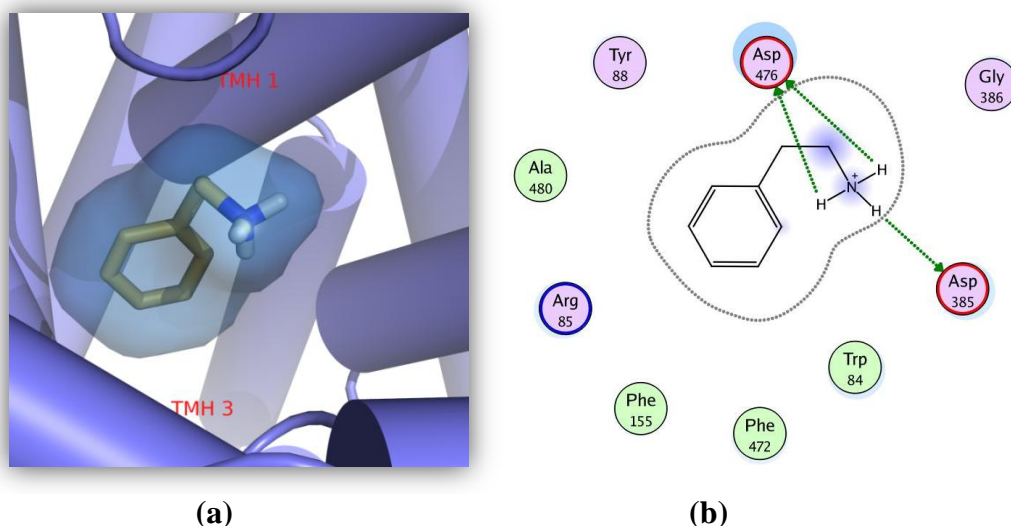
**Figure 5.15.** DAT (subcluster at3)-dopamine binding complex snapshot which is taken from docking studies (a). 2D representation of the atomic interactions between the DAT and dopamine (b).

Figure 5.16 shows DAT structure of the result of subcluster at4 and dopamine complex snapshot which was taken from docking studies. Transmembrane helices 4 and 3 are important to binding with dopamine as seen in Figure 5.16.(a). As shown in Figure 5.16 (b), Pro236, Phe168 and Leu240 are hydrophobic residues and colored in light purple. As shown in Figure 5.16., there are hydrogen bonding interactions between the side chain of dopamine and DAT's residues of Glu174 and Tyr216. Glu174 is acidic residue and shown with a red ring.



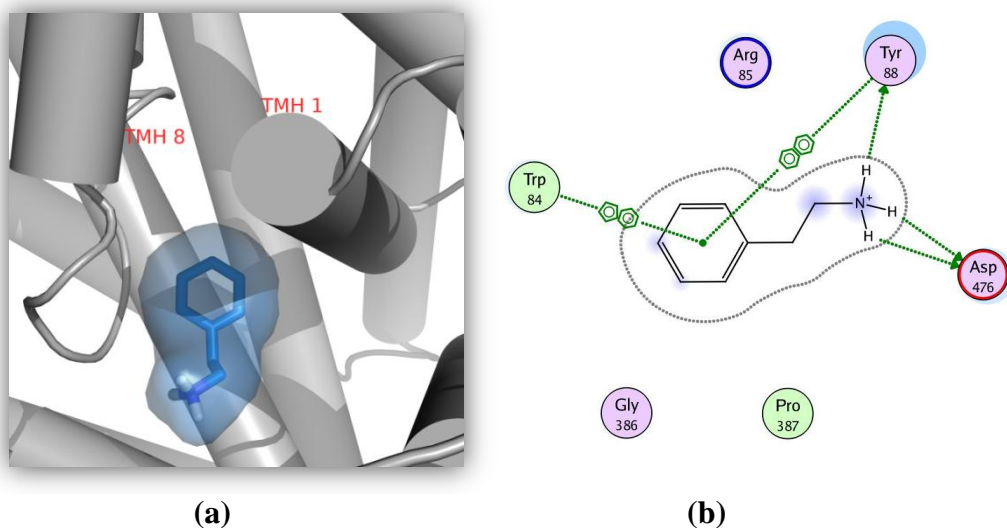
**Figure 5.16.** DAT (subcluster at4)-dopamine binding complex snapshot which is taken from docking studies (a). 2D representation of the atomic interactions between the DAT and dopamine (b).

As shown in Figure 5.17, there are important helices and interactions with residues in the active site of DAT (subcluster at5). The dopamine interacted with transmembrane helices 1 and 3, as seen in Figure 5.17.(a). Asp476, Tyr88, Gly386, Asp385 and Arg85 are polar residues and colored in light purple. Ala480, Phe155, Phe472 and Trp84 are hydrophobic residues and all colored with a green interior. In addition to these, basic residues are further annotated by a blue interior ring, and acidic residues with a red ring. There are hydrogen bonding interactions between the side chain of dopamine and DAT's residues of Asp476 and Asp385 as shown in Figure 5.17.(b).



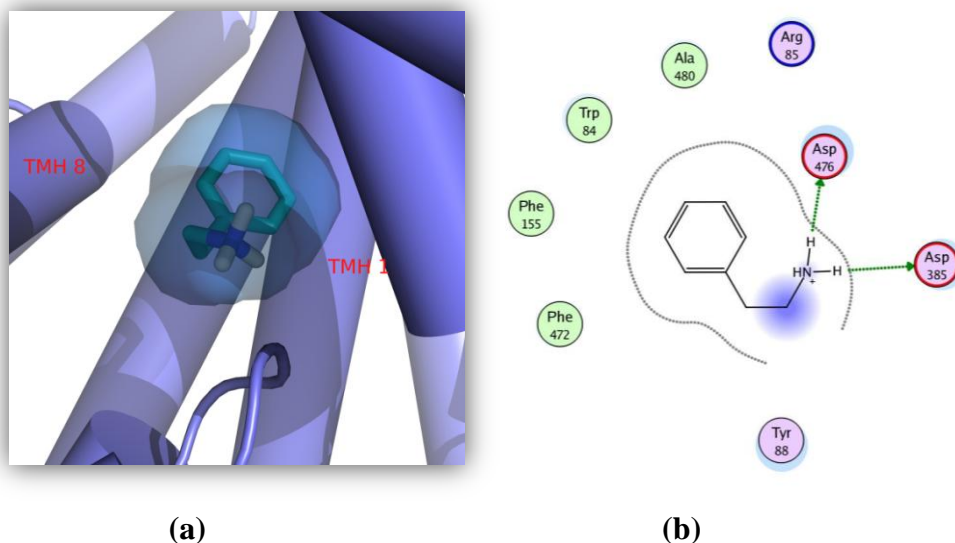
**Figure 5.17.** DAT (subcluster at5)-dopamine binding complex snapshot which is taken from docking studies (a). 2D representation of the atomic interactions between the DAT and dopamine (b).

Dopamine interacted with transmembrane helices 1 and 8 of DAT structure (subcluster at6), as seen in Figure 5.18.(a). In Figure 5.18.(b) the residues around 5Å proximity within the active site of DAT (subcluster at6) are labeled. The residues around the active site, that can have important roles in binding. Trp84 and Pro387 are hydrophobic, Asp476, Tyr88, Gly386 and Arg85 are polar residues. Acidic residues with a red ring and basic residues are further annotated by a blue interior ring. As shown in Figure 5.18.(b), there are hydrogen bonding interactions between the side chain of dopamine and Asp476 and Tyr88 residues of DAT. They are drawn with an arrowhead to denote the direction of the hydrogen bond. On the other hand Trp84 and Tyr88 interacts with the aromatic ring of dopamine.



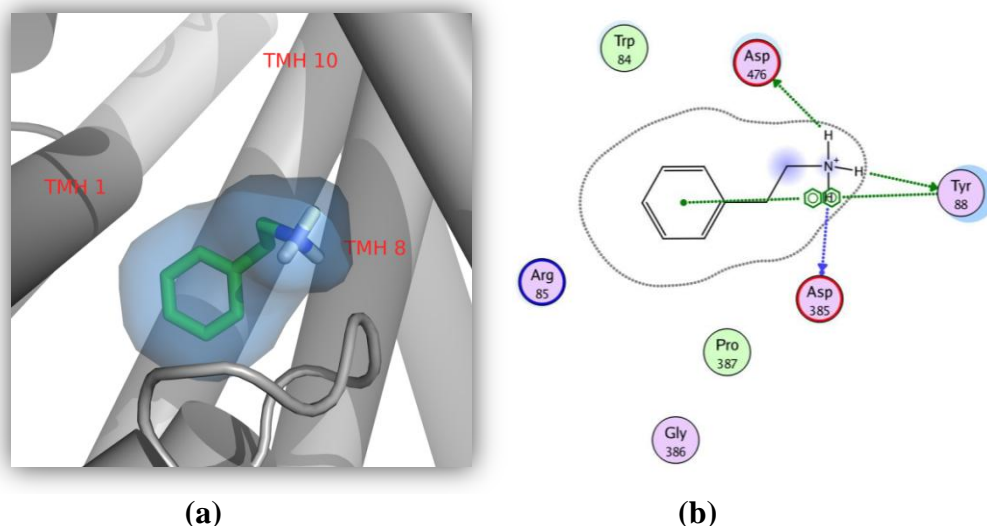
**Figure 5.18.** DAT (subcluster at6)-dopamine binding complex snapshot which is taken from docking studies (a). 2D representation of the atomic interactions between the DAT and dopamine (b).

Transmembrane helices 1 and 8 are important for dopamine binding with DAT (subcluster at7), as seen in Figure 5.19.(a). Hydrophobic residues are Ala480, Trp84, Phe155, Phe472 and all colored with a green interior. In addition to these, polar residues are Arg85, Asp476, Asp385, Tyr88 and colored in light purple. As shown in Figure 5.19.(b), there are hydrogen bonding interactions between DAT's residues of Asp476 and Asp385 and the side chain of dopamine and they are drawn with an arrowhead to denote the direction of the hydrogen bond.



**Figure 5.19.** DAT (subcluster at7)-dopamine binding complex snapshot which is taken from docking studies (a). 2D representation of the atomic interactions between the DAT and dopamine (b).

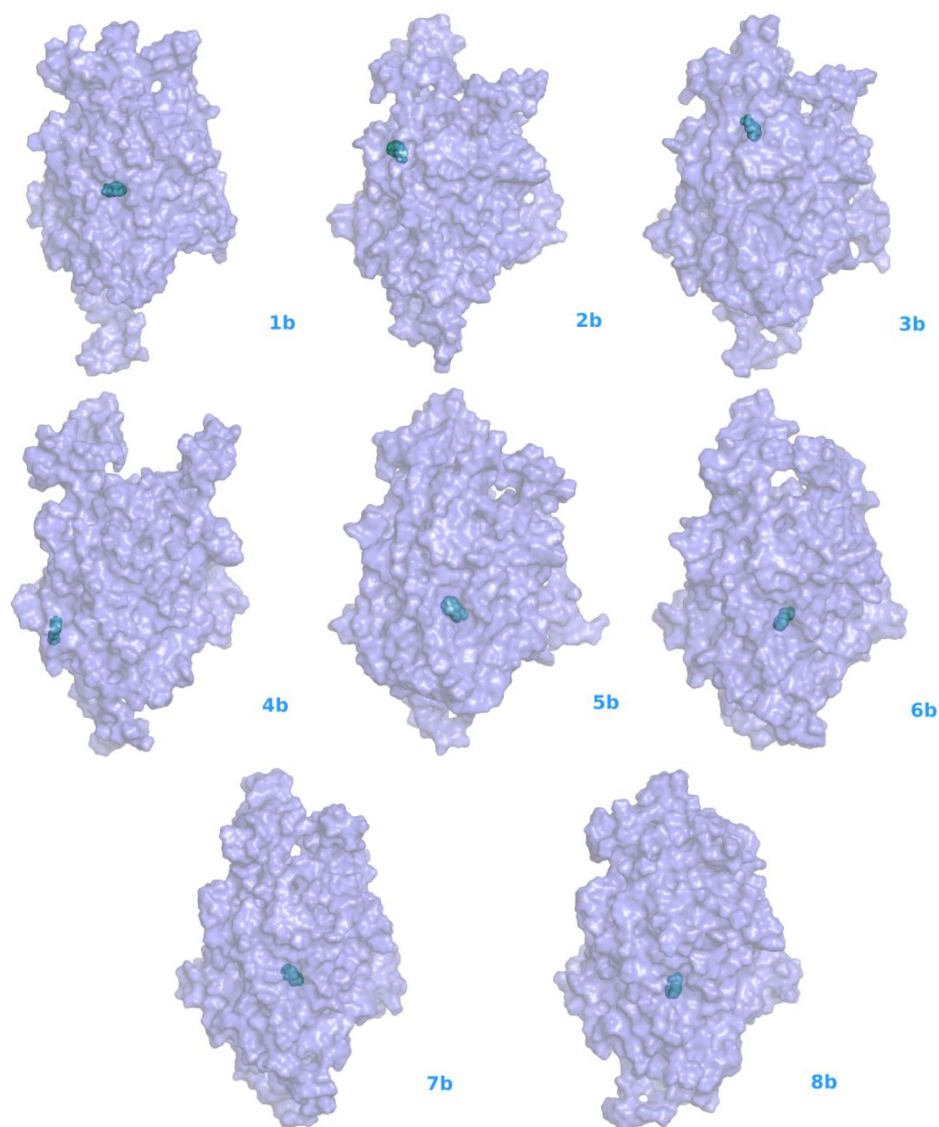
Figure 5.20 shows DAT structure of the result of subcluster at8 and dopamine complex snapshot which was taken from docking studies. The dopamine-binding site in our structure of the result of subcluster at8, was made by unwound regions of transmembrane helices 10, 1 and 8, as seen in Figure 5.20.(a). As shown in Figure 5.20 (b), Trp84 and Pro387 are hydrophobic residues and all colored with a green interior. On the other hand Asp476, Tyr88, Asp385, Gly386 and Arg85 are polar residues and colored in light purple. Basic residues are further annotated by a blue interior ring, and acidic residues with a red ring. As shown in Figure 5.20., there are hydrogen bonding interactions between the side chain of dopamine and DAT's residues of Asp476, Tyr88 and Asp385, they are drawn with an arrowhead to denote the direction of the hydrogen bond. In addition to these, Tyr88 interacts with the aromatic ring of dopamine.



**Figure 5.20.** DAT (subcluster at8)-dopamine binding complex snapshot which is taken from docking studies (a). 2D representation of the atomic interactions between the DAT and dopamine (b).

You can see from the above figures, and explanations, docking results of dopamine and DAT model subclusters clustered of 200 ns simulation according to the binding site regions using a RMSD threshold of 1.3 Å have been analyzed. As shown in these analyzes, dopamine contacted with various helices and residues in different conformations of DAT thereby it forms different binding sites. In the following sections they will be examined in detail in a way that these different binding sites in the protein is depicted in Figure 5.21.





**Figure 5.21.** Autodock different binding site results of dopamine and DAT model subclusters. Clustering was performed based on the binding site regions using a RMSD threshold of 1.3 Å for all simulations. Dopamine is shown in the binding pocket as dots in green, while the binding pocket is represented as molecular surface format, colored with blue.

All the conformations shown in Figure 5.21 were from the same angle for the aligned snapshots of the best members of the cluster.

Several NSS structure-function studies support direct contributions of TMH 1 and 3 to substrate recognition [119-128]. On the other hand in another study on the crystal structure of LeuT which is bacterial homolog of DAT, and two  $Na^+$  bound to the unwound regions of transmembrane helices 1 and 6 suggested that these unwound

regions are relatively flexible and thus may serve as hinges for the conformational transition [150]. Following the classical model, the TM segments 1 and 6, were proposed to move in an alternating fashion relative to TM 3 and 8 [130].

Our results are in agreement with the identification of these segments, as explained above in detail cluster-(3Å) results binding site residues commonly belong to TMH1, TMH3, TMH8, TMH6, TMH10, TMH9 and TMH4 and cluster-(1.3Å) results binding site residues belong to TMH1, TMH3, TMH8, TMH6 and TMH4.

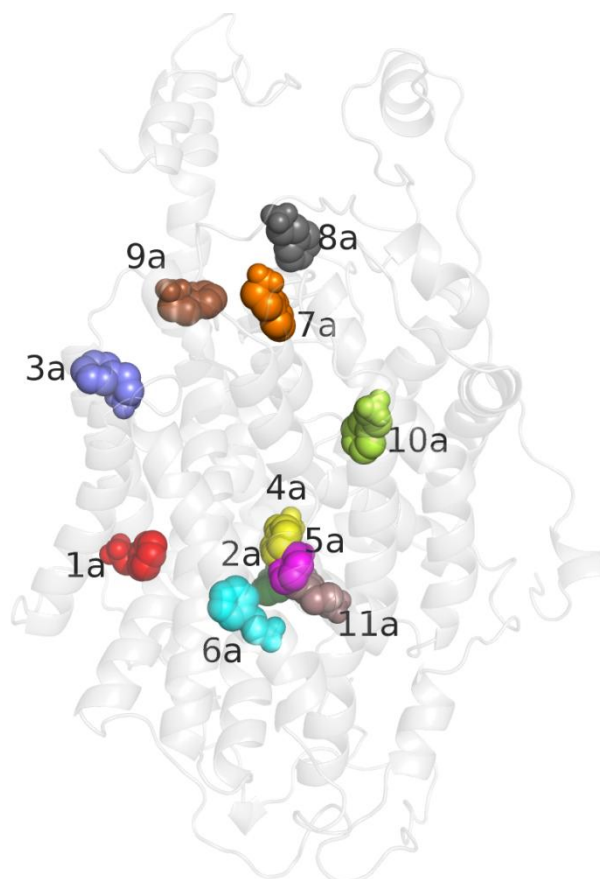
Binding-site residues; Asp 79, Val 152, Tyr 156, Phe 76, Ala 77, Ser 149, Ser 422, Phe 320, Ser 321, Ala 423, Leu 322, Gly 323, Phe 326, Val 328 and Gly 426 are previously determined according to experimental and computational studies as a primary binding site (S1) of dopamine in DAT [108-117,13,23,100]. In our study, cluster-1.3Å docking result binding site residues; Asp 79, Tyr 156, Phe 76, Ser 422, Phe 320 and Ser 321 are similar with previously studies. Other residues of cluster 1.3 docking results and all residues of cluster 3 docking results are different from S1 site residues because many of them belong to S2 site as explained in detail in the following section 5.5.

### **5.2.5 The S1 and S2 binding sites and the substrate translocation pathway of DAT**

The main point of DAT-dopamine complex mechanisms is supposed to be the allosteric effect of ion and substrate-binding on the translocation process. According to computational and experimental studies, the local perturbations are propagated from one end of the transporter to the other and cause important alterations in the preferred state from the binding events in LeuT [31,64-68]. The structural changes which are large-scale are interpretable as the formation of outward and inward-open conformations are thought to accommodate the process of transport. In literature ligand binding in the extracellular vestibule of LeuT which named as S2 binding site is suggested as it affects the one element of the allosteric mechanism which generates the conformational alterations during the propagation of local perturbations instead of large rigid body motions [31].

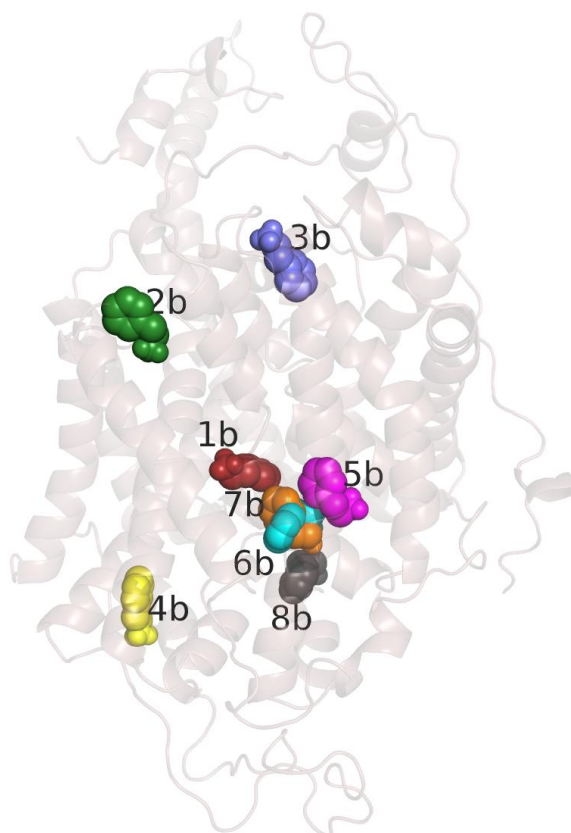
As mentioned before previous molecular dynamics (MD) simulations have identified structural elements important for substrate binding and the formation of an occluded state for dopamine transporter but the involvement of a LeuT-like S2 binding site and any mechanistic role that an S2-bound substrate might have in modulating DAT function in the manner described for LeuT, remain open question than others.

In this thesis, to study the mechanism of dopamine translocation to the intracellular side, we used different conformations of a DAT model which are obtained from clustering as in mentioned previous chapter. And also to explore the pathway related with different binding sites results were investigated. To determine the S1 and S2 sites we used the different states of DAT and position of specific residues which are suggested in previous studies.



**Figure 5.22** Different binding site results of dopamine and DAT model subclusters clustering of all simulations according to the overall structure using a RMSD threshold of 3 Å. DAT is shown as helices in transparent gray. Positions of dopamine in different subclusters represent as dots which is; subcluster 1 in red, subcluster 2 in green, subcluster 3 in blue, subcluster 4 in yellow, subcluster 5 in magenta,

subcluster 6 in cyan, subcluster 7 in orange, subcluster 8 in gray, subcluster 9 in brown, subcluster 10 in limon and subcluster 11 in dirty violet.



**Figure 5.23** Different binding site results of dopamine and DAT model subclusters clustering of all simulations according to the binding site regions using a RMSD threshold of 1.3 Å. DAT is shown as helices in transparent pink. Positions of dopamine in different subclusters represent as dots which is; subcluster 1 in red, subcluster 2 in green, subcluster 3 in blue, subcluster 4 in yellow, subcluster 5 in magenta, subcluster 6 in cyan, subcluster 7 in orange and subcluster 8 in gray

Our characterization of the S1 and S2 sites and the substrate translocation pathway based on the analysis of 19 different docking result which are the DAT different states obtained from 2 different clustering process shown in Figure 5.22 and 5.23.

As shown in the figures, after treatment of docking, dopamine is observed to bound to different regions. We identified here, these regions as a S1, S2 and S1 to extracellular.

The residues forming the S1 site were identified from the docking results of both first and second clustering process. In the S1 site, dopamine resulting binding pose is consistent with previous studies [124-132]. Most residues in contact with the S1 substrate were from TMH 1, TMH 3, TMH 6 and TMH 8 and remained the same in both docking result of clustering, as explained previously section 5.2 and 5.4.

The S2 site residues identified in the first clustering docking results which are subcluster 2, subcluster 4, subcluster 5, subcluster 6 and subcluster 11 were from jointly TMH 1, TMH 3, TMH 8 and TMH 10 and second clustering docking results which are subcluster 5, subcluster 6, subcluster 7 and subcluster 8 were from exactly the same helices region as the first clustering. The composition of the S2 site in LeuT is suggested to be similar to composition of the S2 site in DAT and to include the corresponding (aligned) hydrophobic residues Phe 155, Trp 162 and Phe 472 and a pair of corresponding charged residues, Asp 476 and Arg 85 [13]. These residues consistent with our studies also our TMH region determination for S2 site and consistent with study of Jufang et al [122].

**Table 5.5** Comparison of S1 site residues. Same residues found in these regions are shown in dark.

S1 site residues identified in the literature			S1 site residues identified in the our study		
<b>Phe 76</b>	<b>Tyr 156</b>	Val 328	Ile148	<b>Ser321</b>	<b>Phe320</b>
Ala 77	<b>Phe 320</b>	<b>Asp 421</b>	Gly325	Leu418	Leu80
<b>Asp 79</b>	<b>Ser 321</b>	<b>Ser 422</b>	Ile330	<b>Phe76</b>	<b>Ser422</b>
Ser 149	Leu 322	Ala 423	Val145	Gly75	<b>Asp421</b>
Val 152	Gly 323	Gly 425	Thr144	Val78	<b>Tyr156</b>
Gly 153	Phe 326	Gly 426	Val141	Ala81	<b>Asp79</b>

Residues are shown in table obtained from previous studies and in our study subcluster 10 docking results obtained from the first cluster process and subcluster 1 docking results obtained from the second cluster process.

**Table 5.6** Comparison of S2 site residues. Same residues found in these regions are shown in dark.

S2 site residues identified in the literature			S2 site residues identified in the our study		
<b>Arg 85</b>	<b>Asp 385</b>	<b>Thr 473</b>	<b>Asp476</b>	Glu218	Val471
<b>Phe 155</b>	<b>Gly 386</b>	<b>Asp 476</b>	Hse477	<b>Phe217</b>	Tyr470
Ile 159	<b>Pro 387</b>		<b>Arg85</b>	<b>Ile469</b>	<b>Val221</b>
<b>Trp 162</b>	Phe 391		<b>Asp385</b>	Tyr470	<b>Trp162</b>
<b>Phe 217</b>	Leu 415		<b>Pro387</b>	<b>Phe155</b>	
<b>Val 221</b>	<b>Ile 469</b>		<b>Gly386</b>	<b>Thr473</b>	
Leu 222	<b>Phe 472</b>		Tyr88	<b>Phe472</b>	

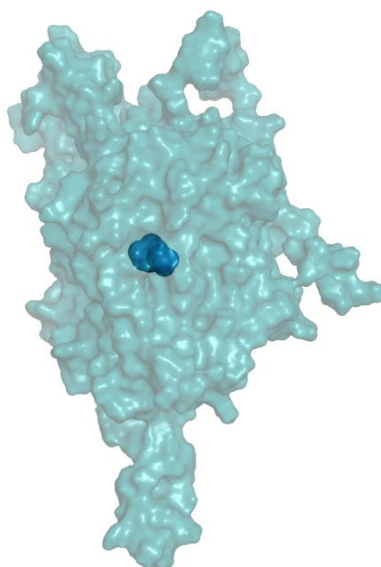
Residues are shown in Table 5.6 obtained from studies in literature [122,31] and in our study subcluster 2, subcluster 4, subcluster 5, subcluster 6 and subcluster 11 docking results obtained from the first clustering process and subcluster 5, subcluster 6, subcluster 7 and subcluster 8 docking results obtained from the second clustering process.

Apart from these 19 different docking results, we have one more result of docking which is obtained from docking process of dopamin and DAT initial structure which is before applying the MD simulation process. Docking was performed on the initial structure of DAT and dopamine to analyzed the binding energy, binding site and how connections they have before applying the MD simulation process shown in Figure 5.24. 100 runs for dopamine were performed.

**Table 5.7** Docking results for initial DAT model-ligand dopamine with AutoDock 4.0 (result of top 10)

Rank	Sub-Rank	Run	Binding Energy(kcal/mol)	Cluster RMSD (Å)	Reference RMSD (Å)
1	1	85	-7.43	0.00	6.16
1	2	51	-7.42	0.08	6.17
1	3	4	-7.42	0.19	6.19
1	4	20	-7.41	0.08	6.17
1	5	66	-7.41	0.11	6.17
1	6	62	-7.41	0.11	6.17
1	7	10	-7.41	0.15	6.17
1	8	89	-7.41	0.66	6.20
1	9	68	-7.41	0.14	6.18
1	10	46	-7.41	0.11	6.17

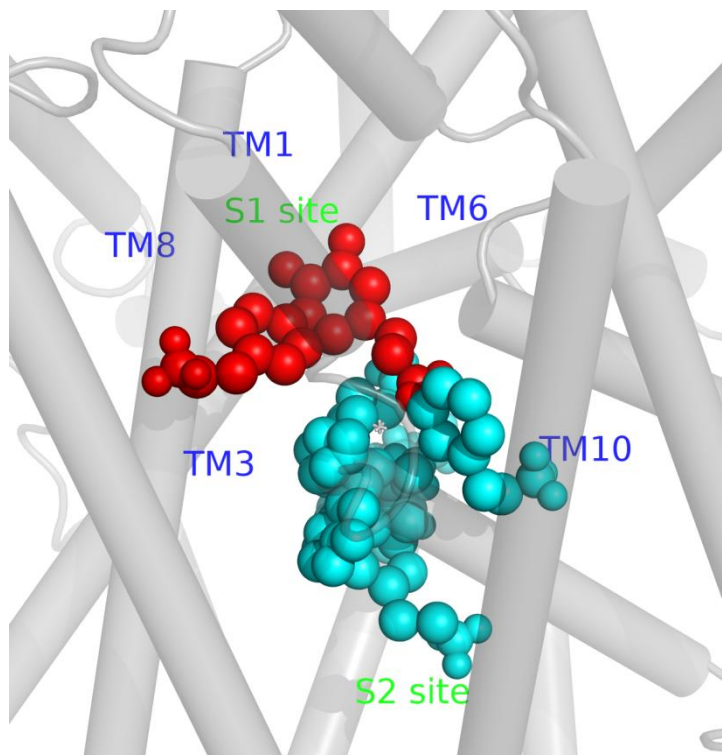
As seen in Table 5.6. , after the docking process with AutoDock 4.0, the binding energies and RMSD values for each run were obtained. The results are classified in ranks and also each run is divided into sub-ranks. For the natural ligand dopamine, the run number 85 which belongs to rank 1 and also sub-rank 1, is the best pose based on binding energies (-7.43 kcal/mol) and it has 5.16 RMSD value. The residues around the activesite, that can have important roles in binding, are Phe326, Ala77, Tyr156, Gly323, Asp79, Ala81, Gly426, Val152, Ser321, Phe320, Leu322, Phe76 and Ser422.



**Figure 5.24** Autodock binding site result of dopamine and initial DAT model. The binding pocket is represented in molecular surface format, colored with cyan. The dopamine molecule shown as dots in blue, in the complex model.

When we analyzed the dopamine-DAT initial docking results as in the latter docking results, we determined the active region of dopamine-DAT corresponds to S1 site according to binding residues and helix.

When we analyze the results of the docking of identified 20 different active region, we saw that 3 of these belong to S1 site and 9 of them belong to the S2 site (Figure 5.25) according to binding of helices and residues.



**Figure 5.25** The substrate binding sites of DAT. S1 site is represented as spheres, colored with red and S2 site is represented as spheres too and colored with cyan. The TMHs 1, 3, 6, 8 and 10 which are interacting with S1 and S2, are shown as a cylindrical helices in gray.

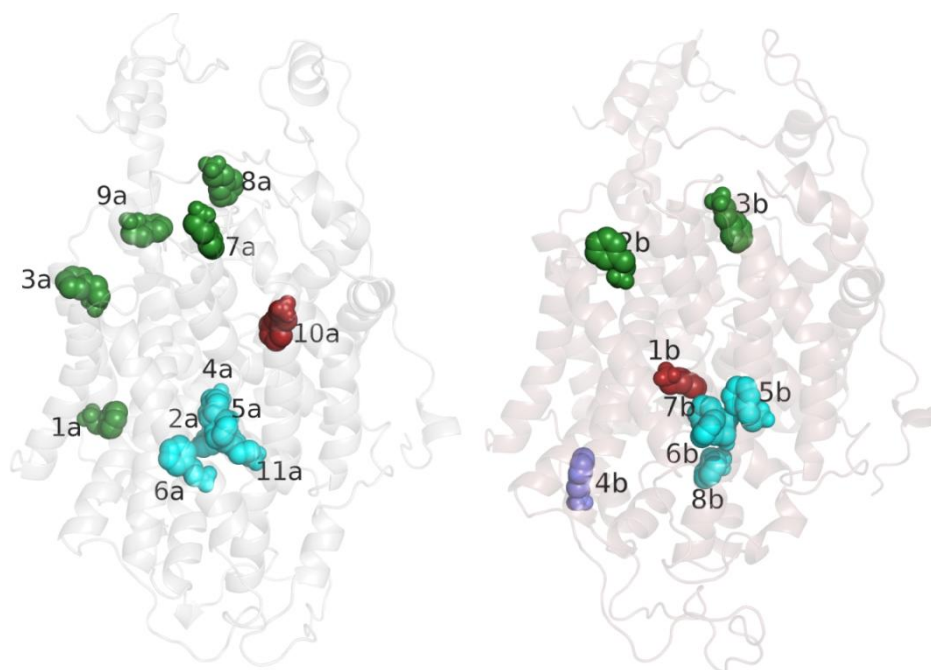
After the determination of S1 and S2 sites, when we analyzed the remaining 8 different active sites we see that, 7 conformations except for one of them is connected as a step by step pathway from the S1 site to the intracellular site.

The structures which are used for the docking were obtained from the MD and for this reason we can say that residues in contact with the substrate as it moves from the S1 site toward the cytoplasmic side through the 200 ns MD simulations. These regions were classified as belonging to the intracellular translocation pathway lined mainly by residues from TMHs 5, 6, 8, 9 and 4, shown in Table 5.8. Thus our determination is consistent with study of Jufang et al [122].



**Table 5.8** Comparison of translocation pathway from the S1 site to the intracellular site residues. Same residues found in these regions are shown in dark.

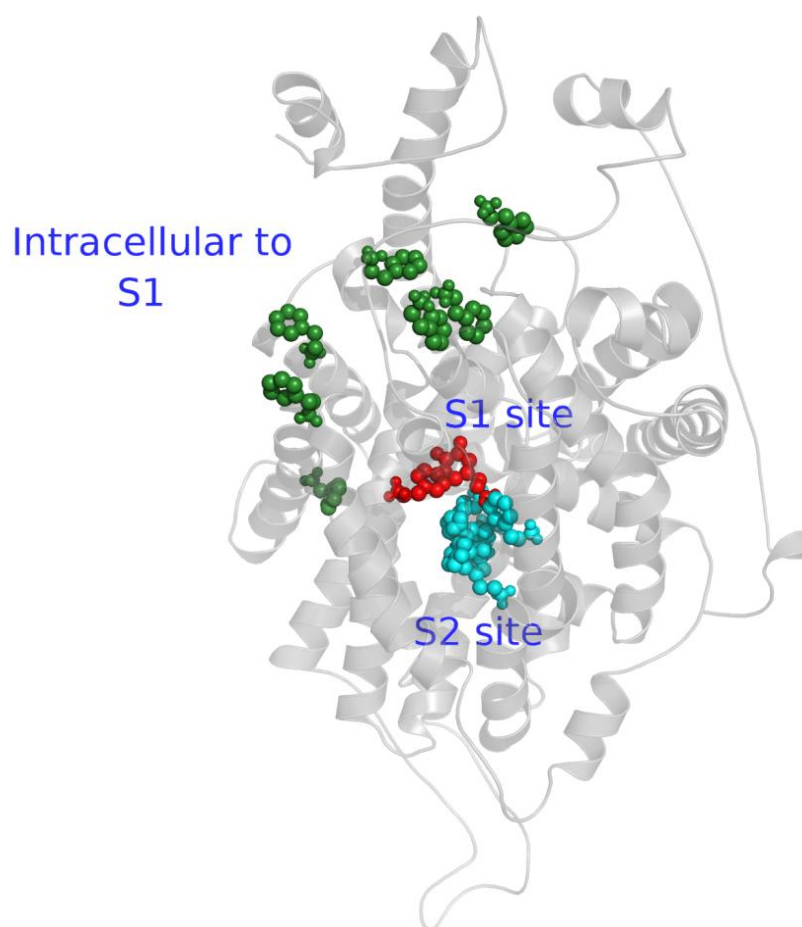
(S1 to Intracellular) Translocation pathway residues identified in the literature			(S1 to Intracellular) Translocation pathway residues identified in the our study		
<b>Arg60</b>	Gly258	Ala331	<b>Arg60</b>	Glu126	<b>Glu428</b>
Trp63	<b>Val259</b>	Phe332	Ile435	Gly127	Lys257
Ser72	Ser262	Tyr335	Glu446	Val430	Arg125
Gly75	Gly263	Met424	<b>Ala128</b>	Ile431	<b>Asp436</b>
<b>Ala128</b>	Val266	<b>Glu428</b>	<b>Leu255</b>	<b>Thr432</b>	<b>Arg445</b>
<b>Leu255</b>	Leu329	Ser429	<b>Val259</b>	<b>Gly433</b>	Leu251
<b>Thr432</b>	<b>Asp 436</b>		Trp256	Leu434	Tyr252
<b>Gly433</b>	<b>Arg445</b>		Ser254	Glu437	Ala129



**Figure 5.26** Different binding site results of dopamine and DAT model subclusters which are obtained from; clustering of all simulations according to the binding site regions using a RMSD threshold of 3 Å (left one) and clustering of all simulations according to the binding site regions using a RMSD threshold of 1.3 Å (right one). DAT is shown as helices in transparent gray (cluster 3) and pink (cluster 1.3). Positions of dopamine in different subclusters are labeled and represented as dots which is; S1 in red, S2 in cyan, the substrate translocation pathway from the S1 site to the intracellular site in green and finally purple is untitled.

Residues are shown in Table 5.8 obtained from literature [122,31] and from our study (subcluster 1, subcluster 3, subcluster 7 and subcluster 9 docking) results obtained from the first clustering process and (subcluster 2 and subcluster 3 docking) results obtained from the second clustering process.

Consequently, using MD, clustering and docking analysis we defined a primary binding site (S1), S2 site and the translocation pathway of dopamine from the S1 site to the intracellular site. You can see in Figure 5.26 and 5.27, our defined regions.



**Figure 5.27** Active sites and translocation pathway of dopamine in DAT which are defined in our study. Positions of dopamine through the simulation are labeled and represented as spheres which is; S1 in red, S2 in cyan, the substrate translocation pathway from the S1 site to the intracellular site in green.

## **Chapter 6**

### **Conclusion**

The dopamine transporter (DAT) is a membrane protein and it transports dopamine across the membrane which is located on the plasma membrane of nerve terminals. By taking into synaptic dopamine ligand into neurons, it plays a critical role in maintaining dopamine homeostasis and in terminating dopamine neurotransmission in the central nervous system. Many membrane proteins undergo very large conformational changes to complete their function. Experimentally, crystallography will, at most, only be able to capture a time and space-averaged snapshot of these distinct states. Therefore, *in silico* methods are used. Molecular Dynamics (MD) is one of these useful tools that, additionally provides information regarding the stability of a membrane protein, can also provide insight into the behavior in which these conformational changes take place.

In this thesis, firstly the structure-function relationship of the human dopamine transporter (DAT) and the dopamine is addressed via Molecular Dynamics (MD) simulations. Throughout the study, we developed three cases. The first case is the dopamine transporter as a ‘DAT’ model, the second is the ‘dopamine’ model and the third is the ‘DAT-dopamine complex’ model. A series of energy minimization and MD simulations of 200 ns for the DAT model, 15 ns for the dopamine model and 20 ns for the DAT-dopamine complex model have been performed by using NAMD 2.7 software package. Afterwards, to study the mechanism of dopamine translocation to the intracellular side we used different conformations of DAT model which are obtained with clustering, to explore the pathway and different binding sites. For the DAT and dopamine binding analysis we used a docking program, AutoDock 4.0. The dopamine-binding modes were determined through the calculation of binding free energies.

In the first part of the study, the structure-function relationship of the DAT is addressed via Molecular Dynamics simulations (MD). After the MD process, the structure alignment performed in VMD for initial DAT and after MD simulation DAT model. The RMSD value of  $C_{\alpha}$  atoms pertaining to these before-after models have been calculated as 7.586 Å for  $C_{\alpha}$  atoms. This number is an indication of DAT's structure have undergone some variations during the Molecular Dynamics Simulation. These variations analyzed and most mobile regions of protein determined. Furthermore 12 TMH regions of our human DAT model identified, comparing with the experimental data. According to analysis profile, the highest stability of the protein is observed at the helix region and we can say that a longer simulation study can be performed to see more mobility on this helix region which are affecting the binding site. Among all transmembrane helices, the most mobile ones are the twelfth and the fifth helices (TMH12 and TMH5).

As it is well known, dopamine is a symporter and is impossible to pass the membrane without dopamine transporter and ions. In second part of the study we embedded the dopamine in the membrane, to see how it behave in the membrane without dopamine transporter and to compare its behavior in a realistic environment. We created the special topology file for dopamine and applied the same MD procedure. After placement of the dopamine in the centre of membrane, is seen that dopamine moving step by step. It went out from membrane as expected.

In third part of our study, we placed the dopamine and dopamine transporter in the membrane, complex form of dopamine and DAT which is created via molecular docking. At this time scales of MD simulation without using SMD (steered molecular dynamics) method, it is not possible to see dopamine binding with dopamine transporter. For this reason, we used the molecular docking method before starting the MD simulation. 2  $Na^{+}$  and 5  $Cl^{-}$  ions are embedded into the membrane with complex structure, to make the total net charge of the system equal to zero.

The dopamine-binding site in our human DAT structure was made by unwound regions of helices 1, 6 and 10, before MD simulation. After MD simulation, dopamine changed its position. The new dopamine-binding site in DAT was made by

unwound regions of helices 1, 8 and 10 which was close to the sites of  $Na^+$  and  $Cl^-$ -binding. In addition to these, the binding site residues changed. According to the commonality of binding residues and transmembrane helices, we can say that MD simulation affected binding of DAT-dopamine and changed the binding site. For comparison DAT and DAT+dopamine simulations, initial 20 ns part of DAT simulation, extracted from 200 ns MD trajectory, is considered. The dynamic behavior of the DAT-dopamine complex and DAT have been monitored by the  $C_\alpha$  RMSD changes. RMSD change of DAT dopamine complex was smaller than that of the corresponding DAT structure without dopamine. On the other hand, when looking the RMSF profile of DAT without dopamine simulation, changing of loop regions can be observed. This indicates that running of MD simulation together with dopamine effects on DAT protein's conformational dynamics. Among all trans membrane helices, the most mobile ones are the twelfth, the fifth and third helices (TMH12, TMH5, TMH3). However, the biggest helix TMH12 is fluctuating through the simulation. The helices TMH1, TMH8 and TMH10 which binding with dopamine, are remain stable with respect to TMH12, TMH5 and TMH3 can be observed.

After examine properties and behaviours of our three model, to see the different conformations of DAT we made clustering analysis according to overall structure and according to binding site. We used for this process DAT model snapshots taken from 200 ns MD trajectories. The program used for cluster analysis is the *kclust* script. In our studies, distinguishable 11 clusters are obtained with a threshold of 3.00 Å RMSD in the first case. For second cluster process, cluster radius 1.3 gave better results and 8 different subcluster are obtained. When we compare the cluster results with the results of MD, we also observed that difference in clusters are based more on the loop regions than the helix regions. This means that the conformational changes observed during the simulation, causing the cluster variations, are mainly resulting from the more flexible loops in the structure. Likewise, when we examine the RMSD analysis results, DAT structure undergoes small fluctuations, that mean not very large movements of structural parts. While the helix parts are stable (fluctuating less), overall small fluctuation seemed to be the cause of transport mechanism. Helix regions stability also supports that the structure of human DAT is evolutionary protected. Furthermore, when compare changes on

the helix regions TM12, TM5, TM1 and TM3 have more differences than others for two cases.

After two different clustering processes, we have obtained 11 from the initial case and 8 from the latter case. Totally 19 different conformations of DAT model were obtained. These 19 different conformations were used for docking analysis in order to understand the binding variations. Each of these conformations, docking process stages are applied and docked with dopamine ligand. 100 runs for dopamine were performed for each subcluster.

According to the experimental studies conducted previously with the DAT-dopamine complex the binding energy value was also found as -7.4 kcal/mol [137]. When we compare this score to our computational docking study, we can see that subcluster-2 and subcluster-4 scores of first cluster process and subcluster 8 scores (-7.31 kcal/mol) of second cluster process show quite close confirming a good agreement.

According to analyzes, dopamine contacted with variously helices and residues in different conformations of DAT thereby it forms different binding sites. In our results, cluster-(3Å) binding site residues commonly belong to TMH1, TMH3, TMH8, TMH6, TMH10, TMH9 and TMH4 and cluster-(1.3Å) binding site residues belong to TMH1, TMH3, TMH8, TMH6 and TMH4. In addition to these, cluster-1.3Å docking result binding site residues; Asp 79, Tyr 156, Phe 76, Ser 422, Phe 320 and Ser 321 are similar with previously studies. Other residues of cluster 1.3 docking results and all residues of cluster 3 docking results are different from S1 site residues because many of them belong to S2 site.

To explore the pathway related with different binding sites results were investigated. To determine the S1 and S2 sites we used the different states of DAT and position of specific residues which are suggested in previous studies.

The residues forming the S1 site were identified from the docking results of both first and second clustering process. In the S1 site, dopamine resulting binding pose is consistent with previous studies [124-132]. Most residues in contact with the

S1 substrate were from TMH 1, TMH 3, TMH 6 and TMH 8 and remained the same in both docking result of clustering, as explained previously section 5.2 and 5.4.

The S2 site residues identified in the first clustering docking results which are subcluster 2, subcluster 4, subcluster 5, subcluster 6 and subcluster 11 were from jointly TMH 1, TMH 3, TMH 8 and TMH 10 and second clustering docking results which are subcluster 5, subcluster 6, subcluster 7 and subcluster 8 were from exactly the same helices region as the first clustering. The composition of the S2 site in LeuT is suggested to be similar to composition of the S2 site in DAT and to include the corresponding (aligned) hydrophobic residues Phe 155, Trp 162 and Phe 472 and a pair of corresponding charged residues, Asp 476 and Arg 85 [13]. These residues consistent with our studies also our TMH region determination for S2 site and consistent with study of Jufang et al [122].

On the other hand, docking was performed on the initial structure of DAT and dopamine to analyzed the binding energy, binding site and how connections they have before applying the MD simulation process. When we analyzed the dopamine-DAT initial docking results as in the latter docking results, we determined the active region of dopamine-DAT corresponds to S1 site according to binding residues and helix.

We identified 20 different active region according to analyze the results of the docking, we saw that 3 of these belong to S1 site and 9 of them belong to the S2 site according to binding of helices and residues.

After the determination of S1 and S2 sites, when we analyzed the remaining 8 different active sites we see that, 7 conformations except for one of them is connected as a step by step pathway from the S1 site to the intracellular site.

The structures which are used for the docking were obtained from the MD and for this reason we can say that residues in contact with the substrate as it moves from the S1 site toward the cytoplasmic side through the 200 ns MD simulations. These regions were classified as belonging to the intracellular translocation pathway lined mainly by residues from TMHs 5, 6, 8, 9 and 4. Thus our determination is consistent with study of Jufang et al [122].

We observed that there is a remarkable agreement between the identities of the key residues in the translocation mechanism. We were able to identify from the simulations and experimental data in the literature.



## REFERENCES

- [1] Amara, S.G., and Sonders, M.S. *Neurotransmitter transporters as molecular targets for addictive drugs*. *Drug Alcohol Depend.* 51, 87–96. (1998).
- [2] Schenk, J.O., George, S.E., Schumacher PD What can be learned from studies of multisubstrate mechanisms of neuronal dopamine transport?, 479(1-3):223-8, Department of Chemistry, Washington State University, 2003.
- [3] Liu, J. and Rost, B., Comparing Function and Structure Between Entire Proteomes. *Protein Sci.*, 10, 1970-1979, 2001.
- [4] Muller, D. J., Wu, N., and Palczewski, K., Vertebrate Membrane Proteins : Structure, Function, and Insights from Biophysical Approaches. *Pharmacol. Rev.*, **60**, 43-78, 2008.
- [5] Giros, B. and Caron, M., Molecular Characterization of the Dopamine Transporter. *Trends Pharmacol. Sci.*, 14, 43-49, 1993.
- [6] Tamm L. K., Arora A., and Kleinschmidt, J. H., Structure and Assembly of  $\beta$ -Barrel Membrane Proteins. *J. Biol. Chem.*, 276, 32399-32402, 2001.
- [7] Speers A. E., and Wu, C. C., Proteomics of Integral Membrane Proteins - Theory and Application. *Chem. Rev.*, 107, 3687-3714, 2007.
- [8] Torres J., Stevens T.J., and Samsó M. Membrane Proteins: the ‘Wild West’ of Structural Biology. *Trends Biochem. Sci.*, 28, 137-144, 2003.
- [9] Midgett, C, R., and Madden, D. R., Breaking the Bottleneck: Eukaryotic Membrane Protein Expression for High-Resolution Structural Studies. *J. Struct. Biol.*, 160, 265-274, 2007.

- [10] Ritz M. C., Lamb, R. J., Goldberg, R., and Kuhar, M. J., Cocaine Receptors on Dopamine Transporters are Related to Self-Administration of Cocaine. *Science*, 237, 1219-1223, 1987.
- [11] Danilenko, U., Analysis of Cocaine Binding Site of Human Dopamine Transporter Using Affinity Labeling and Mass Spectrometry.,M.S., *Petersburg State Chemical Pharmaceutical Academy*, 2003.
- [12] Rudnick, G. Mechanisms of Biogenic Amine Neurotransmitter Transporters, Second Edition ,Totowa, NJ: Humana Press, Inc.,2002.
- [13] Shi, L., Quick, M., Zhao, Y., Weinstein, H., Javitch JA, The Mechanism of a Neurotransmitter: Sodium Symporter-Inward Release of Na<sup>+</sup> and Substrate Is Triggered by Substrate in a Second Binding Site,6, 667-67, 2008.
- [14] Beuming T., Shi L., Javitch J.A., and Weinstein H., A Comprehensive Structure-Based Alignment of Prokaryotic and Eukaryotic Neurotransmitter/Na Symporters (NSS), *Mol Pharmacol* 70:1630–1642, 2006.
- [15] Chen N., Zhen J., and Reith M.E.A., Mutation of Trp84 and Asp313 of the Dopamine Transporter Reveals Similar Mode of Binding Interaction for GBR12909 and Bztpropine as Opposed to Cocaine. *J Neurochem.*,**89**, 853-864, 2004.
- [16] Quick M., Yano H., Goldberg N.R., Duan L., Beuming T., Shi L., Weinstein H, Javitch JA. State-dependent Conformations of the Translocation Pathway in the Tyrosine Transporter Tyt1, a Novel Neurotransmitter: Sodium Symporter from *Fusobacterium nucleatum*, *Biol Chem.* Sep 8; 281 (36):26444-54, 2006.
- [17] Kanner B., I., and Zomot E., Sodium-Coupled Neurotransmitter Transporters. *Chem. Rev.*, 108, 1654-1668, 2008.
- [18] Loland C., Graanas C., Javitch J., and Gether U., Identification of Intracellular Residues in the Dopamine Transporter Critical for Regulation of Transporter and Cocaine Binding. *J. Biol. Chem.*, 279, 3228-38, 2004.

- [19] Sonders, M.S., Quick, M., and Javitch, J.A. How did the neurotransmitter cross the bilayer? A closer view. *Curr. Opin. Neurobiol.* 15, 296–304, 2005.
- [20] Yamashita A., Singh S.K., Kawate T., Jin Y., and Gouaux E., Crystal Structure of a Bacterial Homologue of Na<sup>+</sup>/Cl<sup>-</sup>- Dependent Neurotransmitter Transporters. *Nature*, 437, 215-222, 2005.
- [21] Beuming T., Shi L., Javitch J.A., and Weinstein H., A Comprehensive Structure-Based Alignment of Prokaryotic and Eukaryotic Neurotransmitter/Na Symporters (NSS) Aids in the Use of the LeuT Structure to Probe NSS Structure and Function. *Mol. Pharmacol.*, 70, 1630-1642, 2006.
- [22] Zhou Z., Zhen J., Karpowich N.K., Goetz R.M., Law C.J., Reith M.E., and Wang D., LeuT-Desipramine Structure Reveals How Antidepressants Block Neurotransmitter Reuptake. *Science*, 317, 1390-1393, 2007.
- [23] Huang X., and Zhan C., How Dopamine Transporter Interacts with Dopamine: Insights from Molecular Modeling and Simulation. *Biophys. J.*, 93, 3627-3639, 2007.
- [24] Giros B. and Caron M., Molecular Characterization of the Dopamine Transporter. *Trends Pharmacol. Sci.*, 14, 43-49, 1993.
- [25] Bannon M.J., The Dopamine Transporter: Role in Neurotoxicity and Human Disease. *Toxicol. Appl. Pharmacol.*, 204, 355-360, 2005.
- [26] Iversen, L. Neurotransmitter transporters and their impact on the development of psychopharmacology. *Br. J. Pharmacol.* 147 (Suppl 1), S82–S88, 2006.
- [27] Jackson D. M., Westlind-Danielsson Dopamine receptors: molecular biology, biochemistry and behavioural aspects. *A. Pharmacol. Ther.* 64, 291-369 , 1994.
- [28] Strange P.G., Dopamine receptors: studies on structure and function *Adv. Drug Res.* 28, 313-351, 1996.
- [29] Giros, B., Caron, M.G., Molecular characterization of the dopamine transporter. *Trends Pharmacol. Sci.* 14, 43– 49, 1993.

- [30] Iversen, L.L., Role of transmitter uptake mechanisms in synaptic neurotransmission. *Biophys. J.* 41, 571–591, 1971.
- [31] Nianhang C., Maarten E.A., Reith, Na<sup>+</sup> and the substrate permeation pathway in dopamine transporters, *European Journal of Pharmacology*, 213-221, 2003.
- [32] Boja, J.W., Vaughan, R., Patel, A., Shaya, E.K. and Kuhar, M.J., In Boja, J.W., Vaughan, R., Patel, A., Shaya, E.K. and Kuhar, M.J. (Eds), *Dopamine receptors and transporters*, Marcel Dekker, New York, 611, 1994.
- [33] Aina Westrheim R., Ingebrigt S., Svein G.D., Molecular model of the neural dopamine transporter *Department of Pharmacology, Institute of Medical Biology, University of Tromsø, N-9037 Tromsø, Norway*, 5-6, 2003.
- [34] Bönisch, H., Transport and drug binding kinetics in membrane vesicle preparation. *Methods Enzymol.* 296, 259–278, 1998.
- [35] Sonders, M.S., Zhu, S.-J., Zahniser, N.R., Kavanaugh, M.P., Amara, S.G., Multiple ionic conductances of human dopamine transporter the actions of dopamine and psychostimulants. *J. Neurosci.* 17, 960–967, 1997.
- [36] Chen, N., Trowbridge, C.C., Justice, J.B. Jr., Cationic modulation of human dopamine transporter: dopamine uptake and inhibition of uptake. *J. Pharmacol. Exp. Ther.* 290, 940–949, 1999.
- [37] Earles, C., Schenk, J.O., A multi substrate mechanism for the inward transport of dopamine by the human dopamine transporter expressed in HEK cells and its inhibition by cocaine. *Synapse* 33, 230–238, 1999.
- [38] Li, L.B., Reith, M.E.A., Modeling of the interaction of Naq and Kq with the binding of dopamine and w3HxWIN 35,428 to the human dopamine transporter. *J. Neurochem.* 72, 1095–1109, 1999.

- [39] Li, L.B., Reith, M.E.A., Modeling of the interaction of Naq and Kq with the binding of dopamine and w3HxWIN 35,428 to the human dopamine transporter. *J. Neurochem.* 72, 1095–1109, 1999.
- [40] Meiergerd, S.M., Schenk, J.O., Striatal Transporter for dopamine: Catechol structure-activity studies and susceptibility to chemical modification. *J. Neurochem.* 62, 998–1008, 1994.
- [41] Javitch, J.A., Probing structure of neurotransmitter transporters by substituted-cysteine accessibility method. *Methods Enzymol* 296: 331–346, 1998.
- [42] Loland, C.J., Norregaard L., Gether U., Defining proximity relationships in the tertiary structure of the dopamine transporter. Identification of a conserved glutamic acid as a third coordinate in the endogenous Zn<sup>2+</sup> binding site. *J Biol Chem* 274: 36928–36934, 1999.
- [43] Norregaard, L, Loland CJ, Gether U., Evidence for distinct sodium dopamine- and cocaine-dependent conformational changes in transmembrane segments 7 and 8 of the dopamine transporter. *J Biol Chem* 278: 30587–30596, 2003.
- [44] Lin Z., Itokawa M., Uhl, GR., Dopamine transporter proline mutations influence dopamine uptake, cocaine analog recognition, and expression. *FASEB J* 14: 715–728, 2000.
- [45] Itokawa, M., Lin, Z, Uhl G.R., Dopamine efflux via wild-type and mutant dopamine transporters: alanine substitution for proline-572 enhances efflux and reduces dependence on extracellular dopamine, sodium and chloride concentrations. *Brain Res Mol Brain Res* 108: 71–80, 2002.
- [46] Sen, N., Shi L., Beuming T., Weinstein H., Javitch, J.A., A pincer-like configuration of TM2 in the human dopamine transporter is responsible for indirect effects on cocaine binding. *Neuropharmacology* 49: 780–790, 2005.
- [47] Lin, Z., Uhl, G.R., Proline mutations induce negative-dosage effects on uptake velocity of the dopamine transporter. *J Neurochem* 94: 276–287, 2005.

- [48] Sucic, S., Bryan-Lluka, L.J. Roles of transmembrane domain 2 and the first intracellular loop in human noradrenaline transporter function: pharmacological and SCAM analysis. *J Neurochem* 94: 1620–1630, 2005.
- [49] Quick M., Winther A.M., Shi L., Nissen P, Weinstein H, et al. Binding of an octylglucoside detergent molecule in the second substrate (S2) site of LeuT establishes an inhibitor-bound conformation. *Proc Natl Acad Sci U S A* 106: 5563–5568, 2009.
- [50] Singh, S.K., Yamashita, A., Gouaux, E., Antidepressant binding site in a bacterial homologue of neurotransmitter transporters. *Nature* 448: 952–956, 2007.
- [51] Singh, S.K., Piscitelli, C.L., Yamashita A, Gouaux, E., A Competitive Inhibitor Traps LeuT in an Open-to-Out Conformation. *Science* 322: 1655–1661, 2008.
- [52] Zhou, Z., Zhen, J., Karpowich, N.K., Law, C.J., Reith, M.E., et al. Antidepressant specificity of serotonin transporter suggested by three LeuTSSRI structures. *Nat Struct Mol Biol* 16: 652–657, 2009.
- [53] Zhou, Z., Zhen, J., Karpowich, N.K., Goetz, R.M., Law, C.J., et al. LeuTdesipramine structure reveals how antidepressants block neurotransmitter reuptake. *Science* 317: 1390–1393, 2007.
- [54] Yamashita, A., Singh, S.K., Kawate, T., Yan Jin, Y., Gouaux, E., Crystal structure of a bacterial homologue of Na<sup>+</sup>/Cl<sup>-</sup> dependent neurotransmitter transporters. *Nature* 437: 215–223, 2005.
- [55] Shan, J., Javitch, J.A., Shi, L., Weinstein, H., The Substrate-Driven Transition to an Inward-Facing Conformation in the Functional Mechanism of the Dopamine Transporter. *Department of Physiology and Biophysics, Weill Medical College of Cornell University, New York, New York, United States of America*, 2011.

- [56] Jardetzky, O., Simple Allosteric Model for Membrane Pumps. *Nature* 211: 969–970, 1996.
- [57] Forrest, L.R., Rudnick, G., The rocking bundle: a mechanism for ion coupled solute flux by symmetrical transporters. *Physiology (Bethesda)* 24: 377–386, 2009.
- [58] Forrest, L.R., Tavoulari, S., Zhang, Y.W., Rudnick G, Honig B Identification of a chloride ion binding site in Na<sup>+</sup>/Cl<sup>-</sup>-dependent transporters. *Proc Natl Acad Sci U S A* 104: 12761–12766, 2007.
- [59] Crisman, T.J., Qu, S., Kanner, B.I., Forrest, L.R. Inward-facing conformation of glutamate transporters as revealed by their inverted-topology structural repeats. *Proc Natl Acad Sci U S A* 106: 20752–20757, 2009.
- [60] Enkavi, G., Tajkhorshid, E., Simulation of spontaneous substrate binding revealing the binding pathway and mechanism and initial conformational response of GlpT. *Biochemistry* 49: 1105–1114, 2010.
- [61] Khalili-Araghi, F., Gumbart, J., Wen, P.C., Sotomayor, M., Tajkhorshid, E., et al. Molecular dynamics simulations of membrane channels and transporters. *Curr Opin Struct Biol* 19: 128–137, 2009.
- [62] Li, J., Tajkhorshid, E., Ion-releasing state of a secondary membrane transporter. *Biophys J* 97: L29–31, 2009.
- [63] Quick, M., Yano, H., Goldberg, N.R., Duan, L., Beuming, T., et al. State dependent conformations of the translocation pathway in the tyrosine transporter Tyt1, a novel neurotransmitter: sodium symporter from *Fusobacterium nucleatum*. *J Biol Chem* 281: 26444–26454, 2006.
- [64] Zhao, Y., Quick, M., Shi, L., Mehler, E.L., Weinstein, H., et al. Substrate dependent proton antiport in neurotransmitter: sodium symporters. *Nat Chem Biol* 6: 109–116, 2010.

- [65] Noskov, S.Y., Roux, B., Control of Ion Selectivity in LeuT: Two Na<sup>+</sup> Binding Sites with Two Different Mechanisms. *Journal of Molecular Biology* 377: 804–818, 2008.
- [66] Noskov, S.Y., Molecular mechanism of substrate specificity in the bacterial neutral amino acid transporter LeuT. *Proteins: Structure, Function, and Bioinformatics* 73: 851–863, 2008.
- [67] Shi, L., Weinstein, H., Conformational rearrangements to the intracellular open states of the LeuT and ApcT transporters are modulated by common mechanisms. *Biophys J* 99: L103–105, 2010.
- [68] Zhao, Y., Terry, D., Shi L, Weinstein H, Blanchard SC, et al. Singlemolecule dynamics of gating in a neurotransmitter transporter homologue. *Nature* 465: 188–193, 2010.
- [69] Steinbach, J., P., “*Introduction to Macromolecular Simulation*”, July, 2010.
- [70] Leach, A. R., “*Molecular Modelling: Principles and Applications (Second Edition)*”, *Prentice Hall*, 2001.
- [71] Özcan, Ö., *Exploring the intrinsic dynamics of human beta-2 adrenergic G-protein coupled receptor and its potential use in computational drug design studies*, M.S Thesis, Boğaziçi University, 1991.
- [72] Verlet, L., “Computer Experiments on Classical Fluids. I. Thermodynamical Properties of Lennard--Jones Molecules”, *Physical Review*, Vol. 159, pp. 98-103, 1967.
- [73] Hockney, R., W., “The Potential Calculations on Some Applications”, *Methods in Computational Physics*, Vol. 9, pp. 136--143, 1970.
- [74] Swope, W. C., C. A. Hans, H. B. Peter and R. W. Kent, “A Computer Simulation Method for the Calculation of Equilibrium Constants for the Formation of Physical Clusters of Molecules: Application to Small Water Clusters”, *The Journal of Chemical Physics*, Vol. 76, pp. 637--650, 1982.



- [75] Feig, M. J., J. Karanicolas and C. L. Brooks, "MMTSB Tool Set: Enhanced Sampling and Multiscale Modeling Methods for Applications in Structural Biology", *Journal of Molecular Graphics and Modeling*, Vol.22, pp. 377--395, 2004.
- [76] Terstappen, G. C., and Reggiani, A., In silico research in drug discovery. *Trends Pharmacol Sci.* 22, 23-26, 2001.
- [77] Wallin, E., and von Heijne, G., Genome-wide analysis of integral membrane proteins from eubacterial, archean, and eukaryotic organisms. *Prot. Sci.* 7, 1029-1038, 1998.
- [78] Kukol, A., Molecular modeling of proteins. 2008.
- [79] Beckstein, O., and Sansom, M. S. P. A hydrophobic gate in an ion channel: the closed state of the nicotinic acetylcholine receptor. *Phys. Biol.* 3, 147-159, 2006.
- [80] Hyvönen, M., *Molecular dynamics simulations on phospholipid membranes.*, M.S. Thesis, Department of Physical Sciences, University of Oulu Wihuri Research Institute., 2001.
- [81] Hospital, A., Andrio, P., Fenollosa C., Cicin-Sain, D., Orozco, M. and Lluís Gelpí, J., An integrated web-based platform for molecular dynamics simulations. 2011.
- [82] Huang, Y., M. J. Lemieux, J. Song, M. Auer, and D.-N. Wang. Structure and mechanism of the glycerol-3-phosphate transporter from *Escherichia coli*. *Science*. 301:616–620, 2003.
- [83] Abramson, J., I. Smirnova, V. Kasho, G. Verner, H. R. Kaback, and S. Iwata. Structure and mechanism of the lactose permease of *Escherichia coli*. *Science*. 301:610–615, 2003.

- [84] Yernool, D., O. Boudker, Y. Jin, and E. Gouaux. Structure of a glutamate transporter homologue from *Pyrococcus horikoshii*. *Nature*. 431:811–818, 2004.
- [85] Chen, J.G., Liu-Chen, S. and Rudnick, G., J., External cysteine residues in the serotonin transporter *Biol. Chem.*, 273 (1998) 12675, 1997.
- [86] Williams, K.A., Three-dimensional structure of the ion-coupled transport protein *Nature*, 403 112, 2000.
- [87] Rothman, A., Padan, E. and Schuldiner, S., Topological analysis of NhaA, a Na<sup>+</sup>/H<sup>+</sup> antiporter from *Escherichia coli*. *J. Biol. Chem.*, 271, 32288, 1997.
- [88] Ballesteros, M., Fredriksson, A., Henriksson, J., Nyström, T., Bacterial senescence: protein oxidation in non-proliferating cells is dictated by the accuracy of the ribosomes. *EMBO J* 20: 5280–5289, 2001.
- [89] Palczewski K, Kumasaka T, Hori T, Behnke CA, Motoshima H, Fox BA, Le Trong I, Teller DC, Okada T, Stenkamp RE, Yamamoto M, Miyano M. Source, Crystal structure of rhodopsin: A G protein-coupled receptor. *Department of Ophthalmology, University of Washington, Seattle, WA 98195, USA, Science*. 739-45, 2000.
- [90] Susan, R., George, Gordon, Y.K. ng, Samuel P., George R., Blockade of G Protein-Coupled Receptors and the Dopamine Transporter by a Transmembrane Domain Peptide: Novel Strategy for Functional Inhibition of Membrane Proteins in Vivo, *Biochemistry University*, 2003.
- [91] Giros, B., Mestikawy, S., Godninot, N., Cloning Pharmacological Characterization and Chromosome Assignment of the Human Dopamine Transporter, *Molecular Pharmacology* ; 42:383-390, 1992.
- [92] Isgro, T., Phillips, J., Sotomayor, M., Villa, E., Namd Tutorial, 2003.
- [93] <http://www.ks.uiuc.edu/Training/Tutorials/science/forcefieldtutorial/forcefield.html/node6.html>

- [94] Torres, G.E., Gainetdinov, R.R., and Caron, M.G., Plasma membrane monoamine transporters: structure, regulation and function. *Nat. Rev. Neurosci.* 4, 13–25, 2003.
- [95] Iversen, L., Neurotransmitter transporters and their impact on the development of psychopharmacology. *Br. J. Pharmacol.* 147 (Suppl 1), S82–S88, 2006.
- [96] Amara, S.G., and Sonders, M.S. Neurotransmitter transporters as molecular targets for addictive drugs. *Drug Alcohol Depend.* 51, 87–96, 1998.
- [97] Berendsen, H.J.C., J.P.M. Postma, W.F. Gunsteren, A. DiNola and J.R. Haak, Molecular dynamics with coupling to an external.  *bath. J. Chem. Phys.*, 81: 3684-3689, 1984.
- [98] Giros, B., Jaber, M., Jones, S., Wightman, R.M., Caron, M.G. Hyperlocomotion and indifference to cocaine and amphetamine in mice lacking the dopamine transporter. *Nature* 379, 606–612, 1996.
- [99] Jones, S.R., Gainetdinov, R.R., Jaber, M., Giros, B., Wightman, R.M. Caron M.G., Profound neuronal plasticity in response to inactivation of the dopamine transporter. *Proc. Natl. Acad. Sci. U. S. A.* 95, 4029–4034, 1998.
- [100] Chen, N., Reith, M.E., Structure and function of dopamine transporter. *J. Biochemistry*, 2008.
- [101] Bönisch, H., Transport and drug binding kinetics in membrane vesicle preparation. *Methods Enzymol.* 296, 259–278, 1998.
- [102] Leach, A.R., Molecular Modeling: Principles and Application (2nd Edition), Prentice Hall, 2001.
- [103] Feig, M., J. Karanicolas and C.L. Brooks, “MMTSB Tool Set: enhanced sampling and multiscale modeling methods for applications in structural biology”, *J. Mol. Graph. Model.*, 377-395, 2004.

- [104] Kitayama, S., S. Shimada, H. Xu, L. Markham, M. D. Donovan, and R. G. Uhl. Dopamine transporter site-directed mutations differentially alter substrate transport and cocaine binding. *Proc. Natl. Acad. Sci. USA*. 89:7782–7785, 1992.
- [105] Uhl, G. R., and Z. Lin. The top 20 dopamine transporter mutants: structure-function relationships and cocaine actions. *Eur. J. Pharmacol.* 479:71–82, 2003.
- [106] Ukairo, O. T., C. D. Bondi, A. H. Neuwman, S. S. Kulkarni, A. P. Kozikowski, S. Pan, and C. K. Surratt. Recognition of benztropine by the dopamine transporter (DAT) differs from that of the classical dopamine uptake inhibitors cocaine, methylphenidate, and mazindol as a function of a DAT transmembrane 1 aspartic acid residue. *J. Pharmacol. Exp. Ther.* 314:575–583, 2005.
- [107] Yamashita, A., S. K. Singh, T. Kawate, Y. Jin, and E. Gouaux.. Crystal structure of a bacterial homologue of Na<sup>+</sup>/Cl<sup>-</sup>-dependent neurotransmitter transporters. *Nature*. 437:215–223, 2005.
- [108] Bismuth, Y., M. P. Kavanaugh, and B. I. Kanner. Tyrosine 140 of the  $\gamma$ -aminobutyric acid transporter GAT-1 plays a critical role in neurotransmitter recognition. *J. Biol. Chem.* 272:16096–16102, 1997.
- [109] Chen, J. G., A. Sachpatzids, and G. Rudnick. The third transmembrane domain of the serotonin transporter contains residues associated with substrate and cocaine binding. *J. Biol. Chem.* 272: 28321–28327, 1997.
- [110] Ponce, J., B. Biton, J. Benavides, P. Avenet, and C. Aragon. Transmembrane domain III plays an important role in ion binding and permeation in the glycine transporter GLYT2. *J. Biol. Chem.* 275: 13856–13862, 2000.
- [111] Edvardsen, O., Dahl, S.G., A putative model of the dopamine transporter. *Brain Res Mol Brain Res* 27: 265 – 274, 1994.

- [112] Lin, Z., Wang, W., Kopajtic, T., Revay, R.S., Uhl, G.R., Dopamine transporter: transmembrane phenylalanine mutations can selectively influence dopamine uptake and cocaine analog recognition. *Mol. Pharmacol.* 56, 434–447, 1999.
- [113] Beuming, T., Loland, C.L., The binding sites for cocaine and dopamine in the dopamine transporter overlap. *Nat Neurosci.* 780-789, 2008.
- [114] Morris, G. M., R. Huey, W. Lindstrom, M. F. Sanner, R. K. Belew, D. S. Goodsell, and A. J. Olson, “AutoDock4 and AutoDockTools4: Automated Docking with Selective Receptor Flexibility”, *J. Comput. Chem.*, Vol. 30, pp. 2785–2791, 2009.
- [115] Weiner, S. J., Kollman, P.A., Case, D.A., Singh, U.C., Ghio, C., Alagona, G., Profeta, S., Weiner P.K., A new force field for molecular mechanical simulation of nucleic acids proteins. *J. Am. Chem. Soc.* 106,765-784,1984.
- [116] Goodford, P. J. *J Med Chem* 28, 849. A computational procedure for determining energetically favorable binding sites on biologically important macromolecules. *Med Chem* , 28, 849, 1985.
- [117] Hu, J., Yan, C, A, Tool for calculating binding-site residues on proteins from PDB structures. Department of Computer Science, Utah State University, Logan, UT, USA, 2009.
- [118] Surratt, C.K., Ukairo, O.T., Ramanujapuram S. Recognition of psychostimulants, antidepressants, and other inhibitors of synaptic neurotransmitter uptake by the plasma membrane monoamine transporters. *AAPS J* ;7:E739–E751, 2005.
- [119] Henry, L.K., Adkins, E.M., Han, Q, Blakely RD. Serotonin and cocaine sensitive inactivation of human serotonin transporters by methanethiosulfonates targeted to transmembrane domain I. *J Biol Chem*;278:37052–37063,2003.

- [120] Adkins, E.M., Barker, E.L., Blakely RD. Interactions of tryptamine derivatives with serotonin transporter species variants implicate transmembrane domain I in substrate recognition. *Mol Pharmacol* 2001;59:514–523.
- [121] Barker, E.L., Perlman, M.A., Adkins, E.M., Houlihan, W.J., Pristupa ZB, Niznik HB, Blakely RD. High affinity recognition of serotonin transporter antagonists defined by species-scanning mutagenesis. *J Biol Chem*;273:19459–19468,1998.
- [122] Chen J-G, Rudnick G., Permeation and gating residues in serotonin transporter. *Proc Natl Acad Sci USA*;97:1044–1049, 2000.
- [123] Chen J-G, Sachpatzidis A, Rudnick G. The third transmembrane domain of the serotonin transporter contains residues associated with substrate and cocaine binding. *J Biol Chem* ;272:28321– 28327, 1997.
- [124] Lee, S.H., Chang, M.Y., Lee, K.H., Park, B.S., Lee, Y.S., Chin, H.R. Importance of valine at position 152 for the substrate transport and 2bcarbomethoxy- 3b-(4-fluorophenyl)tropane binding of dopamine transporter. *Mol Pharmacol* ;57:883–889, 2000.
- [125] Melamed, N., Kanner, B.I., Transmembrane domains I and II of the g-aminobutyric acid transporter GAT-4 contain molecular determinants of substrate specificity. *Mol Pharmacol*;65:1452–1461,2004.
- [126] Ukairo, O.T., Bondi, C.D., Newman, A.H., Kulkarni, S.S., Kozikowski AP, Pan, S., Surratt, C.K., Recognition of benztropine by the dopamine transporter (DAT) differs from that of the classical dopamine uptake inhibitors cocaine, methylphenidate, and mazindol as a function of a DAT transmembrane 1 aspartic acid residue. *J Pharmacol Exp Ther* ;314:575–583, 2005.
- [127] Wang, W., Sonders, M.S., Ukairo, O.T., Scott, H., Kloetzel, M.K., Surratt, C.K. Dissociation of high-affinity cocaine analog binding and dopamine uptake inhibition at the dopamine transporter. *Mol Pharmacol*;64:430–439, 2003.

- [128] Zomot, E, Kanner, B.I. The interaction of the g-aminobutyric acid transporter GAT-1 with the neurotransmitter is selectively impaired by sulfhydryl modification of a conformationally sensitive cysteine residue engineered into extracellular loop IV. *J Biol Chem*; 278:42950–42958, 2003.
- [129] Yamashita, A., Singh, S.K., Kawate, T, Yan, Jin Y., Gouaux, E. Crystal structure of a bacterial homologue of Na<sup>+</sup>/Cl<sup>-</sup> dependent neurotransmitter transporters. *Nature* 437: 215–223, 2005.
- [130] Krishnamurthy, H., Piscitelli, C.L., Gouaux, E. Unlocking the molecular secrets of sodium-coupled transporters. *Nature* 459: 347–355, 2009.
- [131] Patrick, C.G., Marti'n ,I., Christopher, K.S., Jeffry, D.M. Molecular dynamics of leucine and dopamine transporter proteins in a model cell membrane lipid bilayer. *Proteins: Structure, Function, and Bioinformatics* 78: 797–811, 2010.
- [132] Indarte, M., Madura, J.D., Surratt, C.K. Dopamine transporter comparative molecular modeling and binding site prediction using the LeuTAa leucine transporter as a template. *Proteins: Structure, Function, and Bioinformatics* 70: 1033–1046, 2008.
- [133] Tatar, G., Structure Prediction of Human DAT and its Binding Analysis, M.S Thesis, Kadir Has University, 2011.